

Cooperative quantum phenomena

Michael Reitz,^{1,2} Christian Sommer,¹ and Claudio Genes^{1,2}

¹*Max Planck Institute for the Science of Light, Staudtstraße 2, D-91058 Erlangen, Germany*

²*Department of Physics, University of Erlangen-Nuremberg, Staudtstraße 7, D-91058 Erlangen, Germany*

(Dated: June 8, 2022)

Quantum cooperativity is evident in light-matter platforms where quantum emitter ensembles are interfaced with confined optical modes and are coupled via the ubiquitous electromagnetic quantum vacuum. Cooperative aspects such as dipole-dipole interactions and subradiance find applications in the design of nanoscale coherent light sources and highly-reflective quantum metasurfaces made up of hundreds of optically trapped atoms, in the implementation of topological quantum optics on subwavelength arrays of emitters, in quantum metrology and quantum information. The quick bursts of radiation from a collection of quasi-indistinguishable emitters provides an alternative approach to standard lasers by introducing superradiant lasers operating at extremely low intracavity power. This tutorial provides a set of theoretical tools to tackle the behavior responsible for the onset of cooperativity in light-matter systems by extending open quantum system dynamics methods, such as the master equation and quantum Langevin equations, to electron-photon interactions in strongly coupled and correlated quantum emitters ensembles. These analytical approaches are then also extended to frequency disordered or vibronically coupled quantum emitter ensembles with wide relevance ranging from atoms in optical lattices, quantum dots in solid state environments or molecular quantum systems.

PACS numbers: 42.50.Nn, 42.50.Ct, 42.50.-p

Contents

I	Introduction	1
II	Cooperativity of light and matter	3
A	Collective radiative emission	3
B	Superradiance and subradiance	4
C	Dicke superradiance	7
D	Cooperative cavity QED	7
E	Superradiant lasers	9
F	Disorder effects	11
III	Subwavelength quantum emitter arrays	12
A	Optical response of two-dimensional arrays	12
B	Towards topological quantum optics	14
C	Quantum emitter rings and chains	17
D	Further remarks	19
IV	Cooperativity in cavity QED	19
A	Quantum Langevin equations	20
B	Cavity QED with subradiant arrays	21
C	Hybrid cavities	22
D	Further remarks	24
V	Quantum optics with molecules	24
A	Holstein Hamiltonian	25
B	Quantum Langevin equations for polarons	27
C	Absorption and emission	28
D	Near-field effects: vibronic dimer model	28
E	Förster resonance energy transfer	29
F	Further remarks	30
VI	Conclusions	31
	Acknowledgments	31
	References	31
	Appendix	35
1	One dimensional transfer matrix theory	35
2	Brownian noise model for vibrational relaxation	36
3	Derivation of the FRET rate	37

I. INTRODUCTION

Some of the most intriguing phenomena in nature, both in the classical and quantum domains, are a product of *cooperative* effects, i.e., they cannot be understood by sole consideration of the individual constituents as they arise from the interplay among them. While at the fundamental science level, the understanding of many of those problems in the quantum domain already poses a great intellectual challenge, there is an ever increasing interest to build, control and harness complex cooperative platforms for emerging quantum technologies [1].

Light-matter platforms provide an optimal playground for the observation and exploitation of quantum cooperative effects. Quantum light, either multimode, as naturally arising in the quantum electromagnetic vacuum or single mode, as confined in the small volume of an optical resonator, can induce strong interactions among quantum emitters (QEs). Cooperativity then occurs naturally under high-density conditions and manifests itself in a strongly modified material response owed to a continuous scattering and re-scattering of photons between the matter constituents. Two main aspects brought on by the common coupling to an electromagnetic environment are dipole-dipole interactions, stemming from a virtual exchange of photons and collective spontaneous emission, stemming from the loss of excitation into the infinite number of the electromagnetic vacuum modes. While the former is included as a coherent effect, the latter is an incoherent one, observable either as an increase (*superradiance*) or a decrease (*subradiance*) in the collective spontaneous emission rate compared to that of an isolated emitter.

Numerous aspects and applications of cooperative

effects in light-matter platforms have been tackled in the past decades. For example, a naturally occurring effect of near-field dipole-dipole interactions is the Förster resonance energy transfer processes in molecular ensembles [2, 3], a key process in photosynthetic light harvesting. Engineered platforms instead, in the form of structured *subwavelength arrays* of quantum emitters, employ near-field exchanges allowing hopping of surface excitations. Such platforms could provide an alternative to linear topological photonic systems [4–6]. A crucial aspect is the existence of an intrinsic non-linearity of the quantum emitters which leads to the emergence of rich many-body quantum phenomena on emitter-thick metasurfaces. Such arrays are ideal platforms for achieving strong light-matter interactions and high fidelities for photon storage capabilities [7, 8] and their subradiance properties are an important resource for applications ranging from quantum information processing [9] to metrology [7, 10, 11]. Individual addressing of a single qubit emitter has been proposed via quantum spin lenses [12] and an approach to quantum networking with composite quantum systems comprised of many atomic arrays has been proposed building on theoretical results showing the production of a Bell entangled superposition quantum state for two distant arrays [13].

Cooperativity is explicitly manifested in the scaling of the subradiant properties of emitter arrays, predicted to scale as \mathcal{N}^{-3} [8] and even as \mathcal{N}^{-5} [14]. This property has been experimentally employed to show near-unity ultra-thin reflectors [15] with potential applications in nano-optomechanics [16, 17], antiresonance spectroscopy [18, 19] and nonlinear quantum optics [20]. In the context of cavity quantum electrodynamics (cQED) [21–24], where matter is interfaced with strongly confined photon modes, superradiance [25, 26] (the quick burst of spontaneous emission from \mathcal{N} indistinguishable quantum emitters) finds application in the operation of superradiant lasers [27, 28]. The combination of quantum metasurfaces with plain mirrors allows for the design of hybrid cavities (optical resonators with one or two frequency dependent end-mirrors), superior in performance to ones made up by plain, frequency-insensitive, mirrors [29].

While many light-matter platforms are designed at the level of *quasi-pure* quantum emitters, i.e. considering mainly electron-photon interactions, a variety of extremely promising directions in quantum engineering are utilizing more complex quantum emitters such as organic molecules, quantum dots or color centers. In particular at the level of organic molecules, the strong confinement of light modes in micro-cavities gives rise to a novel research direction into *vacuum-dressed* or *cavity-dressed* materials, i.e. vacuum-hybridized materials with enhanced properties. At the level of mesoscopic systems, changes in charge conductivity [30–34], energy transfer rates [35, 36], chemical reactivity [37–41] have been experimentally observed and theoretically studied. At the level of single molecules, the focus is in producing

reliable single quantum emitters as single photon sources with application such as entanglement generation or in optical quantum computing. Recent results for example, have shown that a cavity-dressed molecule can act as an almost ideal quantum emitter, exhibiting a close electronic transition [42].

Many of the aforementioned applications can be understood within the formalism of open quantum system dynamics extended to the more complex problem of correlated matter, such as occurring in a coupled quantum emitter ensemble. To this end, this tutorial utilizes two competing, interconnected approaches, one at the level of the density operator time evolution, i.e., the master equation (ME) and the other following time dynamics of system operators, i.e., the quantum Langevin equations (QLEs) approach. As the two formalisms are standard textbook methods describing phenomena such as the spontaneous emission of a single emitter and cavity photon loss (see Refs. [43–46]), this tutorial proceeds with more complex aspects of light-matter interactions such as the emergence of a cooperative ME for coupled quantum emitter systems, introduced in Sec. II A together with the consequential occurrence of subradiance and superradiant properties, which are tackled in Sec. II B (and later utilized in Sec. III B and Sec. II B). The connection to Dicke superradiance [25] is explained in Sec. II C and its relevance to the operation of alternative superradiant, low intracavity power lasers is made in Sec. II E. A simplified, basic theory of lasing for incoherently pumped cavity embedded gain media is also presented in Sec. II E, which allows the understanding of the mechanism of storing coherence in the gain medium instead of cavity photons, as exploited in superradiant lasers. From the master equation, one can then derive the fundamental equations of motion for \mathcal{N} driven emitters and a single driven cavity mode as shown in Sec. II D. These equations are the starting point in showing strong reflection properties of subwavelength emitter arrays (in Sec. III A) and in providing an understanding on how energy dispersion relations and energy bandgaps can be engineered (in Sec. II B) with topological quantum optics implementations. More applications of the master equation for coupled quantum emitters are exemplified in Sec. II C with relevance to quantum metrology, the design of robust quantum memories and of nanoscale coherent light sources with thresholdless lasing capabilities. In Sec. IV we provide a translation of the master equation to the quantum Langevin equations which are then employed towards the analysis of quantum properties of light used for antiresonance spectroscopy in cavity QED and towards the design of narrow-linewidth non-Markovian hybrid cavities. Results previously derived in Sec. III A are used to show improved performance of hybrid cavities utilizing one or two subwavelength reflective arrays as end-mirrors. To understand the more complex dynamics of light-matter interactions in the presence of additional vibrational degrees of freedom typically described by a

Holstein Hamiltonian [47], we describe the application of a recently introduced formalism [48, 49] based on the application of the QLEs to molecular ensembles in Sec. V. We show how perturbative analytical approaches can shed light into processes such as molecular absorption and emission, the emergence of a FRET (Förster resonance energy transfer regime) and can quantitatively explain the modification of the branching ratio of a molecule coupled to a lossy cavity [42]. Finally, the occurrence of near-field effects and subradiance in molecular dimers [50] is tackled in Sec. V D by translating a standard model used in quantum chemistry into the formalism introduced in Sec. II and showing the possibility of engineering subwavelength arrays based on self-assembled systems of chromophores.

II. COOPERATIVITY OF LIGHT AND MATTER

The standard system we will consider in the next sections is that of an ensemble of \mathcal{N} identical quantum emitters modeled for simplicity as hydrogen-like atoms with nuclei fixed in random positions \mathbf{R}_j , where $j = 1, \dots, \mathcal{N}$. The (single) electronic degree of freedom for each emitter is described by quantized momentum $\hat{\mathbf{p}}_j$ and position $\hat{\mathbf{r}}_j$ (relative to its respective nucleus) operators appearing in the Hamiltonian $h_j = \hat{\mathbf{p}}_j^2/(2\mu) + V(\hat{\mathbf{r}}_j)$ consisting of the kinetic energy and an electrostatic potential $V(\hat{\mathbf{r}}_j)$. Out of the infinite set of eigenvectors of h_j , we pick the lowest energy one (and set its energy to zero) $|g_j\rangle$ and assume that all the physics described in the following involves transitions to only one excited state $|e_j\rangle$ at energy ω_0 (we set $\hbar = 1$). This amounts to a two-level system approximation where the unity of the Hilbert space is a sum of only two projectors $\mathbf{1}_j = |g_j\rangle\langle g_j| + |e_j\rangle\langle e_j|$. To quantify transitions between the two levels, we introduce the standard ladder (Pauli) operators $\sigma_j = |g_j\rangle\langle e_j|, \sigma_j^\dagger = |e_j\rangle\langle g_j|$. Their commutator $[\sigma_j^\dagger, \sigma_j] = 2\sigma_j^z$ is the population difference operator. The free Hamiltonian can then be written as $h_j = \omega_0\sigma_j^\dagger\sigma_j$ or alternatively as $h_j = \omega_0\sigma_j^z/2$ (up to a constant energy shift).

To describe the interaction of the emitters with the electromagnetic vacuum, one introduces a fictitious perfectly reflecting box of volume $\mathcal{V} = \ell^3$ and follows a standard quantization procedure for the electromagnetic field imposing periodic boundary conditions [43–46]. This leads to a plane wave expansion of the electric field operator

$$\hat{\mathbf{E}}(\mathbf{r}) = \sum_{\mathbf{k}} \mathcal{E}_k \left(a_{\mathbf{k}} e^{i\mathbf{k}\cdot\mathbf{r}} + a_{\mathbf{k}}^\dagger e^{-i\mathbf{k}\cdot\mathbf{r}} \right) \boldsymbol{\epsilon}_{\mathbf{k}}, \quad (1)$$

where the allowed \mathbf{k} -vectors are multiples of $2\pi/\ell$ on each Cartesian direction and the index \mathbf{k} runs over all possible \mathbf{k} -vectors and also over the two orthogonal polarizations with unit vectors $\boldsymbol{\epsilon}_{\mathbf{k}}$. The bosonic operators follow the commutation $[a_{\mathbf{k}}, a_{\mathbf{k}'}^\dagger] = \delta_{\mathbf{kk}'} \mathbf{1}$ and their action is to create and destroy excitations in a given field

mode. The zero point electric field amplitude is defined as $\mathcal{E}_k = \sqrt{\omega_k/(2\epsilon_0\mathcal{V})}$. The Hamiltonian for the field inside the box can then be written as a sum over an infinite number of bosonic modes $\mathcal{H}_{\text{vac}} = \sum_{\mathbf{k}} \omega_k (a_{\mathbf{k}}^\dagger a_{\mathbf{k}} + 1/2)$.

A. Collective radiative emission

The coupling of light and matter occurs within the formalism of the minimal coupling Hamiltonian [43–46]

$$\mathcal{H} = \sum_{j=1}^{\mathcal{N}} \frac{[\hat{\mathbf{p}}_j - e\hat{\mathbf{A}}(\hat{\mathbf{r}}_j)]^2}{2\mu} + V(\hat{\mathbf{r}}_j) + \mathcal{H}_{\text{vac}}, \quad (2)$$

describing the total quantum system of charges and electromagnetic vacuum modes. Notice that the canonical momentum of the electron is shifted to $\hat{\mathbf{p}}_j = \mu\hat{\mathbf{r}}_j + e\hat{\mathbf{A}}(\mathbf{r}_j)$ where $\hat{\mathbf{A}}(\mathbf{r})$ is the vector potential operator of the electromagnetic field. The observation that the size of the electronic orbital is much smaller than the wavelength $\lambda_0 = 2\pi c/\omega_0$ associated with the optical transition between the two electronic orbitals allows for a length gauge transformation leading to a simplified form of the Hamiltonian

$$\mathcal{H} = \sum_{j=1}^{\mathcal{N}} h_j + \mathcal{H}_{\text{vac}} + \sum_{j=1}^{\mathcal{N}} \hat{\mathbf{d}}_j \cdot \hat{\mathbf{E}}(\mathbf{R}_j). \quad (3)$$

In this so-called *dipole approximation*, the light matter interaction only involves the dipole moment operator $\hat{\mathbf{d}}_j = -e\hat{\mathbf{r}}_j$ and the electric field operator. Under the two-level assumption, the dipole operator is written as $\hat{\mathbf{d}}_j = \mathbf{d}_{\text{eg}}\sigma_j + \text{h.c.}$, where the transition dipole moment is computed between the two states $\mathbf{d}_{\text{eg}} = \langle g_j | \hat{\mathbf{d}}_j | e_j \rangle$ (assuming identical emitters). Moreover, one performs an additional *rotating wave approximation* (RWA) where energy non-conserving terms such as $\sigma_j a_{\mathbf{k}}$ and its Hermitian conjugate are neglected. Under these approximations, the light-matter interaction part of the Hamiltonian can be written as

$$\mathcal{H}_{\text{int}} = \sum_{j=1}^{\mathcal{N}} \left(g_{\mathbf{k}} \sigma_j^\dagger a_{\mathbf{k}} e^{i\mathbf{k}\cdot\mathbf{R}_j} + g_{\mathbf{k}}^* a_{\mathbf{k}}^\dagger \sigma_j e^{-i\mathbf{k}\cdot\mathbf{R}_j} \right), \quad (4)$$

describing a photon-emitter energy exchange at rates $g_{\mathbf{k}} = \mathcal{E}_k \boldsymbol{\epsilon}_{\mathbf{k}} \cdot \mathbf{d}_{\text{eg}}$.

The Hamiltonian \mathcal{H} governs unitary evolution in an infinite-dimensional Hilbert space (owing to the infinite number of electromagnetic modes). One can then use a deterministic Schrödinger equation or equivalently the von-Neumann equation for the system density operator $\rho_{\text{tot}}(t)$ to compute the state of the system at any time. However, this is an extremely complex task requiring an immense computational resource even for small size systems. Instead, in order to drastically reduce complexity, an open system dynamics approach can be taken, which consists in reducing the system of interest to the Hilbert

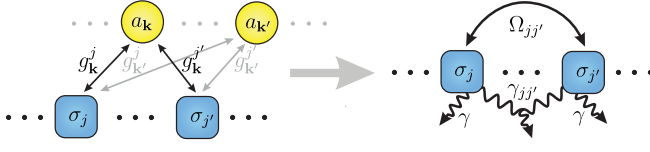


FIG. 1: Schematics of the procedure followed to obtain the open system dynamics formulation for a system of \mathcal{N} quantum emitters (denoted by σ_j and $\sigma_{j'}$) subject to the quantum electromagnetic vacuum. The key point is that, for a pair of emitters, coupling to the *common reservoir modes* (denoted by a_k and $a_{k'}$) gives rise to separation dependent dipole-dipole interactions at rate $\Omega_{jj'}$ as well as to collective decay rates $\gamma_{jj'}$.

space of dimension $2^{\mathcal{N}}$ of the matter part only. The first observation then is that the time-dependent light-matter interaction Hamiltonian can be very simply expressed as $\mathcal{H}_{\text{int}} = \sigma \mathcal{F}^\dagger(t) + \sigma^\dagger \mathcal{F}(t)$ where the time-dependent operator driving the emitter

$$\mathcal{F}(t) = \sum_{j=1}^{\mathcal{N}} g_k a_k e^{i\mathbf{k} \cdot \mathbf{R}_j} e^{i(\omega_k - \omega_0)t}, \quad (5)$$

acts fully in the Hilbert space of the light modes. The procedure then asks that, under the weak light-matter coupling assumption, the electromagnetic degrees of freedom are traced over (as schematically illustrated in Fig. 1) to obtain an equation of motion for $\rho(t) = \text{Tr}_{\text{em}}[\rho_{\text{tot}}(t)]$. The simplifying assumption is the Born-Markov approximation requiring that i) at any time t , the bath density operator is unchanged (thus not time-dependent) and the total system state can be decoupled $\rho_{\text{tot}}(t) = \rho(t) \otimes \rho_{\text{em}}$ and ii) tracing over the electromagnetic vacuum involves two-time correlations of the operator $\mathcal{F}(t)$ which is assumed in the form of a delta function in time. This is a standard procedure widely covered in the literature [45].

Finally, after the previous steps are followed one obtains the quantum master equation in the form

$$\dot{\rho}(t) = i \left[\rho(t), \sum_{j=1}^{\mathcal{N}} h_j + \mathcal{H}_{dd} \right] + \mathcal{L}_e[\rho]. \quad (6)$$

The last term in the master equation above describes irreversible loss of excitation into the electromagnetic vacuum and is expressed in the form of a superoperator defined as

$$\mathcal{L}_e[\rho] = \sum_{j,j'=1}^{\mathcal{N}} \gamma_{jj'} \left[2\sigma_j \rho(t) \sigma_{j'}^\dagger - \sigma_j^\dagger \sigma_{j'} \rho(t) - \rho(t) \sigma_j^\dagger \sigma_{j'} \right]. \quad (7)$$

Notice that this is not in standard, diagonal Lindblad form [44–46] which for a collapse operator \mathcal{O} and collapse rate $\gamma_{\mathcal{O}}$ is defined as

$$\mathcal{L}_\gamma[\rho] = \gamma_{\mathcal{O}} [2\mathcal{O}\rho(t)\mathcal{O}^\dagger - \mathcal{O}^\dagger\mathcal{O}\rho(t) - \rho(t)\mathcal{O}^\dagger\mathcal{O}], \quad (8)$$

and describes decay at rate $\gamma_{\mathcal{O}}$ through a single channel with operator \mathcal{O} .

The decay rates are $\gamma_{jj'} = (3\gamma/2)F(k_0 R_{jj'})$ where the relative distance vector is $R_{jj'} = |\mathbf{R}_j - \mathbf{R}_{j'}|$ and the function of position is defined as

$$F(kR) = \left[1 + \frac{(\mathbf{e}_d \cdot \nabla_{\mathbf{R}})^2}{k^2} \right] \frac{\sin(kR)}{kR}. \quad (9)$$

The rate $\gamma = \omega_0^3 d_{\text{eg}}^2 / (6\pi^3 \epsilon_0)$ is the spontaneous emission rate of a single emitter (note that the decay rate of the excited state population is given by 2γ). The collective radiative decay properties are given by the oscillatory behavior of $F(k_0 R)$ as illustrated in Fig. 2b. Notice that, for emitters separated by much more than λ_0 , the decay becomes purely diagonal as expected for non-interacting, independent emitters.

The coherent term \mathcal{H}_{dd} in Eq. (6) instead describes a dipole-dipole interaction characterized by a virtual exchange of excitation via the vacuum modes without loss of photons

$$\mathcal{H}_{dd} = \sum_{j,j':j \neq j'}^{\mathcal{N}} \Omega_{jj'} \sigma_j^\dagger \sigma_{j'}. \quad (10)$$

The exchange rate $\Omega(R_{jj'}) = -(3\gamma/4)G(k_0 R_{jj'})$ can be obtained from the same function that characterizes the collective decay rates via the definition

$$G(kR) = \frac{c}{\pi \omega^3} \mathcal{P} \int dk \frac{(ck)^3}{ck - \omega} F(kR). \quad (11)$$

The behavior illustrated in Fig. 2(b) shows that the dipole-dipole interaction ceases at large distances, as expected, but diverges at close separations. This is however only an artefact of the initial assumptions that the dipole-electric field interaction is valid at any inter-particle distance. This is of course not true, as for separations of the order of the size of the orbitals, one ends up with a fundamentally quantum many-body problem where the tunneling of electrons between neighboring emitters has to be taken into account (leading to molecule formation, hybridization of orbitals, etc). More involved models, based for example on a quantum electrodynamics density-functional formalism, can then be employed [51].

B. Superradiance and subradiance

The superoperator in Eq. (7) describes non-trivial mutual decay characterized by the matrix Γ made up by the elements $\gamma_{jj'}$. However, this term is not in standard diagonal form (characterized by a single collapse operator) as it is not comprised on \mathcal{N} independent decay channels. One can perform a basis transformation with a matrix \mathbf{T} (such that $\mathbf{T}^{-1} = \mathbf{T}^\top$) which diagonalizes Γ such that $\text{diag}(\tilde{\gamma}_1, \dots, \tilde{\gamma}_{\mathcal{N}}) = \mathbf{T}^\top \Gamma \mathbf{T}$ where $\tilde{\gamma}_k$ is the k th eigenvalue of the decay matrix. Defining a set of collapse operators $\Pi_k = \sum_j T_{jk} \sigma_j$, we can write

$$\mathcal{L}_e[\rho] = \sum_{k=1}^{\mathcal{N}} \tilde{\gamma}_k \left(2\Pi_k \rho \Pi_k^\dagger - \Pi_k^\dagger \Pi_k \rho - \rho \Pi_k^\dagger \Pi_k \right), \quad (12)$$

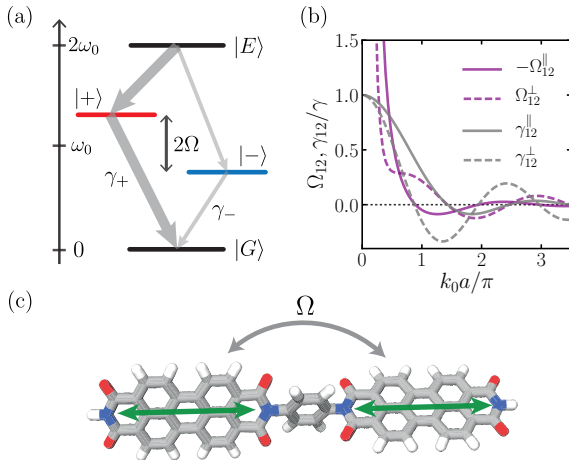


FIG. 2: (a) Decay and eigenstates in the collective two-emitter basis. Superradiant and subradiant decay channels emerge through the formation of symmetric and antisymmetric superposition states. (b) Dipole-dipole coupling Ω_{12} and collective decay rate γ_{12} scaling with normalized interatomic distance k_0a for parallel (\parallel) and perpendicular (\perp) orientation of dipoles (with respect to \mathbf{R}_{12}). (c) Possible experimental realization of strong dipole-dipole couplings for two identical chromophores connected by an insulating bridge of length much smaller than λ_0 . The green arrows represent the orientation of the transition dipoles. Adapted from Ref. [50].

which now describes \mathcal{N} independent decay channels each with collapse operator Π_k and associated loss rate $\tilde{\gamma}_k$.

Two coupled emitters - Let us first make the connection between collective radiative effects and the symmetry of quantum superpositions by considering the simplest example of two quantum emitters separated by distance a . Diagonalization of the decay matrix leads to superradiant/subradiant decay channels characterized by $\gamma_{\pm} = \gamma \pm \bar{\gamma}$ and at the same time renders the Hamiltonian in diagonal form with eigenenergies $\omega_{\pm} = \omega_0 \pm \Omega$. The eigenstates are symmetric/antisymmetric superpositions $|\pm\rangle = (|e\rangle_1 \otimes |g\rangle_2 \pm |g\rangle_1 \otimes |e\rangle_2)/\sqrt{2}$. This is illustrated in Fig. 2a in the collective basis where the other two states are the fully excited one $|E\rangle = |e\rangle_1 \otimes |e\rangle_2$ and the ground state $|G\rangle = |g\rangle_1 \otimes |g\rangle_2$. The splitting between the two levels in the collective basis $2\Omega = 2\Omega_{12}(a)$ as well as the magnitude and the sign of the mutual decay rate $\bar{\gamma} = \gamma_{12}(a)$ depend strongly on the particular choice of dipole orientations as well as on separation (as illustrated in Fig. 2b). However, for distances below half a wavelength $a < \lambda_0/2$, the antisymmetric/symmetric states always have a subradiant/superradiant character. One can understand the connection between state symmetry and radiative properties in terms of an constructive/destructive interference of radiative paths.

The strong scaling of the near-field dipole-dipole coupling with the interparticle distance renders such a

simple system valuable for experimental applications in superresolution imaging. The mechanism is based on the analysis of the emitted light frequency shift and comparison with fluorescence from a single unshifted emitter which allows then for subwavelength resolution. In addition, for strongly coupled emitters, chemical or mechanical means can be employed to correct energy shifts and render the closely spaced emitters indistinguishable such that a source of indistinguishable photons can be achieved. Finally, we remark that subwavelength separations (even at the level of less than 10 nm) could be achieved in assembled molecular dimers [50] where two chromophores are coupled via an insulating bridge (illustrated in Fig. 2c). The mapping of the vibronic dimer model onto two dipole-dipole coupled (vibronic) quantum emitters is detailed in Sec. V D.

The single excitation subspace - While the simultaneous diagonalization of the Lindblad term and the Hamiltonian is generally not possible for $\mathcal{N} > 2$, one can still get some intuition in the nature of cooperative decay in the particular case of \mathcal{N} equally spaced quantum emitters in a 1D chain configuration. Analysis of Eq. (12) leads to a set of subradiant states characterized by decay rates scaling exponentially down with \mathcal{N} . Also, superradiance emerges, which for small distances a is characterized by a rate proportional to \mathcal{N} but eventually saturates with increasing \mathcal{N} (around $\mathcal{N} = \lambda_0/a$, as illustrated in Fig. 3b). As these states are not eigenstates of the Hamiltonian, they can be reached by some excitation scheme that applies the collective operator Π_k^{\dagger} to the ground state $|G\rangle = |g\rangle_1 \otimes |g\rangle_2 \otimes \dots \otimes |g\rangle_{\mathcal{N}}$. However, in practice this is not a trivial task. In Sec. III C we will show how a combination of a magnetic field gradient together with a pulsed laser excitation could instead be used to perform such an action.

Let us now inspect the Hamiltonian in the analytically solvable case where a nearest neighbor approximation is performed. This is justified as the dipole-dipole interactions scales as $R_{jj'}^{-3}$ for distances smaller than a wavelength and thus the nearest neighbor coupling is almost an order of magnitude larger than that of the next to nearest neighbor one. The resulting Hamiltonian is then in the form of a tridiagonal Toeplitz matrix

$$\mathcal{H} = \omega_0 \sum_j \sigma_j^{\dagger} \sigma_j + \sum_j \Omega (\sigma_j^{\dagger} \sigma_{j+1} + \sigma_{j+1}^{\dagger} \sigma_j), \quad (13)$$

where Ω is the coupling between two neighbors. The free Hamiltonian has degenerate energy levels of degeneracy $C_n^{\mathcal{N}} = \mathcal{N}!/(\mathcal{N} - n)!n!$ for a given level of energy $n\omega_0$ where n ranges from 0 for the ground state to \mathcal{N} for the highest excited state. In the single-excitation manifold characterized by the particle basis $|j\rangle = \sigma_j^{\dagger} |G\rangle$ with $j = 1, \dots, \mathcal{N}$, the Hamiltonian can be diagonalized with resulting eigenvalues

$$\epsilon_k = \omega_0 + 2\Omega \cos \left[\frac{\pi k}{\mathcal{N} + 1} \right], \quad (14)$$

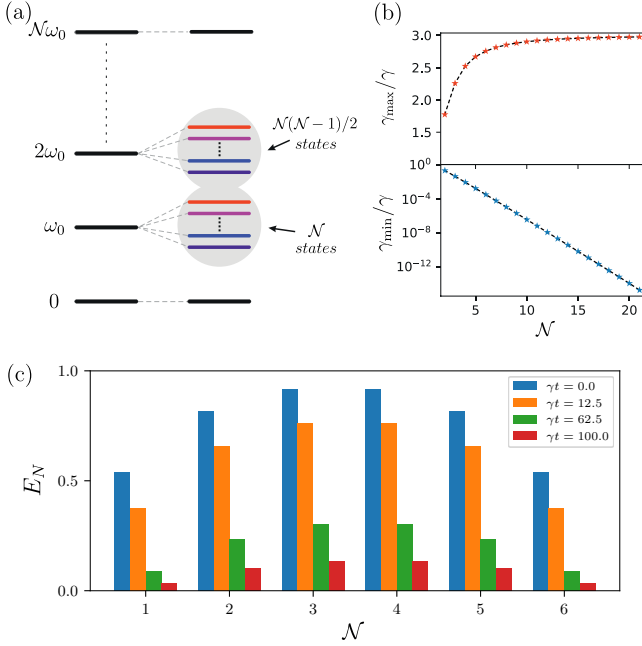


FIG. 3: (a) Energy scheme of the collective N -emitter system. The C_n^N -fold degeneracy of a given n -excitation manifold is lifted by the dipole-dipole interactions and contains states with superradiant (red) and subradiant (blue) character. (b) Decay rates of most superradiant γ_{\max} and most subradiant state γ_{\min} for an equidistant chain with lattice constant $\lambda_0/4$ as a function of N in the single-excitation manifold. The decay rate of the subradiant state shows an exponential scaling with the number of emitters. (c) Entanglement of six-emitter equidistant chain with separation $a = 0.1\lambda_0$ which is initialized in the most subradiant state $|k = N\rangle$. The logarithmic negativity of each emitter with respect to the $N - 1$ other emitters is plotted for different points in time.

for an index k running from 1 to N . The corresponding eigenstates of the Hamiltonian are then described in the collective (exciton) basis

$$|\tilde{k}\rangle = \sum_j \sqrt{\frac{2}{N+1}} \sin\left(\frac{\pi k j}{N+1}\right) |j\rangle = \sum_j f_{jk} |j\rangle. \quad (15)$$

Notice that the reverse transformation is straightforward $|j\rangle = \sum_k f_{jk} |\tilde{k}\rangle$. The transformation also holds at the level of operators $\tilde{\sigma}_k = \sum_j f_{jk} \sigma_j$ which sees the diagonal form of the Hamiltonian as $\mathcal{H} = \sum_k \epsilon_k \tilde{\sigma}_k^\dagger \tilde{\sigma}_k$. In Fig. 3a we illustrate the eigenvalues of the Hamiltonian up to the second excitation manifold. Notice that the energy levels have been color coded to illustrate their subradiant (blue) versus superradiant (red) character. This specific subradiant properties of the lower energy states will be employed in Sec. III C to illustrate a procedure for the generation of robust quantum memories based on collective quantum emitter states. To compute the decay rates of the Hamiltonian eigenstates, we will use the master equation to derive the equation of motion for the population

component $\rho_{kk} = \langle \tilde{k} | \rho | \tilde{k} \rangle$. We arrive at

$$\dot{\rho}_{kk} = -i\epsilon_k \rho_{kk} - \sum_{k'} \left\{ \sum_{jj'} \gamma_{jj'} f_{jk} f_{j'k'} \right\} (\rho_{kk'} + \rho_{k'k}), \quad (16)$$

which shows that the eigenstates of the Hamiltonian couple within the first excitation manifold in addition to the decay to the ground state. The diagonal elements can then be estimated by setting $k = k'$ to derive $\tilde{\gamma}_k = \sum_{jj'} \gamma_{jj'} f_{jk} f_{j'k}$ and more explicitly

$$\tilde{\gamma}_k = \frac{2}{N+1} \sum_{jj'} \gamma_{jj'} \sin\left(\frac{\pi k j}{N+1}\right) \sin\left(\frac{\pi k j'}{N+1}\right). \quad (17)$$

From this expression, one can derive a scaling of subradiant states with roughly N^{-3} which will be utilized for cavity antiresonance spectroscopy applications in Sec. IV B. Notice that this scaling with N^{-3} for $\tilde{\gamma}_k$ is weaker than the exponential one as the eigenstates of the Hamiltonian do not correspond to the superpositions obtained by the collective operators Π_k^\dagger applied to the ground state. More generally, as shown in Ref. [14], scalings with N^{-s} in between the N^{-3} obtained by direct diagonalization of the Hamiltonian and the exponential one obtained by diagonalization of the collective Lindblad term can be obtained, in particular $s = 5$ in Ref. [14].

The collective eigenstates of the dipole-dipole Hamiltonian (both super- and subradiant ones) commonly feature high degrees of entanglement [52, 53] rendering them as an interesting resource for quantum information processing; highly subradiant states are of course even more useful due to the increased lifetime of correlations. Even if two-pair quantum correlations are only moderate, the overall entanglement can be large as each individual emitter is highly entangled with all the other emitters. To this end we analyze the logarithmic negativity [54], which is an entanglement monotone. For a bipartite system consisting of the subsystems A and B , it is defined as

$$E_N(\rho) = \log_2 (|\rho^{T_A}|), \quad (18)$$

where ρ^{T_A} denotes the partial transpose with respect to the subsystem A and $|\cdot|$ is the tracenorm. In Fig. 3c, we show the time evolution of the state with $k = N$. At distinct time points, we compute the logarithmic negativity for each emitter (i.e., we choose our bipartite system to consist of the i th emitter and the rest of the chain). One can see, that the amount of bipartite entanglement is significantly larger in the center of the chain, even in the initial state. Over time, this behavior is retained and correlation is only slowly lost due to excitation loss of the chain. Even at $t = 100\gamma^{-1}$ there still is considerable entanglement in the system.

C. Dicke superradiance

Let us now go beyond the single-excitation manifold and consider a famous example introduced by Dicke [25] which shows the generation of a superradiant pulse from an ensemble of indistinguishable quantum emitters. The model assumes an idealized case of \mathcal{N} quantum emitters within a very small volume and neglects their dipole-dipole interactions. While this is an unrealistic assumption, we will indicate later in Sec. II E how such a model is relevant for the physics of lasing in what is known as bad (lossy) cavity superradiant lasers [27].

In the following we will make use of the Bloch sphere illustration in Fig. 4a, where \mathcal{N} two-level systems can be described by a collective spin of length $\mathcal{N}/2$. This follows from $1/2 \otimes 1/2 \otimes \dots \otimes 1/2 = 0 \oplus 1 \oplus \dots \oplus \mathcal{N}/2$ for \mathcal{N} even and $1/2 \otimes 1/2 \otimes \dots \otimes 1/2 = 1/2 \oplus 3/2 \oplus \dots \oplus \mathcal{N}/2$ for \mathcal{N} odd (the tensor product space of dimensions $2^{\mathcal{N}}$ of \mathcal{N} spins $1/2$ can be written as a direct sum of spaces of different sizes). We can then introduce collective spin operators $S_z = \sum_j \sigma_j^z/2$ and $S = \sum_j \sigma_j$ and the total spin $\mathbf{S}^2 = S_z^2 + (S^\dagger S + S S^\dagger)/2$. As in the standard angular momentum algebra, it is then possible to find a collective basis, known as the *Dicke basis* of \mathbf{S}^2 and S_z , indexed by two quantum numbers $|s, m_s\rangle$

$$\mathbf{S}^2 |s, m_s\rangle = s(s+1) |s, m_s\rangle, \quad (19a)$$

$$S_z |s, m_s\rangle = m_s |s, m_s\rangle. \quad (19b)$$

The spin quantum number s can take either integer or half-integer values and is bounded by $0, 1/2 \leq s \leq \mathcal{N}/2$ where the zero holds for even and the $1/2$ holds for odd values of \mathcal{N} . The so-called inversion quantum number m_s which measures the projection of the collective spin onto the z -axis can take values from $-s \leq m_s \leq s$ and equals $-\mathcal{N}/2$ in the ground state $|G\rangle = |g\rangle^{\otimes \mathcal{N}}$ and $\mathcal{N}/2$ in the fully excited state $|E\rangle = |e\rangle^{\otimes \mathcal{N}}$. The ladder operators S and S^\dagger act on the Dicke states as

$$S^\dagger |s, m_s\rangle = \sqrt{(s-m_s)(s+m_s+1)} |s, m_s+1\rangle, \quad (20a)$$

$$S |s, m_s\rangle = \sqrt{(s+m_s)(s-m_s+1)} |s, m_s-1\rangle. \quad (20b)$$

In a closed system interacting with the electromagnetic field, the interactions are mediated by S and S^\dagger . Thereby the selection rules for optical transitions are given by $\Delta m_s = \pm 1$, $\Delta s = 0$ and the Hilbert space splits into non-interacting subspaces defined by the quantum number s with dimension $2s+1$ (illustrated in Fig. 4a).

Let us now describe the phenomenon of Dicke superradiance in the ideal case where all mutual decay rates are equal and maximal $\gamma_{jj'} = \gamma$. A trivial observation is now that the Lindblad decay term assumes a very simple form with a single superradiant decay channel and collective collapse operator

$$\mathcal{L}_e[\rho] = \gamma [2S\rho S^\dagger - S^\dagger S\rho - \rho S^\dagger S]. \quad (21)$$

We will follow the time evolution under such a Lindblad term for an initially fully excited ensemble characterized

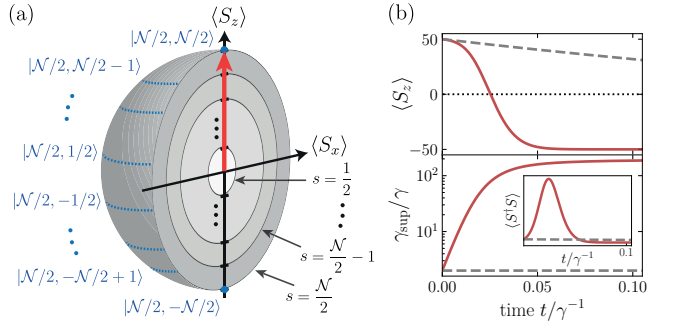


FIG. 4: (a) Cross section of collective \mathcal{N} -emitter Bloch sphere (for an odd number of spins) showing an onion-like structure with Bloch vector (red) pointing towards the north pole representing the fully excited state $|E\rangle$. The lines of latitude (blue dotted lines) correspond to the $|\mathcal{N}/2, m_{\mathcal{N}/2}\rangle$ states. (b) Dicke superradiance for $\mathcal{N} = 100$ emitters initialized in the fully excited state $|E\rangle$: Top shows time dynamics of $\langle S_z \rangle$ while bottom shows the normalized decay rate $\gamma_{\text{sup}} = -\partial_t \langle S_z \rangle / (\langle S_z \rangle + \mathcal{N}/2)$. The inset shows the time evolution of $\langle S^\dagger S \rangle$ with superradiant ‘burst’ reaching a maximum when $\langle S_z \rangle = m_s$ reaches zero. The dashed grey lines show the result for pure exponential decay of independent, uncoupled emitters.

by the state vector $|\mathcal{N}/2, \mathcal{N}/2\rangle$. Notice that the action of the collapse operator cannot take the system out of the $s = \mathcal{N}/2$ symmetric manifold containing $\mathcal{N} + 1$ Dicke states. We can derive an equation of motion for the population difference operator average $\langle \dot{S}_z \rangle = -2\gamma \langle S^\dagger S \rangle$ which simply states that the loss rate is proportional to the emitted intensity. For a single quantum emitter one has $\langle \sigma^\dagger \sigma \rangle = \langle \sigma_z \rangle + 1/2$, implying that the spontaneous emission always follows an exponential law. The population difference of a collective Dicke state $|s, m_s\rangle$ decays instead at a state-dependent rate $2\gamma \langle S^\dagger S \rangle = 2\gamma(s + m_s)(s - m_s + 1)$. For the initially fully excited state, the decay rate is $2\gamma\mathcal{N}$ which is the same as expected for \mathcal{N} independently decaying emitters. However, particle-particle correlations start building up during the evolution and by the time the $|\mathcal{N}/2, 0\rangle$ state (for even \mathcal{N}) is reached, the emission is superradiant and scales approximately as $\gamma\mathcal{N}^2/2$ (see Fig. 4b). Notice that the crucial effect of correlations can be distinguished by rewriting $\langle S^\dagger S \rangle = \langle \sum_i \sigma_i^\dagger \sigma_i \rangle + \langle \sum_{i \neq j} \sigma_i^\dagger \sigma_j \rangle$. Using that the sum over populations is given by $\langle \sum_i \sigma_i^\dagger \sigma_i \rangle = s + m_s$, the dipole-dipole correlation between particles i and j can be estimated as $\langle \sigma_i^\dagger \sigma_j \rangle = (s^2 - m_s^2) / (\mathcal{N}(\mathcal{N} - 1))$, reaching a maximum of approximately $1/4$ for $m_s = 0$ and becoming zero for $m_s = \pm s$.

D. Cooperative cavity QED

An observation can be immediately made on the scaling of the zero-point electric field amplitude \mathcal{E}_k with \mathcal{V}^{-1} : stronger fields per photon mode are achieved for smaller

mode volumes. A celebrated example of such a platform exhibiting stronger light-matter interactions is the co-planar cavity design known as a Fabry-Perot cavity comprised of two highly reflective parallel mirrors. For a distance ℓ between the mirrors, such a setup defines resonances conditioned by $\ell = n\lambda/2$. The fundamental mode has therefore a wavelength of 2ℓ with frequency $\omega = \pi c/\ell$ and higher harmonics are multiples of this mode. The quantity $\omega_{\text{FSR}} = \pi c/\ell$ is known as the free spectral range and gives the frequency difference between consecutive optical resonances of the structure. Assuming two mirrors positioned at $z = 0$ and $z = \ell$ and a transverse area \mathcal{S} of the supported optical resonances, one can proceed in quantizing the field inside the optical resonator by associating bosonic operators a_n to all resonances and writing the total Hamiltonian as $\mathcal{H}_c = \sum_n \omega_n a_n^\dagger a_n$. The electric field operator can then be decomposed as

$$\hat{\mathbf{E}}(z) = \sum_n \mathcal{E}_n (a_n + a_n^\dagger) \sin(k_n z) \epsilon_n, \quad (22)$$

where the sum runs over all allowed wavevectors $k_n = n\pi/\ell$ and the zero-point electric field amplitude $\mathcal{E}_n = \sqrt{\omega_n/(2\epsilon_0\ell\mathcal{S})}$ and all polarizations ϵ_n are assumed orthogonal to the z -direction. For all situations we will consider in the following a single cavity mode which suffices to describe the underlying physics so that we will denote the cavity mode simply by a at frequency ω_c .

Perfect mirrors define infinitely sharp resonances; in order to allow the in-coupling of light into the optical resonator side mirrors with slightly less than unit reflectivity are used. For a double-sided optical resonator, the localized resonances can then couple to the infinite number of modes to the left and right of the cavity, leading to a loss of the intracavity excitations. This loss can be described within the master equation formalism. To this end, we follow a phenomenological model where photons from mode a can tunnel to the left $b(\omega)$ and right $c(\omega)$ continuum of free radiation modes via the tunneling Hamiltonian $\mathcal{H}_{\text{int}} = \int d\omega i[V(\omega)b(\omega) + W(\omega)c(\omega)]a^\dagger + \text{h.c.}$. The model assumes an exchange interaction with frequency-dependent rates $V(\omega)$ and $W(\omega)$. One can then exactly follow the procedure utilized in Sec. II A for spontaneous emission by approximating $\rho_{\text{tot}} = \rho \otimes \rho^{(\text{L})} \otimes \rho^{(\text{R})}$ where $\rho^{(\text{L,R})} = |\text{vac}\rangle_{\text{L,R}} \langle \text{vac}|_{\text{L,R}}$. Similarly to Eq. (5) one can now define an operator acting only on the modes outside the cavity

$$\mathcal{F}(t) = \int d\omega [V(\omega)b(\omega) + W(\omega)c(\omega)]e^{-i(\omega-\omega_c)t}. \quad (23)$$

In the next step, a Born-Markov approximation is performed which assumes the tunneling rates as constant around ω_c and sees the definition of effective photon loss rates through the left $\kappa_L = \pi V(\omega_c)^2$ and through the right $\kappa_R = \pi W(\omega_c)^2$ mirrors. Finally, the reduced master equation for the cavity mode can be written in Lindblad form

$$\mathcal{L}_\kappa[\rho] = \kappa [2a\rho a^\dagger - a^\dagger a\rho - \rho a^\dagger a], \quad (24)$$

where $\kappa = \kappa_R + \kappa_L$ encompasses total losses via both mirrors. Imperfect mirrors also allow the driving of the cavity mode. For example, let us now assume driving of the cavity from the left with a continuous wave laser with power \mathcal{P} . This can be included in the following Hamiltonian:

$$\mathcal{H}_\ell = i\eta(a^\dagger e^{-i\omega_\ell t} - a e^{i\omega_\ell t}), \quad (25)$$

where the drive amplitude is $\eta = \sqrt{2\kappa\mathcal{P}/\omega}$. The equation of motion for the expectation value of the cavity operator can be derived from the master equation leading to

$$\langle \dot{a} \rangle = -\kappa \langle a \rangle - i(\omega_c - \omega_\ell) \langle a \rangle + \eta, \quad (26)$$

which in steady state (reached by requiring that $\langle \dot{a} \rangle = 0$) describes an expected Lorentzian response $\langle a \rangle_{\text{ss}} = \eta/(\kappa + i(\omega_c - \omega_\ell))$ of the cavity field with linewidth κ and resonance ω_c .

Let us consider now \mathcal{N} identical quantum emitters (but subject to some frequency disorder) with transition frequencies ω_j and which are placed inside an optical cavity around a single optical mode of interest. For emitter j positioned at z_j within the cavity volume, the dipolar interaction is characterized by a position-dependent coupling strength $g_j = \mathcal{E}_{\text{deg}} \sin(kz_j)$. The light-matter Hamiltonian describing excitation exchange between the emitters and the cavity mode can then be casted in the standard Tavis-Cummings form

$$\mathcal{H}_{\text{TC}} = \sum_{j=1}^{\mathcal{N}} \omega_j \sigma_j^\dagger \sigma_j + \omega_c a^\dagger a + \sum_{j=1}^{\mathcal{N}} (g_j a \sigma_j^\dagger + g_j^* \sigma_j a^\dagger). \quad (27)$$

At the Hamiltonian level, one can already see that the cavity mode only couples to a *bright* superposition defined by the bright operator $\sum_j g_j \sigma_j$ which can lead to effects such as collective strong coupling. In Sec. II F we will see that disordered ensembles can couple this cavity-defined bright mode to the other possible $\mathcal{N} - 1$ *dark* superpositions. In addition, for dense, interacting ensembles one adds to the above Hamiltonian the dipole-dipole interactions \mathcal{H}_{dd} defined in Eq. (10) and the collective decay terms as defined in Eq. (7). Moreover, one can also include a scenario where direct driving of the emitters is included by the following Hamiltonian

$$\bar{\mathcal{H}}_\ell = i \sum_{j=1}^{\mathcal{N}} \bar{\eta}_j (\sigma_j^\dagger e^{-i\bar{\omega}_\ell t} - \sigma_j e^{i\bar{\omega}_\ell t}), \quad (28)$$

where a single laser at frequency $\bar{\omega}_\ell$ illuminates the whole ensemble with individual amplitudes $\bar{\eta}_j$.

From the master equation with Hamiltonian $\mathcal{H}_{\text{TC}} + \mathcal{H}_{dd} + \mathcal{H}_\ell + \bar{\mathcal{H}}_\ell$ and loss rates incorporated in the term $\mathcal{L}_\kappa[\rho] + \mathcal{L}_e[\rho]$ one can now derive equations of motion for the expectation values of both matter and light operators by writing for example $\langle \dot{\sigma}_j \rangle = \text{Tr}[\sigma_j \dot{\rho}]$. The set of coupled equations is not closed, i.e., expectation values of single operators are coupled to two-operator correlations which

again couple to three or more operator correlations and so on. However, in a first approximation one can assume weak driving which ensures that some factorization of operators under the approximation $\langle \sigma_z^j \rangle \approx -1$ can occur. This approximation is sufficient to describe the linear optical response as used throughout Sec. III A. In Sec. II E instead, we will go beyond this approximation to describe population-inverted systems exhibiting lasing behavior.

By denoting the expectation values by $\alpha = \langle a \rangle$ and $\beta_j = \langle \sigma_j \rangle$, one can then derive a solvable set of coupled linear first order differential equations

$$\dot{\alpha} = -(\kappa - i\omega_c)\alpha - i \sum_{j=1}^N g_j \beta_j + \eta e^{-i\omega_\ell t} \quad (29a)$$

$$\dot{\beta}_j = -i\omega_j \beta_j - ig_j \alpha - \sum_{j'=1}^N \mathcal{M}_{jj'} \beta_{j'} + \bar{\eta}_j e^{-i\bar{\omega}_\ell t}, \quad (29b)$$

where the collective effects coming from the coherent and incoherent emitter-emitter interactions are contained in the off-diagonal elements of the matrix $\mathcal{M}_{jj'} = (i\Omega_{jj'} + \gamma_{jj'})$ (while the diagonal elements $\mathcal{M}_{jj} = \gamma_{jj}$ give the independent decay dynamics). The equations above give the linear response of an ensemble of quantum emitters either to direct laser illumination or to illumination via a cavity mode. They are the starting point for example for deriving the optical response of a two-dimensional subwavelength array as shown in Sec. III A (by setting $g_j = 0$ and $\eta = 0$), for quantifying the band structure surface resonances in Sec. III B or for the derivation of a cooperatively enhanced Purcell effect and antiresonance applications in Sec. IV B (by setting $\bar{\eta}_j = 0$). In Sec. II F they will also be particularized to the situation where $\Omega_{jj'} = 0$ and $\gamma_{jj'} = 0$ (for $j \neq j'$) to quantify the effect of inhomogeneous broadening on the coherent emitter-cavity interaction strength. Moreover, to incorporate non-classical properties of light, such as squeezing, we will extend them to the purely quantum regime in Sec. IV A within the quantum Langevin equation approach.

Let us quickly review a few standard concepts of cavity QED with non-interacting ensembles by setting $\bar{\eta}_j = 0$ as well as $\Omega_{jj'} = 0$ and $\gamma_{jj'} = \gamma \delta_{jj'}$. In steady state, the normalized transmission of the cavity $t = \kappa \alpha / \eta$ can be easily computed as

$$t = \kappa \left[\kappa + i(\omega_c - \omega_\ell) + \sum_{j=1}^N \frac{|g_j|^2}{\gamma + i(\omega_j - \omega_\ell)} \right]^{-1}. \quad (30)$$

Depending on the magnitude of the loss rates relative to the coupling strength, one can distinguish between fundamentally distinct regimes. For $N = 1$, diagonalization of Eqs. (29) leads to normal mode splitting when $g > |\kappa - \gamma|/2$ with new frequencies $\omega_{\pm} = \omega_0 \pm \sqrt{g^2 + (\kappa - \gamma)^2/4}$ (on resonance $\omega_0 = \omega_c$). The difference $\omega_+ - \omega_-$ is known as the vacuum Rabi splitting (VRS). The newly formed quantum states in such a strong coupling regime are hybrid light-matter ones,

i.e., polaritons $(|g1\rangle \pm |e0\rangle)/\sqrt{2}$ and can be read in the cavity transmission t as two well-separated peaks. For $N > 1$, the collective strong coupling regime can be defined when $g_N > |\kappa - \gamma|/2$ with a collective coupling rate $g_N = \sqrt{\sum_j |g_j|^2}$. The loss rates of the polaritons are equal in this regime $(\kappa + \gamma)/2$. One can also identify a weak coupling regime for which $\gamma < g_N < \kappa$ but with a strong cooperativity $\mathcal{C}_N = g_N^2 / (\kappa \gamma) \gg 1$. For many emitters equally coupled to the cavity mode, the cooperativity shows a collective enhancement proportional to N . For a single emitter, this regime (known as the Purcell regime) leads to a renormalization of the intrinsic spontaneous emission rate to $\gamma(1 + \mathcal{C})$ understood as the addition of a new decay channel via cavity loss. A scan of t as a function of laser frequency shows in such a case a dip in the cavity transmission around $\omega_\ell = \omega_0$ known as a cavity antiresonance. The case of N coupled emitters will be presented in Sec. IV showing that the addressing of collective subradiant resonances can lead to a superlinear $\propto N^4$ scaling of \mathcal{C}_N .

E. Superradiant lasers

The results and equations derived in the previous two subsections are already sufficient for a basic understanding of the main advantages presented by superradiant lasers (as treated in Refs. [27, 28, 55]). First, we will assume a minimal model for a laser comprised of a cavity containing an incoherently pumped gain medium. Under certain conditions (described by the existence of a pumping threshold) a non-zero intracavity field amplitude can be obtained, which signifies a coherent light output, i.e., lasing. The distinction between the good and bad cavity regimes (behavior quantified by the cavity losses) will then be seen to characterize the difference between standard and superradiant lasers. Finally, we will make the connection between superradiant lasing and superradiance as described by Eq. (21) in Sec. II C by deriving an effective master equation for the gain medium solely.

The minimal model assumes N identical emitters undergoing decay with the standard Lindblad term (as defined in Eq. (8)) \mathcal{L}_γ (and collapse operator σ_i) while additionally incoherently pumped with a Lindblad term \mathcal{L}_{γ_p} (and collapse operator σ_i^\dagger). The pump can for example be realized as illustrated in Fig. 5a by incoherent excitation into an intermediate level $|i\rangle$ followed by fast decay to the lasing level $|e\rangle$. For $\gamma_p > \gamma$ population inversion can be produced, however without exciting the emitter dipoles $\langle \sigma_j \rangle(t) = 0$. To produce a non-zero average dipole moment, which would correspond to the generation of non-thermal light, the coupling to the optical resonator is crucial. From the Hamiltonian in Eq. (27) (with $g_j = g$ and $\omega_0 = \omega_c$) supplemented with the two Lindblad terms (and in terms of collective operators defined in Sec. III C),

we can write the equations of motion:

$$\langle \dot{a} \rangle = -\kappa \langle a \rangle - ig \langle S \rangle, \quad (31a)$$

$$\langle \dot{S} \rangle = -(\gamma + \gamma_p) \langle S \rangle + 2ig \langle a S_z \rangle, \quad (31b)$$

$$\langle \dot{S}_z \rangle = -2(\gamma + \gamma_p) \langle S_z \rangle + ig \langle a^\dagger S - a S^\dagger \rangle + \mathcal{N}(\gamma_p - \gamma). \quad (31c)$$

The above set of equations is generally not solvable. However, an expansion around averages $a = \alpha + \delta a$, $S = s + \delta S$ and $S_z = s_z + \delta S_z$ where all δa , δS and δS_z are zero averaged quantum noise terms, can lead to a simplification. The observation (which one can eventually infer from numerical simulations) is that $\langle \delta a \delta S \rangle \ll \alpha s$ (and similar for all other two-operator correlations) in the limit that \mathcal{N} is large. In such a case, a much simpler set of equations can be obtained for averages

$$\dot{\alpha} = -\kappa \alpha - igs, \quad (32a)$$

$$\dot{s} = -(\gamma + \gamma_p)s + 2ig\alpha s_z, \quad (32b)$$

$$\dot{s}_z = -2(\gamma + \gamma_p)s_z + ig(\alpha^* s - \alpha s^*) + \mathcal{N}(\gamma_p - \gamma). \quad (32c)$$

Let us now assume that a steady state can be reached (by setting all derivatives to zero) in which case the solution of the above equations yields a population difference $s_z = 1/(2\mathcal{C}_p)$, with $\mathcal{C}_p = g^2/[\kappa(\gamma + \gamma_p)]$, the cavity field intensity (photon number)

$$|\alpha|^2 = \frac{1}{\kappa} \left[\frac{\mathcal{N}(\gamma_p - \gamma)}{2} - \frac{\gamma + \gamma_p}{2\mathcal{C}_p} \right], \quad (33)$$

and the dipole coherence $|s|/|\alpha| = \kappa/g$. The expression above is positive only above a lasing threshold (signifying the existence of a lasing steady state), which can be derived by finding the required values for the pumping strength γ_p . Requiring that in the lasing regime one has $|\alpha|^2 > 0$, yields a quadratic equation with upper and lower thresholds given by

$$\gamma_p^\pm = \frac{g^2 \mathcal{N}}{2\kappa} - \gamma \pm \sqrt{\frac{g^2 \mathcal{N}}{\kappa} \left(\frac{g^2 \mathcal{N}}{4\kappa} - 2\gamma \right)}. \quad (34)$$

If $\mathcal{N}g^2/\kappa$ is large compared to γ , the thresholds can be approximated as $\gamma_p^- \approx \gamma$, $\gamma_p^+ \approx \mathcal{N}g^2/\kappa$. Note that the lower threshold corresponds to achieving population inversion while the upper threshold implies that a too large incoherent pumping rate γ_p also prevents the formation of coherence in the system.

While the analysis above is valid in any regime, the great advantage brought on by superradiant lasers is that the coherence is stored in the gain medium which means that the laser linewidth is unaffected by common problems in optical resonators operating at large intracavity powers (such as thermal vibrations of the end mirrors). This can be seen in the ratio $|s|/|\alpha| = \kappa/g$ which indicates that for $\kappa \gg g$ the intracavity field can be negligible while the gain medium coherence is very large [see Figs. 5b,c].

Let us now provide an alternative understanding of the superradiant lasing problem, by connecting to Sec. II C

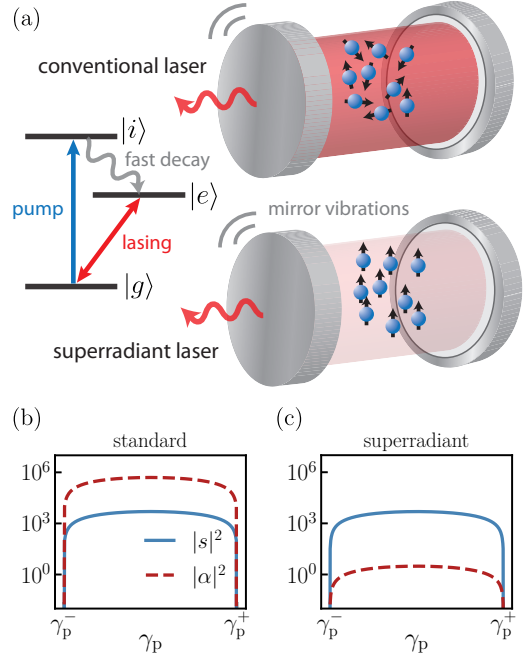


FIG. 5: (a) A gain medium is represented by an incoherently pumped (via intermediate state $|i\rangle$) three-level system with lasing occurring on the $|e\rangle$ - $|g\rangle$ -transition. In a standard laser, stimulated emission produces a large intra-cavity field amplitude exhibiting coherence past threshold. In a superradiant laser, the intra-cavity field amplitude is instead kept small and coherence is stored in the collective atomic dipole thus protecting the laser linewidth from thermal effects. (b) Behavior of intra-cavity photon number $|\alpha|^2$ and coherence $|s|^2$ in the standard, good cavity regime ($\kappa = 0.1g$) and (c) in the superradiant, bad cavity regime ($\kappa = 40g$). Other parameters are $\gamma = 10^{-2}g$ and $\mathcal{N} = 200$. Notice that the upper threshold $\gamma_p^+ \approx \mathcal{N}g^2/\kappa$ is very different in both regimes.

which we do by focusing on sketching the derivation of an effective master equation for the \mathcal{N} emitters in the case of a lossy cavity. We assume at time $t = 0$ the emitters to be fully inverted, while the cavity mode is in the $|\text{vac}\rangle$ vacuum state. We neglect spontaneous emission into free space as the cavity will provide a dominant channel of energy loss by imposing that its decay rate κ is much larger than $g\sqrt{\mathcal{N}}$. The evolution of the system is then described by

$$\dot{\rho}_{\text{tot}}(t) = i [\rho_{\text{tot}}(t), \mathcal{H}] + \mathcal{L}_{\text{cav}}[\rho_{\text{tot}}]. \quad (35)$$

We notice first that the collapse operator a only couples to the total spin ladder operators S and S^\dagger which insures that the dynamics only takes place within the symmetric manifold with maximal spin length $\mathcal{N}/2$. The second observation is that, owing to the quick loss rate κ which is much larger than the coherent light-matter exchange rate $g\sqrt{\mathcal{N}}$, the cavity field is permanently in a very low occupancy state. Therefore we proceed by applying the standard master equation procedure where we assume the crude factorization $\rho_{\text{tot}}(t) = \rho(t) \otimes |\text{vac}\rangle \langle \text{vac}|$ at all

times. The next step is in evaluating two-time correlation terms with the new time-dependent field operator $\mathcal{F} = ga$ (equivalent to the expression in Eq. (5)). The situation is now much simpler than in the free space spontaneous emission case, as one can use the two-time correlations $\langle a(t')a^\dagger(t'') \rangle = e^{-\kappa(t'-t'')}$ to find an effective damping rate g^2/κ . The dynamics can then be reduced to the atomic subspace and incorporated in a master equation

$$\dot{\rho}(t) = i[\rho(t), \mathcal{H}_0] + \mathcal{L}_e^{\text{cav}}[\rho], \quad (36)$$

with $\mathcal{H}_0 = \omega [S_z + (\mathcal{N}/2)\mathbb{1}]$ and the cavity-induced collective spontaneous emission

$$\mathcal{L}_e^{\text{cav}}[\rho] = \frac{g^2}{\kappa} (2S\rho S^\dagger - S^\dagger S\rho - \rho S^\dagger S). \quad (37)$$

The resulting dynamics is of course identical to the one described in Sec. II C showing the emergence of quick bursts of light as superradiant pulses but with a rate established by the cavity g^2/κ . The effect is the spontaneous synchronization of dipoles by the cavity to give rise to the superradiant lasing regime. Here, the lossy cavity acts mainly as a communication bus to drive the synchronization between the atoms and the average photon number inside the cavity is typically well below one. For example Ref. [27] reports the realization of a superradiant laser with an average photon number of less than 0.2 and a single-atom cooperativity $\mathcal{C} = 7.7 \cdot 10^{-3}$. Superradiant lasers have been shown to yield extremely narrow millihertz linewidths and can operate in a steady state regime achieved by continuous repumping of the lasing transition [28].

F. Disorder effects

Let us now address the question of disorder as it plays a great role in ensembles of quantum emitters where coupling to embedding matrices can lead to strong inhomogeneous broadening. Let us quantify frequency disorder by assuming a set of transition frequencies ω_j , inhomogeneously distributed around ω_0 with a distribution function $p(\delta)$ normalized to unity $\int_{-\infty}^{\infty} p(\delta) d\delta = 1$. In particular we choose a Gaussian distribution of frequencies $p(\delta) = (1/\sqrt{2\pi w^2})e^{-\delta^2/(2w^2)}$. We write $\omega_j = \omega_0 + \delta_j$ and have $\langle \delta_j \rangle_{\text{cl}} = 0$ while the variance is $\langle \delta_j^2 \rangle_{\text{cl}} = w^2$. We also restrict in the following the discussion to the case of identical couplings $g_j = g$ (for all j).

For $w = 0$ we note that the cavity couples only to a symmetric superposition $\hat{B} = \sum_j \sigma_j / \sqrt{\mathcal{N}}$, i.e., a *bright state*, with a collective coupling strength $g_{\mathcal{N}} = \sqrt{\mathcal{N}}g$. The other $\mathcal{N}-1$ combinations define *dark states* which are obtainable by a Gram-Schmidt algorithm that leads to all vectors orthogonal to the bright state and to each other. However, a simple choice of coefficients is indicated by a discrete Fourier transform $\hat{D}_k = 1/\sqrt{\mathcal{N}} \sum_{j=1}^{\mathcal{N}} e^{-i2\pi j k / \mathcal{N}} \sigma_j$. We index the dark state manifold for $k = 1, \dots, \mathcal{N}-1$ and note that for $k = \mathcal{N}$ we have $\hat{D}_{\mathcal{N}} = \hat{B}$. The equations of

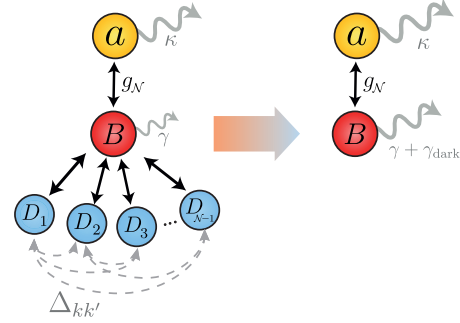


FIG. 6: In the case of disorder, the dark modes are coupled to the bright mode and to each other while the bright mode couples to the cavity mode with rate $g_{\mathcal{N}}$. Elimination of the dark, cavity uncoupled modes then leads to an effective two hybridized mode problem (cavity mode and bright collective state) with renormalized loss rates.

motion for $\mathcal{B} = \langle \hat{B} \rangle$, $\mathcal{D} = \langle \hat{D} \rangle$ and $\alpha = \langle a \rangle$ become (in a frame rotating at ω_0)

$$\dot{\mathcal{D}}_k = -\gamma \mathcal{D}_k - i \sum_{k'=1}^{\mathcal{N}} \Delta_{kk'} \mathcal{D}_{k'} - ig_{\mathcal{N}} \alpha \delta_{kN}, \quad (38a)$$

$$\dot{\alpha} = -(\kappa - i\Delta_c) \alpha - ig_{\mathcal{N}}^* \mathcal{D}_{\mathcal{N}} + \eta, \quad (38b)$$

with the cavity detuning $\Delta_c = \omega_c - \omega_0$ and the couplings between the collective states are defined as $\Delta_{kk'} = 1/\mathcal{N} \sum_{j=1}^{\mathcal{N}} \delta_j e^{-i2\pi j(k-k')/\mathcal{N}}$. For $k = \mathcal{N}$, the equations above indicate that the bright state couples to the cavity mode with the standard $g_{\mathcal{N}}$ rate, while also being coupled to all dark states.

Non-Markovian regime - We proceed (see Fig. 6) to eliminate the dark state manifold in an exact way without making a Markovian approximation (which would imply that the dark state reservoir has no memory and therefore it would allow to set all derivatives of \mathcal{D}_k to zero). Instead, we formally integrate the equations for \mathcal{D}_k to obtain

$$\dot{\mathcal{B}}(t) = -(\gamma + i\bar{\delta}) \mathcal{B}(t) - \int_{-\infty}^{\infty} dt' f(t-t') \mathcal{B}(t') - ig_{\mathcal{N}} \alpha, \quad (39)$$

where the memory kernel generally describes a non-Markovian loss process. In the mesoscopic limit $\mathcal{N} \rightarrow \infty$, one finds

$$f(t-t') \approx \Theta(t-t') w^2 e^{-i(\bar{\delta} - i\gamma)(t-t')} \text{sinc}(2w(t-t')). \quad (40)$$

This now allows to identify the Markovian regime discussed in the next paragraph, where the condition that the disorder $w \gg \gamma$ implies that the kernel $f(t-t')$ tends towards a delta function.

Markovian limit - In the Markovian limit, the elimination of the dark state manifold is straightforward as all the derivatives \mathcal{D}_k for $k \neq \mathcal{N}$ can be set to zero. This

means $\mathcal{D}_k = -\sum_{k'}(\mathcal{A}^{-1})_{kk'}\Delta_{k'N}\mathcal{B}$ with the matrix

$$\mathcal{A} = \begin{pmatrix} (\bar{\delta} - i\gamma) & \Delta_{12} & \dots & \Delta_{1(N-1)} \\ \Delta_{21} & (\bar{\delta} - i\gamma) & \dots & \Delta_{2(N-1)} \\ \vdots & \vdots & \ddots & \vdots \\ \Delta_{(N-1)1} & \Delta_{(N-1)2} & \dots & (\bar{\delta} - i\gamma) \end{pmatrix}, \quad (41)$$

and $\bar{\delta} = \Delta_{kk} = \sum_{j=1}^N \delta_j/N$. The Markovian kernel is explicitly $f(t-t') = (i\delta_{\text{dark}} + \gamma_{\text{dark}})\delta(t-t')$, containing an effective frequency shift δ_{dark} and a loss rate γ_{dark} derived from $\delta_{\text{dark}} + i\gamma_{\text{dark}} = \sum_{k,k'=1}^{N-1} \Delta_{Nk}(\mathcal{A}^{-1})_{kk'}\Delta_{k'N}$. In the mesoscopic limit, one can further simplify the expression of the loss rate and derive scaling laws where $\gamma_{\text{dark}} = w^2/\gamma$ for $\gamma \gg w$ and $\gamma_{\text{dark}} = \pi w/4$ for $w \gg \gamma$. Moreover, both $\bar{\delta}$ and δ_{dark} vanish in this regime. The dependence of the VRS on disorder can then be obtained by diagonalizing the dynamics in the reduced cavity-bright state subspace

$$\text{VRS} \approx \Im \left\{ 2\sqrt{(\gamma + \gamma_{\text{dark}} - \kappa)^2/4 - g_N^2} \right\}. \quad (42)$$

The expression above shows that a large degree of disorder (on the order of κ) can lead to a strong reduction of the VRS and consequently pull the system out of the collective strong coupling regime. In Ref. [56] a more detailed derivation is provided that shows that particles which have a large detuning with respect to the cavity frequency, or a very lossy behavior are effectively pulled out of the macroscopic superposition participating in the strong coupling condition. This in turn leads to the degradation of the VRS described by the equation above.

III. SUBWAVELENGTH QUANTUM EMITTER ARRAYS

The interplay between dipole-dipole interactions and subradiance in quantum emitter ensembles leads to a multitude of applications of one- and two-dimensional subwavelength arrays such as in nonlinear quantum optics [20], nano-optomechanics [17], the design of quantum metamaterials with magnetic response at optical frequencies [57, 58], as platforms for quantum information processing [12, 13, 59] or as chiral light-matter interfaces [60]. These applications are based on the fact that such structures can support collective surface resonances that interact in a controllable fashion with impinging fields.

We will first apply the formalism from Sec. II D to derive the optical response of two dimensional subwavelength arrays around certain confined surface mode resonances [61–63] and describe a regime recently experimentally tackled showing close to unity reflectivity for arrays of optically trapped atoms [15]. Within the same formalism, but with the additional application of a Bloch ansatz, we then study the dispersion relations of the surface modes on platforms as depicted in Fig. 7a showing the occurrence of bandgaps and Dirac points. This direction has recently

emerged showing the promise of subwavelength arrays for topological quantum optics implementations [4, 5].

We finally provide illustrations on emitter chains and rings aimed at showing the usefulness of subradiance as a resource for: i) improved frequency sensitivity (as shown in Refs. [10, 64]), ii) robust quantum memories [52] and iii) the design on nanoscale coherent light sources as recently proposed in Ref. [65].

A. Optical response of two-dimensional arrays

We will consider the situation depicted in Figs. 7a,b where the two-dimensional periodic array of quantum emitters is positioned in the x - y plane. To derive the linear optical response of such a structure, we will make use of Eqs. (29) (without the cavity mode so that $g_j = 0$) where the excitation is in the form of a plane wave with wavenumber k_0 impinging at normal incidence, along the z -axis.

The electric field (source field) at some position \mathbf{r} emitted by a collection of emitters, each located at \mathbf{r}_j , takes the following expression in the far field limit [19, 62]

$$\mathcal{E}_{\text{dip}}(\mathbf{r}, t) = -\frac{3\gamma}{2d_{\text{eg}}} \sum_j \beta_j(t) \left(\frac{e^{ik_0|\mathbf{r}-\mathbf{r}_j|}}{k_0|\mathbf{r}-\mathbf{r}_j|} \right). \quad (43)$$

The total amplitude is given by the sum of dipole radiated fields, which, in the linear regime, are proportional to the expectation value of the individual particle dipole operators β_j . We will aim at describing the response only in the z -direction: the total field can then be written as the sum of the incident field and the field radiated by the emitters

$$\mathcal{E}(z) = \mathcal{E}_{\text{in}} e^{ik_0 z} + \mathcal{E}_{\text{dip}}(z). \quad (44)$$

Let us first look at the single emitter case where the radiated field is a dipole pattern with the z -direction amplitude

$$\mathcal{E}(z) = \mathcal{E}_{\text{in}} \left[e^{ik_0 z} + \frac{\alpha\pi}{\epsilon_0\lambda_0^2} \frac{e^{ik_0|z|}}{|z|} \right], \quad (45)$$

falling off with increasing distance z . We have introduced the single-atom polarizability $\alpha = d_{\text{eg}}\beta/\mathcal{E}_{\text{in}}$ which can be expressed in terms of the wavelength, linewidth and detuning $\Delta = \bar{\omega}_\ell - \omega_0$ as $\alpha = -(3\epsilon_0\lambda_0^3)/(4\pi^2)\gamma/(\Delta + i\gamma)$. The extinction cross section of a quantum emitter σ_{ext} (i.e., the effective area seen by an impinging photon) can be related to the polarizability via $\sigma_{\text{ext}}(\Delta) = k_0 \Im(\alpha)/\epsilon_0$ which in the case of resonant illumination simply becomes $\sigma_{\text{ext}}(0) = 3\lambda_0^2/(2\pi)$. Notice the interesting aspect that the cross section is much larger (proportional to λ_0^2) than the square of the actual size of the electronic orbital which can be a million times smaller.

For a collection of periodically arranged dipoles, under the assumption that the array is quasi-infinite and that one only looks in the far field, the outgoing field is roughly

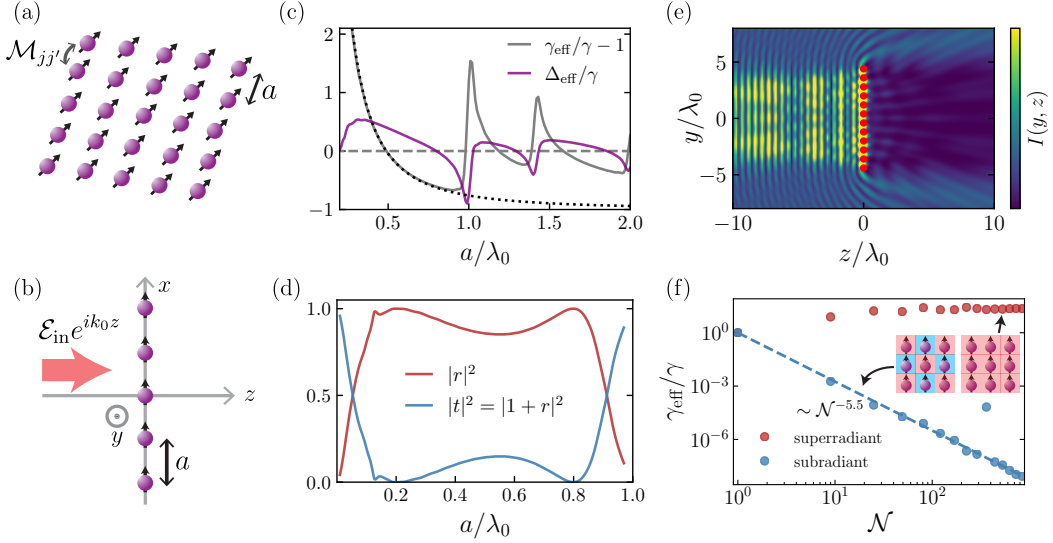


FIG. 7: (a) A two-dimensional quantum emitter array illustrated as a regular pattern of near-field coupled dipoles with lattice constant a . (b) The array is placed in the x - y plane and is illuminated by a plane wave with wavenumber k_0 . (c) Effective decay rate γ_{eff} and frequency shift Δ_{eff} of an array consisting of 20×20 atoms as a function of a/λ_0 . The dotted black curve shows the approximation $\gamma_{\text{eff}} = \gamma \frac{3}{4\pi} (\lambda_0/a)^2$ valid for lattice constants $a < \lambda_0$. (d) Reflection $|r|^2$ and transmission coefficient $|t|^2$ for the same array as a function of the lattice constant a (for resonant illumination of the emitters). (e) Calculated intensity profile $I(y, z)$ (in arbitrary units) in the y - z plane for an array of 12×12 atoms (indicated by red dots) with lattice constant $a = 0.8\lambda_0$ which is resonantly illuminated by a plane wave. (f) Targeted addressing of super- and subradiant states of a 2D array with $a = 0.1\lambda_0$ as a function of the number of emitters in the array \mathcal{N} . As indicated in the inset, subradiant states are targeted by illumination with antisymmetric phases $f_j = (-1)^j$ in a checkerboard pattern while superradiant states are obtained from uniform illumination. The effective decay rate of the subradiant states scales proportional to $\mathcal{N}^{-5.5}$ as shown by the dashed line. Note that here we always matched the detuning of the incident field to the collective resonance of the array $\bar{\omega}_\ell - \omega_0 = \Delta_{\text{eff}}$.

a plane wave. In the case of *constant, or symmetric illumination*, where the phase and amplitude of the incident field are the same at the position of each dipole we use

$$\dot{\beta}_j = -i\omega_0\beta_j - \sum_{j'=1}^N \mathcal{M}_{jj'}\beta_{j'} - i\eta e^{-i\bar{\omega}_\ell t}, \quad (46)$$

which are obtained from the more general Eqs. (29) in the absence of a cavity field and with the particular choice that $\omega_j = \omega_0$ and $\bar{\eta}_j \rightarrow -i\eta$ (corresponds to driving with $\eta(\sigma_j^\dagger + \sigma_j)$ and Rabi frequency $\eta = d_{\text{eg}}\mathcal{E}_{\text{in}}$). One can observe that a simplification arises as each dipole will respond the same and the average expectation value $\beta_j = \beta$ can be easily estimated from the equation above. The sum over the spatial distribution along the z -direction can be estimated by a plane wave expansion as (assuming an infinite 2D array of dipoles)

$$\begin{aligned} \sum_j \frac{e^{ik_0|z\mathbf{e}_z - \mathbf{r}_j|}}{|\mathbf{z}\mathbf{e}_z - \mathbf{r}_j|} &= \sum_{m,n=-\infty}^{\infty} \frac{e^{ik_0\sqrt{(ma)^2 + (na)^2 + z^2}}}{\sqrt{(ma)^2 + (na)^2 + z^2}} \\ &= \frac{2\pi i}{a^2} \sum_{m,n=-\infty}^{\infty} \frac{e^{ik_{mn}|z|}}{k_{mn}}, \end{aligned} \quad (47)$$

where $k_{mn} = \sqrt{k_0^2 - (2\pi m/a)^2 - (2\pi n/a)^2}$ is real if $(a/\lambda_0)^2 \geq m^2 + n^2$. For a subwavelength lattice, this

can then only be fulfilled by $m, n = 0$ while all other contributions describe evanescent waves which do not propagate into the far field. One can finally express the source field radiated by the dipoles in the far field limit as

$$\mathcal{E}_{\text{dip}}(z) = i\pi \left(\frac{\lambda_0}{a} \right)^2 \frac{\alpha_{\text{eff}}}{\epsilon_0 \lambda_0^3} \mathcal{E}_{\text{in}} e^{ik_0|z|}, \quad (48)$$

with a renormalized effective polarizability as opposed to the single emitter case $\alpha_{\text{eff}} = d_{\text{eg}} \sum_j \beta_j / (\mathcal{N} \mathcal{E}_{\text{in}})$ expressed as

$$\alpha_{\text{eff}} = -\frac{3\epsilon_0\lambda_0^3}{4\pi^2} \frac{\gamma}{\Delta - \Delta_{\text{eff}} + i\gamma_{\text{eff}}}. \quad (49)$$

The cooperative decay rates and frequency shifts γ_{eff} , Δ_{eff} are computed as real and imaginary parts of the inverse of the sum over all elements of the inverse interaction matrix $\mathcal{M}_{jj'}^{-1}$

$$\gamma_{\text{eff}} + i\Delta_{\text{eff}} = \frac{\mathcal{N}}{\sum_{jj'} \mathcal{M}_{jj'}^{-1}}. \quad (50)$$

We illustrate in Fig. 7c the behavior of these collective rates as a function of the lattice constant a . We note that similarly to the two-particle interactions discussed in Sec. II A, the real and imaginary parts are not independent

but can be connected by a Kramers-Kronig relation. Regions with $\gamma_{\text{eff}} < \gamma$ (negative values in Fig. 7c) correspond to collective subradiant behavior and are of particular interest. One can see that a special operation point occurs e.g. at $a/\lambda_0 \approx 0.8$ where the collective frequency shift vanishes while a pronounced subradiant behavior remains, facilitating the experimental realization of subradiant optical mirrors with cold atoms in an optical lattice [15].

Notice that the effective cross section per emitter can be considerably increased as, on resonance, one has $\sigma_{\text{ext}}^{\text{eff}}(0) = \sigma_{\text{ext}}(0)/\gamma/\gamma_{\text{eff}}$. For $a < \lambda_0$ one can furthermore approximate the effective decay rate $\gamma_{\text{eff}} = 3\gamma(\lambda_0/a)^2/(4\pi)$ [see Fig. 7c] showing a decrease by a factor of roughly 2.68 around the optimal operation point at $a/\lambda_0 \approx 0.8$. This can also be connected to an increase in the overall reflectivity of the array. To derive this, we write $\mathcal{E}_{\text{dip}}(z) = r\mathcal{E}_{\text{in}}e^{ik_0|z|}$ where the complex amplitude reflectivity reads

$$r = -i \frac{\gamma_{\text{eff}}}{(\bar{\omega}_\ell - \omega_{\text{eff}}) + i\gamma_{\text{eff}}}, \quad (51)$$

while the transmission is obtained as $t = 1 + r$ and we defined the frequency of the collective mirror resonance as $\omega_{\text{eff}} = \omega_0 + \Delta_{\text{eff}}$. In Fig. 7d we plot the absolute square of these quantities as a function of the lattice constant. One can see that, while generally the reflectivity of the array is high over a broad range of separations, for certain values of $a/\lambda_0 \approx (0.2, 0.8)$ the atomic dipoles can even act as a perfect mirror and reflect the entire input field with unit efficiency [62]. Moreover, for the whole region where the approximation $\gamma_{\text{eff}} = 3\gamma(\lambda_0/a)^2/(4\pi)$ holds, the mirror shows no losses (quantified by the scattering outside the z -axis mode), i.e., $|r|^2 + |t|^2 = 1$. This is of course only valid in the absence of any other channels of non-radiative decay (at rate γ_{nr}), in which case the denominator of r acquires an extra term $i(\gamma_{\text{eff}} + \gamma_{\text{nr}})$. The resulting intensity distribution of the total electric field is shown in Fig. 7(e), revealing that the emitters can indeed shut off the transmission of an incident plane wave for $z > 0$.

Notice that the expressions above are only valid under *symmetric illumination* conditions, which is the typically relevant and achievable experimental situation. The gain in reflectivity then arises only around some optimal operation point and it is not scalable as it maximally reaches an enhancement factor of around $4\pi \times 0.8^2/3 \approx 2.68$ at $a = 0.8\lambda_0$. To fully exploit the scalability of subradiance with \mathcal{N} , one could instead assume *antisymmetric, or phased* illumination conditions. For example, Fig. 7f shows that extremely narrow resonances scaling as $\mathcal{N}^{-5.5}$ can be reached for very dense arrays at $a = 0.1\lambda_0$ with asymmetric phases in a checkerboard pattern where $f_j = (-1)^j$ (deviations from the scaling are due to imperfect addressing of subradiant states). In such a case, one needs to first compute the expectation values of $\langle \sigma_j \rangle = \langle \sigma \rangle f_j$ (where f_j is the assumed excitation phase pattern) and recompute the dipole field in Eq. (43) by reestimating the spatial sum.

B. Towards topological quantum optics

Up to this point, we have solved for collective resonances and their associated collective radiation rates by a direct diagonalization of the Hamiltonian with near-field coupling terms. One can however take a solid state approach where the array provides a crystalline structure for the quasi-excitations propagating on its surface. As the simplest example, let us first revisit the one-dimensional equidistant chain of \mathcal{N} emitters with identical frequencies as already discussed in Sec. II B described by the Hamiltonian

$$\mathcal{H} = \omega_0 \sum_j \sigma_j^\dagger \sigma_j + \sum_{j' \neq j} \Omega_{jj'} \sigma_j^\dagger \sigma_{j'}. \quad (52)$$

We first assume nearest neighbor (NN) coupling $\Omega_{jj'} = \Omega \delta_{jj'}$ which insures translational symmetry with periodicity a (equivalently stated, the unit cell contains one site only). We impose *periodic boundary conditions* (PBC) to simulate the mesoscopic case by asking that at the edge $\Omega_{1\mathcal{N}} = \Omega$. We then ask the question: what kind of excitations can propagate in this chain, i.e., what kind of dispersion relations such excitations will exhibit. To this end, we start with the equations of motion for the expectation values $\beta_j = \langle \sigma_j \rangle$

$$\dot{\beta}_j = -i\omega_0 \beta_j - i\Omega \beta_{j-1} - i\Omega \beta_{j+1}. \quad (53)$$

In a compact matrix formulation, we rewrite $\dot{\mathbf{v}} = M\mathbf{v}$ where $\mathbf{v} = (\beta_1, \dots, \beta_{\mathcal{N}})^\top$ and the drift matrix is expressed as a circulant Toeplitz matrix

$$M = -i \begin{pmatrix} \omega_0 & \Omega & 0 & \dots & 0 & \Omega \\ \Omega & \omega_0 & \Omega & \dots & 0 & 0 \\ 0 & \Omega & \omega_0 & \dots & 0 & 0 \\ \vdots & \vdots & \vdots & \ddots & \vdots & \vdots \\ 0 & 0 & 0 & \dots & \omega_0 & \Omega \\ \Omega & 0 & 0 & \dots & \Omega & \omega_0 \end{pmatrix}. \quad (54)$$

The direct diagonalization of the matrix above gives the expected \mathcal{N} collective modes listed in Sec. II B with a state index from 1 to \mathcal{N} . However, we now instead will be looking for a dispersion relationship with a quasi-momentum q , to which end we plug the ansatz $\beta_j = A_q e^{i(qaj - \omega t)}$ into Eq. (53) which straightforwardly leads to the following dispersion relation

$$\omega(q) = \omega_0 + 2\Omega \cos(qa). \quad (55)$$

From the application of the PBCs we have $\beta_1 = \beta_{\mathcal{N}+1}$ which leads to $qa\mathcal{N} = 2\pi m$ where m is an integer. This indicates that the allowed quasimomenta are $q = 2\pi m/(\mathcal{N}a)$ and we can fix the first Brillouin zone to $m \in \{-\mathcal{N}/2, \mathcal{N}/2\}$ corresponding to q from $-\pi/a$ (left propagating wave) to π/a (right propagating wave). The

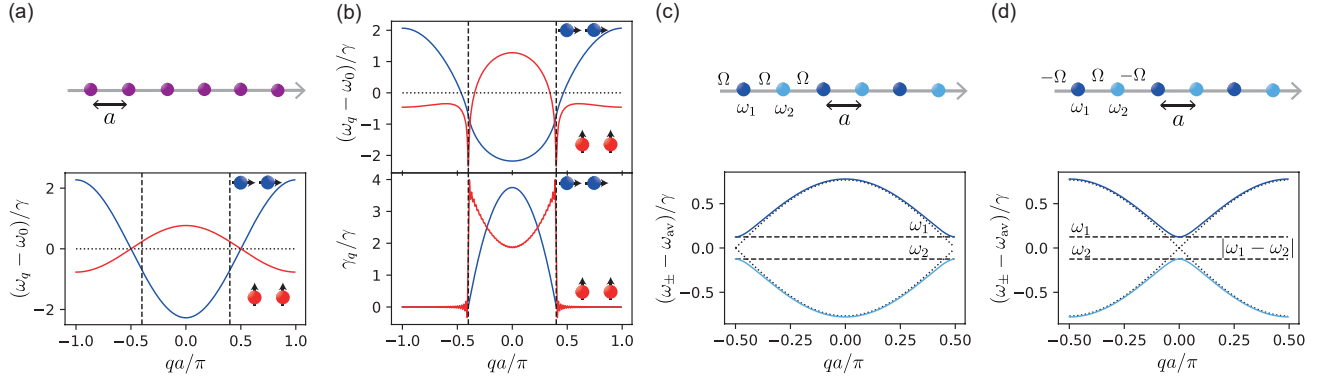


FIG. 8: (a) Energy band structure for a simplified model of a chain of identical emitters with nearest neighbor coupling only for two different alignments of dipoles (perpendicular and parallel to the chain). (b) Top: Band structure considering the exact expression of near-field coupling and in the presence of collective radiative decay. Bottom: Corresponding decay rate as a function of the quasi momentum q . The light cone characterized by $\omega = c|q|$, here plotted at the two level resonance $\omega_0 = ck_0$ is indicated by the dashed black lines. Parameters are $a/\lambda_0 = 0.2$ with $N = 200$ as in [8]. (c) Bandstructure for a chain of equidistant emitters harboring two different species alternately arranged. (d) Additionally, when the interaction between the emitters has an alternating sign, we obtain a Dirac cone at $q = 0$ (for the case of degenerate frequencies $\omega_1 = \omega_2$).

resulting dispersion relations for two arrangements of dipoles (parallel and perpendicular to the chain axis) are indicated in Fig. 8a.

Beyond NN with dissipation - The results presented above describe a simplified model where only nearest neighbor interactions are employed and spontaneous emission is disregarded. The analysis of the full equation of motion including dissipation

$$\dot{\beta}_j = -i(\omega_0 - i\gamma)\beta_j - \sum_{j' \neq j} (i\Omega_{jj'} + \gamma_{jj'})\beta_{j'}, \quad (56)$$

that takes into account the exact behavior of $\Omega_{jj'}$, $\gamma_{jj'}$ (as defined in Sec. II A) shows the following dispersion relation for a one dimensional chain

$$\omega(q) + i\gamma(q) = \omega_0 - i\gamma + \sum_{k \neq j} (\Omega_{jk} - i\gamma_{jk}) e^{iqa(k-j)}, \quad (57)$$

which includes the collective dissipation aspects as well. The result is illustrated in Fig. 8b and compared with the approximation analytically obtained for NN coupling in Fig. 8a. The corresponding collective decay is plotted in the lower panel of Fig. 8b, which characterizes mostly subradiant states towards the edge of the Brillouin zone and indicates mostly superradiance for states of small quasi-momentum (in accordance to results presented in Ref. [8]).

Emerging bandgaps - Let us now consider a slightly more complex structure with alternating emitter frequencies ω_1 and ω_2 and identical NN couplings at rate Ω (as illustrated in Fig. 8c). One then immediately notices that this implies a lattice with a double unit cell. We denote the two types of emitters as $(\beta_j^{(1)}, \beta_j^{(2)})$ where the j index now goes from 1 to $N/2$ (such that we keep the chain

length at Na). The dipole-dipole interaction now couples the two kind of emitters with each other within the unit cell and also between neighboring unit cells

$$\dot{\beta}_j^{(1)} = -i\omega_1\beta_j^{(1)} - i\Omega\beta_{j-1}^{(2)} - i\Omega\beta_j^{(2)}, \quad (58a)$$

$$\dot{\beta}_j^{(2)} = -i\omega_2\beta_j^{(2)} - i\Omega\beta_{j+1}^{(1)} - i\Omega\beta_j^{(1)}. \quad (58b)$$

We now ask for propagating waves with the following profile $\beta_j^{(1)} = A_q e^{i(2qa_j - \omega t)}$ and $\beta_j^{(2)} = B_q e^{i(2qa_j - \omega t)}$ and plug in this ansatz into the above equation to result in the following eigenvalue problem

$$\begin{pmatrix} \omega_1 - \omega(q) & \Omega(1 + e^{-i2qa}) \\ \Omega(1 + e^{i2qa}) & \omega_2 - \omega(q) \end{pmatrix} \begin{pmatrix} A_q \\ B_q \end{pmatrix} = 0. \quad (59)$$

Two types of eigenvalues $\omega_{\pm}(q)$ result from diagonalization of the above matrix corresponding to two distinct energy bands

$$\omega_{\pm}(q) = \frac{\omega_1 + \omega_2}{2} \pm \sqrt{\left(\frac{\omega_1 - \omega_2}{2}\right)^2 + 4\Omega^2 \cos^2(qa)}. \quad (60)$$

The particularity of the system is that the two bands exhibit a bandgap $|\omega_1 - \omega_2|$ in the center of the first Brillouin zone (as depicted in Fig. 8c). The PBC now impose that $\beta_1^{(1)} = \beta_{N/2+1}^{(1)}$ which leads to the condition $q = \pi m/(Na)$. The first Brillouin zone is now defined by $m \in \{-N/2, N/2\}$ corresponding to q varying between $-\pi/(2a)$ to $\pi/(2a)$.

Dirac points - Further complexity in the band structure can be engineering by assuming alternating coupling strengths (for example from Ω to $-\Omega$ for consecutive pairs as in Fig. 8d). Noticing that this situation is again characterized by a double unit cell, we follow the same steps

as above to ask for two kind of propagating waves and reach the following eigenvalue problem

$$\begin{pmatrix} \omega_1 - \omega(q) & \Omega(1 - e^{-i2qa}) \\ \Omega(1 - e^{i2qa}) & \omega_2 - \omega(q) \end{pmatrix} \begin{pmatrix} A_q \\ B_q \end{pmatrix} = 0. \quad (61)$$

which leads to the following dispersion relation for the two branches

$$\omega_{\pm}(q) = \frac{\omega_1 + \omega_2}{2} \pm \sqrt{\left(\frac{\omega_1 - \omega_2}{2}\right)^2 + 4\Omega^2 \sin^2(qa)}, \quad (62)$$

with the quasi-momentum varying as above between $-\pi/(2a)$ to $\pi/(2a)$. The resulting dispersion curve plotted in Fig. 8d shows the emergence of an avoided crossing which exhibits a Dirac point at frequency degeneracy $\omega_1 = \omega_2$.

Berry phase - A particularly interesting case occurs for identical frequency emitters (transition frequency ω_0) with alternating interaction strengths Ω_1 and Ω_2 . This can be mapped onto the Su-Schrieffer-Heeger (SSH) model [66], which for electrons describes the emergence of bulk insulating phases distinguished by topological invariants and which in nature occurs in polyacetylene molecules. As

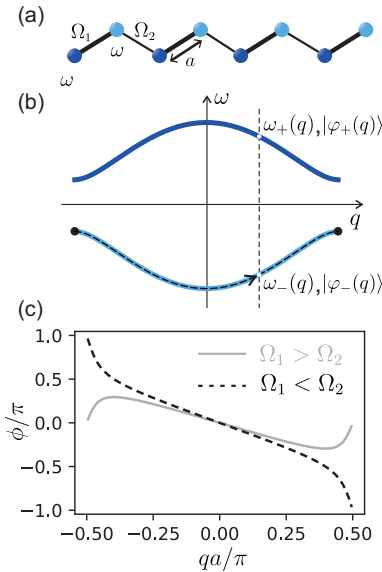


FIG. 9: (a) Chain with alternating dipole-dipole couplings forming the geometry of the Su-Schrieffer-Heeger (SSH) model. (b) Two distinct bands emerge, separated by a bandgap $2|\Omega_1 - \Omega_2|$ and with shape independent of the relation $\Omega_1 \leq \Omega_2$. The vertical dashed line shows the corresponding energies and eigenvectors corresponding to a given parameter q . The arrow in the lower band shows the path chosen for the integration to derive the accumulated phase from one end to the other one of first Brillouin zone. (c) The accumulated phase on the lower energy branch shows considerable differences between the case of $\Omega_1 > \Omega_2$ and that of $\Omega_1 < \Omega_2$.

before we write the equations of motion

$$\dot{\beta}_j^{(1)} = -i\omega_0\beta_j^{(1)} - i\Omega_2\beta_{j-1}^{(2)} - i\Omega_1\beta_j^{(2)}, \quad (63a)$$

$$\dot{\beta}_j^{(2)} = -i\omega_0\beta_j^{(2)} - i\Omega_2\beta_{j+1}^{(1)} - i\Omega_1\beta_j^{(1)}. \quad (63b)$$

and testing for the two kind of waves propagating as $\beta_j^{(1)} = A_q e^{i(2qa_j - \omega t)}$ and $\beta_j^{(2)} = B_q e^{i(2qa_j - \omega t)}$ we obtain the following eigenvalue problem

$$\begin{pmatrix} \omega_0 - \omega & \Omega_1 + \Omega_2 e^{-i2qa} \\ \Omega_1 + \Omega_2 e^{i2qa} & \omega_0 - \omega \end{pmatrix} \begin{pmatrix} A_q \\ B_q \end{pmatrix} = 0. \quad (64)$$

Here we will focus both on the energy dispersion curves but also on the characteristics of their corresponding eigenstates. The eigenvalues are given by

$$\omega_{\pm}(q) = \omega_0 + \sqrt{(\Omega_1 - \Omega_2)^2 + 4\Omega_1\Omega_2 \cos^2(qa)}. \quad (65)$$

While the band structure is insensitive to the exchange of Ω_1 with Ω_2 , the eigenvectors are not. The normalized eigenstates are analytically expressed in vector form as

$$|\varphi_{\pm}(q)\rangle = \frac{1}{\sqrt{2}} \begin{pmatrix} \pm e^{-i\phi(q)} \\ 1 \end{pmatrix}, \quad (66)$$

where the q -dependent phase is given by the following relation

$$e^{-i\phi(q)} = \frac{\Omega_1 + \Omega_2 e^{-i2qa}}{\sqrt{\Omega_1^2 + \Omega_2^2 + 2\Omega_1\Omega_2 \cos 2qa}} \quad (67)$$

The eigenvalue problem can now be written formally as $\mathcal{H}(q)|\varphi_n(q)\rangle = \omega_n(q)|\varphi_n(q)\rangle$ (where n stands for \pm). We now proceed by assuming that a path $q(t)$ is taken, with $q(t=0) = -\pi/(2a)$ and $q(\tau) = \pi/(2a)$; this is illustrated in Fig. 9b, particularized to the lower energy band. By moving adiabatically slow, tunneling to the orthogonal eigenstate is not allowed. Generally, we can then write the state of the system at any time t as $|\psi(t)\rangle = e^{-i\theta(t)}|\varphi_n(q(t))\rangle$ where the time-dependent phase could be computed directly by the application of the time-ordered evolution operator with a time-dependent Hamiltonian to the initial state. However, a more elegant solution comes from simply writing the Schrödinger equation $\mathcal{H}(q(t))|\psi(t)\rangle = i\partial_t|\psi(t)\rangle$ explicitly, to arrive at an equation for the phase

$$(\partial_t\theta(t))|\varphi_n(q(t))\rangle = \omega_n(q(t))|\varphi_n(q(t))\rangle - i\partial_t|\varphi_n(q(t))\rangle. \quad (68)$$

We sandwich the equation above with $\langle\varphi_n(q(t))|$ and integrate to obtain two distinct contributions. The integral of the energy over the whole band vanishes as the final and initial point are equal in energy. The second contribution is path dependent and reads

$$\theta(\tau) = -i \int_0^{\tau} \langle\varphi_n(q(t))|\partial_t|\varphi_n(q(t))\rangle dt. \quad (69)$$

The integration over time can be turned into a path integration such that

$$\theta = -i \int_{q(0)}^{q(\tau)} \langle\varphi_n(q)|\partial_q|\varphi_n(q)\rangle dq. \quad (70)$$

This describes the path-dependent Berry phase where $A_n(q) = \langle \varphi_n(q) | \partial_q | \varphi_n(q) \rangle$ can be identified as the Berry potential. The Berry phase is gauge invariant for closed integration loops. In general the temporal aspect of the adiabatic deformation is a more or less fictitious process but it is helpful to unravel the topological structure. Integrating the Berry phase for our Hamiltonian $\mathcal{H}(q)$ over the Brillouin zone $(-\pi/(2a), \pi/(2a))$ for the lower band results in

$$\nu = \frac{1}{\pi} \oint A_-(q) dq = \begin{cases} 0 & \Omega_1 > \Omega_2 \\ 1 & \Omega_1 < \Omega_2 \\ \text{undef.} & \Omega_1 = \Omega_2 \end{cases} \quad (71)$$

where the matrix element is easily computed from the vector expression of the eigenstates in Eq. (66) to result in $A_-(q) = (1/2)d\phi(q)/dq$. For differentiation we use the following expression for $\phi(q) = \arctan 2(\Omega_1 + \Omega_2 \cos(2qa), \Omega_2 \sin(2qa))$ and we note that ν is similar to a winding number. The result of the integral is a topological invariant showing that two cases $\Omega_1 > \Omega_2$ and $\Omega_1 < \Omega_2$ with the same band structure outcome are topologically different which is expressed by the Berry phase for a closed parameter path. In order to go from one topological phase ν in the bulk to another here given by smoothly varying Ω_1 and Ω_2 , one needs to cross a point ($\Omega_1 = \Omega_2$) where the bandgap is zero which would violate adiabaticity. This shows that Hamiltonians for the two insulating phases occurring for $\Omega_1 > \Omega_2$ and $\Omega_1 < \Omega_2$ are not adiabatically equivalent which is manifested in the difference of the topological invariant. In the case of open boundary conditions one finds that the number of edge states forms a topological invariant as well [67].

C. Quantum emitter rings and chains

Subradiance can be exploited towards applications in quantum metrology for sensitive frequency detection as well as in quantum information for the engineering of robust quantum memories. Moreover, subradiant biomimetic rings can aid to the design of nano-scale light sources acting as thresholdless nano-lasers. To describe these effects, we make use here of the collective master equation in the single excitation regime introduced in Sec. II B and of the Bloch sphere representation introduced in Sec. II C.

Quantum metrology - Ramsey interferometry is routinely used in quantum metrology for the most sensitive measurements of optical clock frequencies. The conventional method of separated oscillatory fields [68] assumes an ensemble of initially ground state atoms illuminated by a laser of frequency ω_ℓ in two consecutive steps separated by time τ . The two pulses are assumed to be instantaneous and tuned as $\pi/2$ pulses that can be visualized as $\pi/2$ rotations around the y -axis on the collective Bloch

sphere of radius $\mathcal{N}/2$ (introduced in Sec. II C). After the interrogation time τ the population difference $\langle S_z \rangle (\omega_\ell)$ is monitored as a function of the laser frequency. Its behavior is sinusoidal where the argument is the total accumulated phase $(\omega - \omega_\ell)\tau$ stemming from the mismatch of the (drifting, variable) laser frequency ω_ℓ and the constant frequency separation of the emitter ground and excited states ω . Analysis of the monitored population difference curve indicates a minimal sensitivity:

$$\delta\omega = \min \left[\frac{\Delta S^z(\omega, \tau)}{|\partial_\omega \langle S^z \rangle(\omega, \tau)|} \right], \quad (72)$$

where the minimization is performed with respect to ω . For weakly decaying emitters ($\gamma \ll \tau^{-1}$), the sensitivity is simply $1/(\tau\sqrt{\mathcal{N}})$ and can obviously be optimized by using longer interrogation times and more emitters. However, longer interrogation times bring decay into play, while operation at higher densities achieved by increasing \mathcal{N} indefinitely are marked by the onset of cooperative effects such as dipole-dipole shifts and super/subradiance.

For independently decaying emitters, the application of the master equation introduced in Sec. II leads to a simple analytical solution for both $\langle S_z \rangle$ and ΔS^z allowing one to estimate $[\delta\omega]_{\text{indep.}} = e^{\Gamma\tau/2}/(\tau\sqrt{\mathcal{N}})$. Further optimization with respect to the interrogation time gives an optimal $\tau_{\text{opt}} = 2/\Gamma$ and optimal sensitivity $\Gamma e/2\sqrt{\mathcal{N}}$, which shows that the main impediment of Ramsey interferometry subject to radiative loss is the limited interrogation times available. This expression hints towards a deterioration of the sensitivity in the case of equally illuminated dense ensembles where symmetric collective states are addressed which are typically characterized by superradiant behavior.

To protect against such detrimental effects, Refs. [10, 64] introduced an alternative procedure which uses an additional step in the Ramsey sequence aimed at hiding the collective states into decoherence free subspaces. To this end one complements the $\pi/2$ pulse with a phase distribution pulse, which for a particular atom j is represented by a rotation around the z -direction with the angle $\varphi_j^{(m)} = 2\pi m(j-1)/\mathcal{N}$, where $m = 1, \dots, [\mathcal{N}/2]$ and $[\mathcal{N}/2]$ is the integer before $\mathcal{N}/2$. The first generalized Ramsey pulse operator of such an asymmetric Ramsey technique is then

$$\mathcal{R}_1 = \bigotimes_j \mathcal{R}_z^{(j)} \left[\varphi_j^{(m)} \right] \cdot \mathcal{R}_y^{(j)} \left[\frac{\pi}{2} \right]. \quad (73)$$

The action of this phase distribution pulse is illustrated in Fig. 10a on the single particle Bloch sphere. In the second step, after the free evolution where robustness is now expected owing to the folding of the collective state into subradiant part of the Bloch sphere, at time τ the phase spread is (instantaneously) reversed and a $\pi/2$ pulse follows leading to the second generalized Ramsey pulse

$$\mathcal{R}_2 = \bigotimes_j \mathcal{R}_y^{(j)} \left[\frac{\pi}{2} \right] \cdot \mathcal{R}_z^{(j)} \left[-\varphi_j^{(m)} \right]. \quad (74)$$

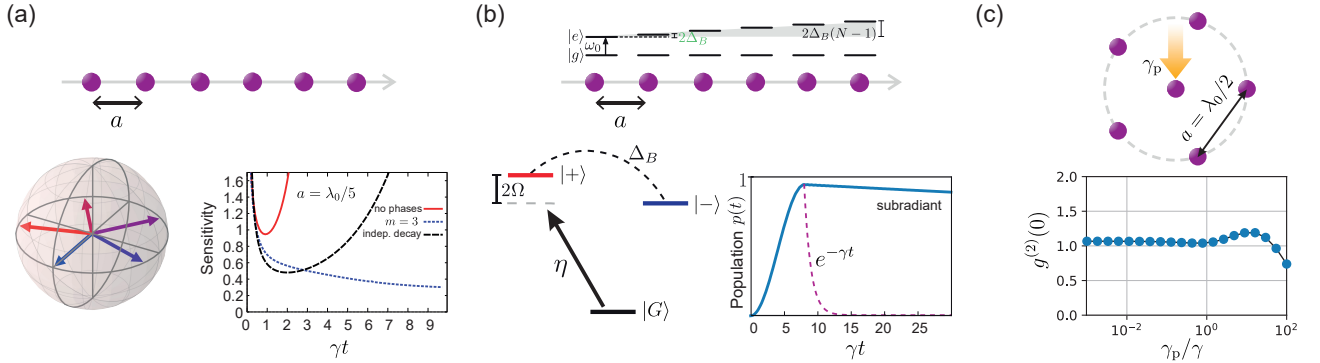


FIG. 10: (a) Ramsey metrology with phased excitation (shown on the individual spin Bloch sphere) for a chain of 6 emitters. Minimum sensitivity is plotted against interrogation time τ showing improved sensitivity for $m = 3$ (blue, dotted curve) as opposed to the independent case (black, dashed) or symmetric illumination (red, full line). (b) Phased excitation achieved via magnetic field gradient. For two coupled emitters, adiabatic population transfer to the robust state is achieved via detuned illumination of the symmetric state and subsequent transfer to the robust asymmetric state via the magnetic field. The population reaches values close to unity and decays much slower than $e^{-\gamma t}$. (c) Subwavelength structure ($a = \lambda_0/2$) of a ring resonator made of 5 quantum emitter surrounding an incoherently pumped central emitter. The second-order correlation function at zero delay $g^{(2)}(0)$ is presented as function of the pumping rate γ_p .

Finally, detection takes place as before and the sensitivity is minimized with respect to frequency to obtain results as shown in Fig. 10a. Here, the sensitivity for symmetric illumination is worse than that for independent emitters while the interrogation times and consequently the minimum frequency sensitivity can be considerably increased for phased excitations with $m \neq 0$. Further results and analytical considerations can be found in Refs. [10, 64].

Quantum memories - We now restrict the discussion to the single-excitation manifold of a 1D emitter chain. Here, we aim at targeting collective subradiant states as they show both robustness against decoherence while exhibiting multipartite entanglement. As pointed out in Sec. II B, eigenstates of the dipole-dipole Hamiltonian with lower energy typically exhibit subradiance. To access such states, one can proceed by first selecting them with individual addressing by tailoring the laser light amplitude to fit the shape of the collective state one wishes to address. For example, for a collective state $|k\rangle$ introduced in Sec. II B one can provide geometrical matching with the following driving Hamiltonian

$$\mathcal{H}_k = \eta \sum_{j=1}^N \sin \left(\frac{\pi k j}{N+1} \right) (\sigma e^{i\omega_\ell t} + \sigma^\dagger e^{-i\omega_\ell t}). \quad (75)$$

Moreover, imposing the condition for resonance by setting $\omega_\ell = \epsilon_k$ insures that states far enough from the desired targeted one are only weakly populated. In Ref. [52] it is shown that enhanced lifetimes much larger than γ^{-1} can be reached by such tailored excitation.

While tailored phase excitation with subwavelength resolution might pose great challenges, alternative methods could be envisioned: for example, symmetric

addressing could be combined with the application of a magnetic field gradient. The effect of magnetic field gradient applied along the direction of the emitter chain is to progressively shift the excited state by a quantity $\Delta_j = \Delta_B(j-1)$ from the first emitter with $j = 1$ to the end of the chain $j = N$. During the duration τ of an applied laser pulse, this amounts to a rotation around the z -axis of the Bloch vector of each emitter by the angle $\Delta_j \tau$. For a conveniently chosen duration τ , the effective phase difference between neighboring emitters can be controlled: for example with the choice $\Delta_B \tau = \pi$ a completely asymmetric superposition can be constructed. For example, for two coupled emitters, Fig. 10b shows results for pulsed adiabatic transfer of population from the ground state to the asymmetric state by a simultaneous off-resonant drive of the symmetric state and the action of the magnetic field gradient. The population then ends up in the protected asymmetric state which then decays much slower than the timescale defined by γ^{-1} . More results and analytical calculations for larger systems sizes can be found in Ref. [52].

Nanoscale coherent light sources - A closely spaced (on the subwavelength scale) ensemble of quantum emitters can act as a thresholdless laser, i.e., a coherent light source [65]. The configuration depicted in Fig. 10d shows a central emitter acting as a gain medium, pumped by incoherent light at some rate γ_p and coupled to the optical modes defined by the geometry of the extra emitters on the ring. One can apply then the formalism of Sec. II E, where a minimal model for lasing has been introduced, to solve the master equation of such a system under the assumption of incoherent pumping with a σ^\dagger collapse operator.

A first observation is that the physics of the system

can be reduced to solely the interaction of the symmetric mode $|\psi_{\text{sym}}\rangle = (1/\sqrt{\mathcal{N}}) \sum_j |j\rangle = \sigma_{\text{sym}}^\dagger |G\rangle$ of the ring resonator with the central atom. The reduced Hamiltonian is then

$$\mathcal{H}_{\text{ring}} = \Omega_{\text{sym}} \sigma_{\text{sym}}^\dagger \sigma_{\text{sym}} + \sqrt{\mathcal{N}} \Omega (\sigma_{\text{sym}}^\dagger \sigma + \text{h.c.}), \quad (76)$$

and the decay of the system which is governed by $\mathcal{L}[\rho] = \mathcal{L}_\gamma[\rho] + \mathcal{L}_{\gamma_b}[\rho] + \mathcal{L}_{\text{sym}}[\rho]$. For favorable geometries, it is possible to obtain a subradiant decay rate for the symmetric mode of the ring resonator. Additionally, such configurations can reduce the dissipative coupling of the central atom, strengthening the lossless transport of population from the central atom to the ring. We can now analyze the emitted light properties by using the fact that the far field is proportional to the sum of the dipole operators such that we can define the normalized second-order correlation function at zero time delay

$$g^{(2)}(0) = \frac{\sum_{ijkl} \langle \sigma_i^\dagger \sigma_j^\dagger \sigma_k \sigma_l \rangle}{\left| \sum_{mn} \langle \sigma_m^\dagger \sigma_n \rangle \right|^2}. \quad (77)$$

Numerical simulations, plotted in Fig. 10c show a close to unity $g^{(2)}(0)$ indicating a coherent state as an output of such a thresholdless laser. For higher pumping rates antibunching of light is expected.

D. Further remarks

One and two-dimensional ensembles of coupled quantum emitters arranged in regular patterns provide an ideal platform for achieving strong light-matter interactions and high fidelities for photon storage capabilities [7, 8]. Their subradiance properties are an important resource for applications ranging from quantum information processing [9] to metrology [7, 10, 11], excitation transfer [69–71] and it is envisioned that one can build quantum matter in a bottom-up approach from nanoscopic lattices of atoms and photons [9]. A single subradiant array has been shown to act as an ideal quantum memory with efficient storage and retrieval [11] and it has been suggested [15] that this geometry could lead to vast improvements in the error bound of quantum memories. Regular or honeycomb lattices of three level systems in a V -configuration, where time reversal symmetry is broken by the application of a magnetic field, have been proposed as platforms for studying topological phenomena with strongly interacting photons [4, 5] and further improvements have been proposed in the form of interfacing the arrays with two-dimensional photonic crystals [6]. A crucial aspect of these proposals that distinguish them from linear topological photonic systems is the intrinsic non-linearity of the quantum emitters which could lead to a rich many body physics dynamics on such subradiant lattices. Furthermore, composite quantum systems comprised of many atomic arrays could

find applications in quantum networking: at the level of two distant layers, nonlocal entangled Bell superposition states have been shown to exist [13]. While quantum information processing at the level of atomic layers require qubit encoding on delocalized spin states over the whole array, quantum spin lenses have been recently introduced, where incoming flying qubit photons can be mapped and stored in single atoms [12].

IV. COOPERATIVITY IN CAVITY QED

We now go a step further by considering systems exhibiting cooperative surface resonances, as analyzed in Sec. III A and Sec. III B but with an extra degree of freedom introduced by a cavity-confined field mode, i.e. in the context of cQED. In the limit of low reflectivity, such systems have been shown to act as quick frequency switchers [18] and to give rise to enhanced optical nonlinearities [19]. In the high reflectivity limit, such as theoretically predicted in Refs. [61, 62] and experimentally proven in Ref. [15], we introduce the necessary steps, as laid out in Ref. [29], to derive the correct input-output formalism for optical resonators made up of subwavelength arrays as end-mirrors.

In the weak reflectivity limit, the array reacts as a strongly dispersive optical element within a short frequency window but it does not, at the same time, considerably change the spatial profile of the cavity mode (owing to its weak reflectivity). The treatment is then perturbative, within the standard Tavis-Cummings formalism and non-trivial effects occur such as enhanced optical nonlinearities and the reach of an enhanced collective Purcell effect with a cooperativity scaling up to $\propto \mathcal{N}^4$ (for a 1D arrangement).

In the opposite case, where the emitter array acts as a near-unity reflectivity end-mirror, a *hybrid cavity* design emerges where asymmetric transmission profiles can be achieved, potentially much narrower than those obtained with frequency-independent mirrors of comparable reflectivity. For such designs, the standard input-output theory and the master equation for the photon mode losses (from Sec. II D) loses validity, as tunneling of photons strongly depends on the frequency of the tunneling photons. We present a general roadmap to derive the correct input-output relations for optical cavities comprised of either one or two of such end-mirrors. We remark that this is not limited to subradiant emitter arrays but also extendable to patterned subwavelength gratings or photonic crystal structures [72–75] and semiconducting monolayers [76–78].

We will start this chapter by introducing the formalism of quantum Langevin equations, which allows for a more in-depth understanding of how system operators evolve in time and is here employed to compute quantum correlation functions of operators at different times.

A. Quantum Langevin equations

The master equation formalism previously utilized is based on discarding the state of the environment and focusing on the dynamics of the reduced density operator of the much smaller system of interest. An alternative approach are quantum Langevin equations (also called Heisenberg-Langevin equations) [45, 79] which follow the evolution at the level of system operators instead of system states, i.e. its density operator. In essence, the formalism consists in supplementing the Heisenberg equations of motion with the proper dissipation and fluctuation terms. The application of such a system of equations can provide analytical insight in a variety of systems ranging from molecules [48] to optomechanics [80].

Mapping the ME onto QLEs - For open system dynamics described by loss in Lindblad form, a direct transformation between the master equation and the QLE formulation exists that reads [45]

$$\dot{\mathcal{O}} = \frac{i}{\hbar} [\mathcal{H}, \mathcal{O}] - [\mathcal{O}, c^\dagger] \left\{ \gamma_c c + \sqrt{2\gamma_c} c_{\text{in}} \right\} + \left\{ \gamma_c c^\dagger + \sqrt{2\gamma_c} c_{\text{in}}^\dagger \right\} [\mathcal{O}, c]. \quad (78)$$

The equation above is applied to a generic system operator \mathcal{O} and needs to be applied to each individual Lindblad collapse operator c acting at rate γ_c and with associated input noise c_{in} . The input noise is zero averaged $\langle c_{\text{in}} \rangle = 0$, delta-correlated in time $\langle c_{\text{in}}(t) c_{\text{in}}^\dagger(t') \rangle = \delta(t - t')$ (all other correlations vanish) and satisfies the following commutation relation $[c_{\text{in}}(t), c_{\text{in}}^\dagger(t')] = \delta(t - t')$. For linear evolution, such an equation can be formally integrated and expectation values of correlations containing any number of operators can be obtained.

We will proceed by first exemplifying the derivation and solution to a QLE applied to a lossy bosonic field corresponding to a decaying and externally driven optical cavity mode. Then we introduce the input-output relations allowing one to read intracavity light-matter interactions in the cavity output. Finally, we introduce a set of coupled linear QLEs for an ensemble of coupled, collectively decaying quantum emitters within the same optical cavity mode and show how quantum correlations can be computed. We will then utilize QLEs in Sec. IV B for the description of subradiant arrays in optical cavities and in Sec. IV C for the description of hybrid cavities. An extension of the QLEs to include electron-vibron coupling will be introduced in Sec. V.

QLEs and input-output relations. - For a driven, lossy, single-sided optical cavity, Eq. (78) yields the following QLE

$$\dot{a} = -(\kappa + i\omega_c)a + \eta e^{-i\omega_\ell t} + \sqrt{2\kappa}a_{\text{in}}. \quad (79)$$

Notice that an expectation value of the equation above simply reproduces Eq. (26) which has been instead derived directly from the master equation. The more general Langevin equation also allows for an exact solution obtainable by formal integration. We separate this solution into a transient and steady state part $a(t) = a_{\text{tr}}(t) + a_{\text{ss}}(t)$. While the transient part $a_{\text{tr}}(t)$ decays away on a timescale defined by the cavity loss κ^{-1} , the steady state part $a_{\text{ss}}(t)$ dominates in the long time (steady state) limit

$$a_{\text{tr}}(t) = a(0)e^{-\kappa t}e^{-i\omega_c t}, \quad (80a)$$

$$a_{\text{ss}}(t) = \int_0^t dt' (\eta e^{-i\omega_\ell t'} + \sqrt{2\kappa}a_{\text{in}}(t')) e^{-(\kappa + i\omega_c)(t-t')}. \quad (80b)$$

It is important to notice that the inclusion of the noise terms in such equations is crucial: while the commutator $[a_{\text{tr}}(t), a_{\text{tr}}^\dagger(t)] = e^{-2\kappa t}$ decays away, the commutator $[a_{\text{ss}}(t), a_{\text{ss}}^\dagger(t)] = 1 - e^{-2\kappa t}$ maintains the standard bosonic commutation relation $[a(t), a^\dagger(t)] = 1$ at every time during evolution.

In addition to the equation of motion for the cavity field amplitude operators, the full description of the optical cavity includes the input-output relation

$$a_{\text{out}} + a_{\text{in}} = \sqrt{\kappa}a(t), \quad (81)$$

which allows for the derivation of the properties of the cavity output mode. For example, the average shows that the cavity transmission can be simply written as: $t = \langle a_{\text{out}} \rangle / \eta = \sqrt{\kappa} \langle a \rangle / \eta$ (as already used and consistent with the result of Eq. (26) in Sec. II).

QLEs for cooperative cavity QED - We now assume a cavity mode coupled to \mathcal{N} interacting emitters, as a system described by the Hamiltonian $\mathcal{H}_{\text{TC}} + \mathcal{H}_{dd} + \mathcal{H}_\ell + \mathcal{H}_e$ and loss rates incorporated in the terms $\mathcal{L}_\kappa[\rho] + \mathcal{L}_e[\rho]$ (as introduced in Sec. IID). In a first step, we notice that the decay terms are not in Lindblad form, thus we perform a diagonalizing transformation to bring it into the form of \mathcal{N} independent decay channels as described by Eq. (12) (such that Eq. (78) can then be directly applied). We also only consider the low excitation limit $\langle \sigma_j^z \rangle \approx -1$. This discards the nonlinear response of the dipoles leading to a collective Kerr nonlinear effect [19]. One then obtains a set of coupled linear differential equations

$$\dot{a} = -(\kappa - i\Delta_c)a - i \sum_j g_j \sigma_j + \sqrt{2\kappa}a_{\text{in}}, \quad (82a)$$

$$\dot{\sigma}_j = i\Delta\sigma_j - ig_j a - \sum_{j'} \mathcal{M}_{jj'} \sigma_{j'} + \sqrt{2\gamma} \sigma_{\text{in}}^j. \quad (82b)$$

The input noise terms σ_{in}^j (stemming from the coupling of the emitters to the electromagnetic modes outside the solid state angle covered by the cavity field) are considered here as zero-averaged and delta-correlated in time $\langle \sigma_{\text{in}}^j(t) \sigma_{\text{in}}^{j',\dagger}(t') \rangle = (\gamma_{jj'}/\gamma) \delta(t - t')$ as a consequence of the low excitation assumption (for the more complex case of

high excitation we refer to Refs. [19, 45]). We can write the equations above in a compact form in terms of the matrix $\mathbf{M}(\Delta) = -i\Delta\mathbb{1} + i\Omega + \Gamma$ and the coupling vector $\mathbf{G} = (g_1, g_2, \dots, g_N)^\top$. Additionally defining the vectors $\boldsymbol{\sigma} = (\sigma_1, \dots, \sigma_N)^\top$ and $\boldsymbol{\sigma}_{\text{in}} = (\sigma_{\text{in}}^1, \dots, \sigma_{\text{in}}^N)^\top$, Eqs. (82) express as

$$\dot{a} = -(\kappa - i\Delta_c)a - i\mathbf{G}^\top \boldsymbol{\sigma} + \sqrt{2\kappa}a_{\text{in}}, \quad (83a)$$

$$\dot{\boldsymbol{\sigma}} = -\mathbf{M}(\Delta)\boldsymbol{\sigma} - i\mathbf{G}a + \sqrt{2\gamma}\boldsymbol{\sigma}_{\text{in}}. \quad (83b)$$

This is the starting point for the next subsection where we compute the classical and quantum response of a weakly excited transverse 1D or 2D array of coupled quantum emitters to a driven cavity mode.

B. Cavity QED with subradiant arrays

Let us now consider a weakly reflecting array placed transversely to the axis of a standard optical cavity. In the presence of near-field couplings, the system undergoes dynamics describable at the level of averages by Eqs. (29) and at the fully quantum level by Eqs. (82). We will assume a vector \mathbf{G} containing all the cavity-emitter couplings and later particularize to symmetric coupling (where all couplings are equal to g) and antisymmetric phased coupling (with alternating $(-1)^j g$ couplings). Assuming a single cavity drive, one can then easily deduce the cavity transmission as

$$t = \frac{\kappa}{i\Delta_c + \kappa + \mathbf{G}^\top \mathbf{G} / [i\Delta_{\text{eff}}(\Delta) + \gamma_{\text{eff}}(\Delta)]}, \quad (84)$$

where the effective Δ -dependent collective energy shifts and linewidths are derived from the matrix $\mathbf{M}(\Delta) = -i\Delta\mathbb{1} + i\Omega + \Gamma$ as real and imaginary parts

$$\gamma_{\text{eff}}(\Delta) + i\Delta_{\text{eff}}(\Delta) = \frac{\mathbf{G}^\top \mathbf{G}}{\mathbf{G}^\top \mathbf{M}^{-1}(\Delta) \mathbf{G}}. \quad (85)$$

These expressions are the equivalents of the decay rates and shifts for free space arrays given in Eq. (50) where the addressing of collective resonances is now controlled via the choice of cavity couplings instead of the drive.

Enhanced cooperativity - Notice that one can now proceed by introducing a modified \mathcal{N} emitter effective cooperativity

$$C_{\text{eff}}(\Delta) = \frac{\mathbf{G}^\top \mathbf{G}}{\kappa\gamma_{\text{eff}}(\Delta)}. \quad (86)$$

As mentioned in Sec. II D, for a single emitter the cooperativity is independent on the emitter properties (dipole moment, decay rate) and simply depends on the cavity finesse. For \mathcal{N} uncoupled emitters the same holds true and only a linear increase with \mathcal{N} will be obtained. For coupled emitters, an interesting decoupling

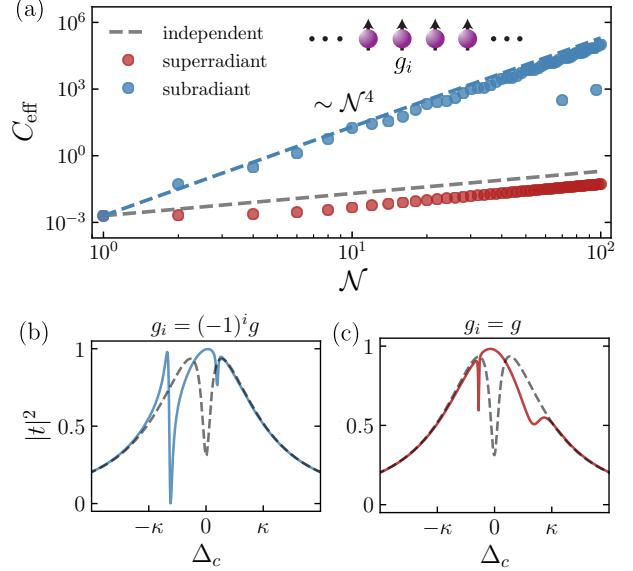


FIG. 11: (a) Effective cooperativity C_{eff} of a cavity-embedded chain of emitters as a function of \mathcal{N} for the superradiant (red, symmetric addressing $g_i = g$) and subradiant (blue, antisymmetric addressing $g_i = (-1)^i g$) case. Parameters: $a = 0.1\lambda$, $\gamma = \kappa/20$, $g = \kappa/100$. The bottom half shows the cavity transmission functions for (b) antisymmetric and (c) symmetric excitation of 4 equally spaced emitters for $a = 0.07\lambda$, $g = \kappa/10$. The grey dashed curves shows the result for independent emitters. In all plots, the dipole moments were chosen perpendicular to the chain.

of the dipole moment in the direction of the cavity (quantified by the term $\mathbf{G}^\top \mathbf{G}$) from the collective radiative properties $\gamma_{\text{eff}}(\Delta)$ can be achieved. As γ_{eff} is not a natural constant of the ensemble, but strongly dependent on the relative positioning and phase of individual emitters, one can reach subradiant states with $\gamma_{\text{eff}} \ll \gamma$. By proper design of the cavity transverse field amplitude profile, the numerator can at the same time be maximized, resulting in a scaling up of C_{eff} well above the independent emitter case $\mathcal{N}g^2/(\kappa\gamma)$. This is illustrated in Fig. 11a where a scaling with \mathcal{N}^4 for a 1D chain is shown possible. In Figs. 11b and c, we consider scans of the cavity transmission for a system of four coupled emitters. The system will have three subradiant and one superradiant state with resonances given by Eq. (14) (the superradiant state is located at $\omega_0 + 2\Omega \cos(\pi/5)$). We address the system either antisymmetrically with $\mathbf{G} = (g, -g, g, -g)^\top$ [Fig. 11b] or symmetrically with $\mathbf{G} = (g, g, g, g)^\top$ [Fig. 11c]. While antisymmetric excitation overlaps with two subradiant states, symmetric excitation overlaps with one subradiant and one superradiant state. In Ref. [18] it is shown that phased excitation could be realized by using the higher order TEM-modes of the optical cavity. Alternatively, one could use symmetric addressing around the optimal points utilized experimentally in Ref. [15] or symmetric addressing combined with a magnetic field gradient as in Ref. [52].

Quantum correlations - From the equations of motion for operators Eqs. (83), one can go a step further and fully analyze the quantum properties (second order correlation function for light $g^{(2)}$, bipartite entanglement, squeezing properties etc) of both the photon and matter counterparts. To this end, one can cast Eqs. (83) in convenient vector form as $\dot{\mathbf{v}} = \mathbf{A}\mathbf{v} + \mathbf{N}\mathbf{v}_{\text{in}}$ for the vectors $\mathbf{v} = (a, a^\dagger, \boldsymbol{\sigma}, \boldsymbol{\sigma}^\dagger)^\top$, $\mathbf{v}_{\text{in}} = (a_{\text{in}}, a_{\text{in}}^\dagger, \boldsymbol{\sigma}_{\text{in}}, \boldsymbol{\sigma}_{\text{in}}^\dagger)^\top$ with the drift matrix expressed in compact form as

$$\mathbf{A} = \begin{pmatrix} -(\kappa - i\Delta_c) & 0 & -i\mathbf{G}^\top & \mathbf{0}^\top \\ 0 & -(\kappa + i\Delta_c) & \mathbf{0}^\top & i\mathbf{G}^\top \\ -i\mathbf{G} & \mathbf{0} & -\mathbf{M}(\Delta) & \mathbf{0} \\ \mathbf{0} & i\mathbf{G} & \mathbf{0} & -\mathbf{M}^*(\Delta) \end{pmatrix}. \quad (87)$$

We have defined the vector $\mathbf{0}$ containing \mathcal{N} zeros and $\mathbf{0}$ is a $\mathcal{N} \times \mathcal{N}$ matrix with only zeros. The matrix multiplying the input noise operators is

$$\mathbf{N} = \begin{pmatrix} \sqrt{2\kappa} & 0 & \mathbf{0}^\top & \mathbf{0}^\top \\ 0 & \sqrt{2\kappa} & \mathbf{0}^\top & \mathbf{0}^\top \\ \mathbf{0} & \mathbf{0} & \sqrt{2\gamma}\mathbb{1} & \mathbf{0} \\ \mathbf{0} & \mathbf{0} & \mathbf{0} & \sqrt{2\gamma}\mathbb{1} \end{pmatrix}. \quad (88)$$

Formally integrating this system of linearly coupled equations gives the solution

$$\mathbf{v}(t) = e^{\mathbf{A}t}\mathbf{v}(0) + \int_0^t dt' e^{\mathbf{A}(t-t')}\mathbf{N}\mathbf{v}_{\text{in}}(t'). \quad (89)$$

If all eigenvalues of the drift matrix are negative, the system is stable and will go towards a steady state (i.e. the transient term $e^{\mathbf{A}t}$ vanishes). From the steady state solution only, one can then define a correlation matrix $\mathbf{V} = \langle \mathbf{v}(t)\mathbf{v}^\top(t) \rangle$ which can be expressed as

$$\mathbf{V} = \int_0^t dt' e^{\mathbf{A}(t-t')}\mathbf{D}e^{\mathbf{A}^\top(t-t')}, \quad (90)$$

where we used that $\langle \mathbf{v}_{\text{in}}(t')\mathbf{v}_{\text{in}}^\top(t'') \rangle = \mathbf{C}\delta(t' - t'')$ and defined the diffusion matrix as $\mathbf{D} = \mathbf{N}\mathbf{C}\mathbf{N}^\top$. The matrix containing the correlations can be readily obtained as

$$\mathbf{C} = \begin{pmatrix} 0 & 1 & \mathbf{0}^\top & \mathbf{0}^\top \\ 0 & 0 & \mathbf{0}^\top & \mathbf{0}^\top \\ \mathbf{0} & \mathbf{0} & \mathbf{0} & \Gamma/\gamma \\ \mathbf{0} & \mathbf{0} & \mathbf{0} & \mathbf{0} \end{pmatrix}. \quad (91)$$

For the covariance matrix, one can then derive the Lyapunov equation using integration by parts

$$\begin{aligned} \mathbf{A}\mathbf{V} + \mathbf{V}\mathbf{A}^\top &= \int_0^t dt' \mathbf{A}e^{\mathbf{A}(t-t')}\mathbf{D}e^{\mathbf{A}^\top(t-t')} + \mathbf{V}\mathbf{A}^\top = \\ &= -e^{\mathbf{A}(t-t')}\mathbf{D}e^{\mathbf{A}^\top(t-t')} \Big|_0^t - \mathbf{V}\mathbf{A}^\top + \mathbf{V}\mathbf{A}^\top = \\ &= -\mathbf{D}. \end{aligned} \quad (92)$$

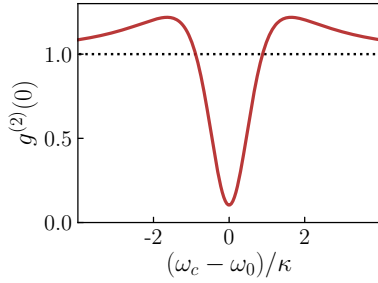


FIG. 12: Second-order optical correlation function $g^{(2)}(0)$ of a driven emitter-cavity system as a function of the cavity-emitter detuning $\omega_c - \omega_0$. Parameters: $\gamma = 0.1\kappa$, $\eta = 5 \cdot 10^{-3}\kappa$, $g = 0.3\kappa$.

Alternatively, one can also perform a Fourier analysis to turn the system of differential equations to an algebraic set of coupled equations $i\omega\mathbf{v}(\omega) = \mathbf{A}\mathbf{v}(\omega) + \mathbf{N}\mathbf{v}_{\text{in}}(\omega)$, which allows to relate the intra-cavity operators to the input noise via

$$\mathbf{v}(\omega) = (i\omega\mathbb{1} - \mathbf{A})^{-1}\mathbf{N}\mathbf{v}_{\text{in}}(\omega). \quad (93)$$

Furthermore, one can relate the input fields directly to the output fields by using the fact that in the time domain $\mathbf{v}_{\text{out}}(t) = \mathbf{N}^\top\mathbf{v}(t) - \mathbf{v}_{\text{in}}(t)$ and therefore one can express $\mathbf{v}_{\text{out}}(\omega) = \mathbf{F}(\omega)\mathbf{v}_{\text{in}}(\omega)$, where $\mathbf{F}(\omega) = [\mathbf{N}^\top(i\omega\mathbb{1} - \mathbf{A})^{-1}\mathbf{N} - \mathbb{1}]$. In the frequency domain, the δ -correlations are preserved for the output fields $\langle \mathbf{v}_{\text{out}}(\omega)\mathbf{v}_{\text{out}}^\top(\omega') \rangle = \mathbf{S}_{\text{out}}(\omega)\delta(\omega + \omega')$, where the two-operator correlations are completely encoded in the spectrum matrix given by

$$\mathbf{S}_{\text{out}}(\omega) = \mathbf{F}(\omega)\mathbf{C}\mathbf{F}^\top(-\omega). \quad (94)$$

While this suffices to characterize the two-operator correlations of the system, also higher-order correlations (e.g. four-operator correlations) can be of interest. We note that all higher order correlations can be expressed as a sum over two-point correlations via the Isserlis' theorem. An example of such a correlation is the the $g^{(2)}$ -function already considered in Sec. III C, characterizing the photon statistics of the system. It is defined in steady state as

$$g^{(2)}(\tau) = \frac{\langle a^\dagger(t)a^\dagger(t+\tau)a(t+\tau)a(t) \rangle_{\text{ss}}}{\langle a^\dagger(t)a(t) \rangle_{\text{ss}}^2}. \quad (95)$$

Non-classical light sources show sub-Poissonian statistics $g^{(2)}(0) < 1$ (antibunching), implying that it becomes unlikely for photons to be detected in pairs. In Fig. 12 this is illustrated for the coupled cavity-emitter system where the mechanism originates from the anharmonicity of the Jaynes-Cummings ladder, allowing only single photons inside the cavity.

C. Hybrid cavities

We now aim to provide a theoretical framework for hybrid cavities where subwavelength arrays are to be used

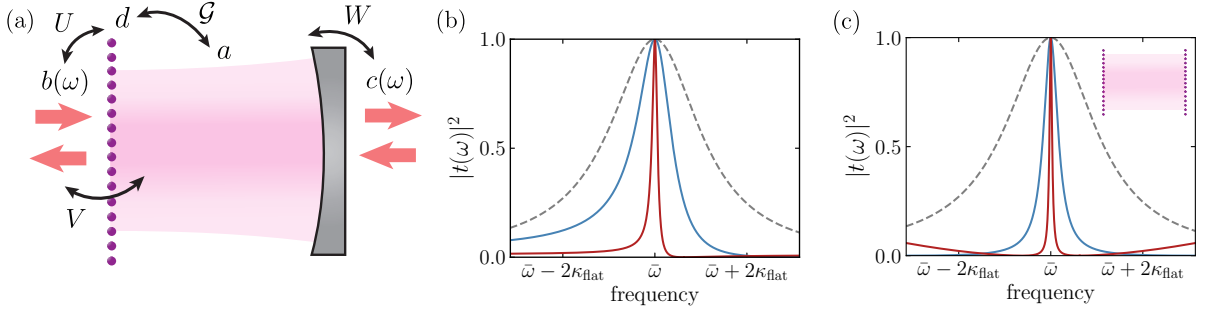


FIG. 13: (a) A hybrid cavity comprised of an atomic array (left mirror) and a standard, flat frequency mirror (right). The cavity mode a interacts with two external continua $b(\omega)$, $c(\omega)$ and the surface-confined mode on the array d . (b) Cavity response for $\zeta_0 = 10$. The grey dashed line is the expected Lorentzian profile with linewidth $\kappa_{\text{flat}} = \omega_{\text{FSR}}/(2\pi\zeta_0^2)$ in the Markovian regime where $\gamma_d = \omega_{\text{FSR}}$. For narrower mirror linewidths $\gamma_d = \omega_{\text{FSR}}/20$ (blue line) and $\gamma_d = \omega_{\text{FSR}}/100$ (red line) the cavity shows an asymmetric transmission profile with a strongly reduced linewidth at the level of γ_d/ζ_0 . (c) Transmission profile for a double sided hybrid cavity, where also the right mirror is replaced by an atomic array (same values for γ_d as in (b)) shows a symmetric response with an even narrower linewidth.

as end mirrors as suggested in Refs. [15, 29, 62]. The standard quantum optics approach of deriving open system dynamics described both in Sec. II and supplemented by input-output relations in Sec. IV is based on the assumption that the tunneling rate of photons between a cavity-confined mode a and the outside continuum of modes ($b(\omega)$ to the left and $c(\omega)$ to the right) is flat around the cavity resonance. This assumption is strongly modified in the case of subwavelength reflective arrays and the presence of a surface-confined resonance (mode d) has to explicitly be taken into account (see illustration in Fig. 13a). The roadmap to construct an input-output quantum theory for such hybrid cavities follows the steps described in Ref. [29] where it has been applied to photonic crystal mirrors. The procedure consists of three steps: i) the derivation of equations of motion for cavity field operators based on a coupled modes model where the photon-exchange processes between modes a and d are included, ii) the derivation of the cavity amplitude transmission from a classical transfer matrix approach based on the expression of the reflectivity of the array $r(\omega)$ derived in Sec. III and iii) the extraction of the phenomenologically introduced parameters by matching the predictions of the two theories. We apply this procedure here to a hybrid cavity made of one flat mirror and one subwavelength array and point out expected improvements in the cavity finesse where the hybrid design makes use of two emitter array mirrors.

Coupled modes theory - We consider the situation depicted in Fig. 13a where mode a is coupled to mode d at some complex rate \mathcal{G} and the photon tunneling rates $U, V, W \in \mathbb{R}$ are frequency independent. Tunneling will then give rise to loss rates $\kappa_L = \pi V^2$, $\kappa_R = \pi W^2$, $\gamma_d = \pi U^2$ (as detailed in Sec. II D). The dynamics is then

described by the Langevin equations

$$\dot{a} = -(i\omega_a + \kappa)a - \mathcal{G}d + \sqrt{2\kappa_L}b_{\text{in}} + \sqrt{2\kappa_R}c_{\text{in}}, \quad (96a)$$

$$\dot{d} = -(i\omega_d + \gamma_d)d - \mathcal{G}a + \sqrt{2\gamma_d}b_{\text{in}}, \quad (96b)$$

showing that the mode a is subject to two types of noises: b_{in} , entering through the left and c_{in} , entering through the right mirrors. In a first approximation, we will consider that the surface-confined mode reacts to the same noise term b_{in} consisting of modes on the left of the cavity but extra independent noise terms stemming for example from nonradiative losses could be added. The total decay rate is $\kappa = \kappa_L + \kappa_R$ and the input fields have the usual non-vanishing correlation functions $\langle b_{\text{in}}(t)b_{\text{in}}^\dagger(t') \rangle = \delta(t - t')$ [and similarly for $c_{\text{in}}(t)$]. The associated output fields follow the input-output relations $b_{\text{out}} = b_{\text{in}} - \sqrt{2\kappa_L}a - \sqrt{2\gamma_d}d$, and $c_{\text{out}} = c_{\text{in}} - \sqrt{2\kappa_R}a$.

We are mainly interested here in deriving the free parameters in the coupled modes model, i.e., \mathcal{G} , ω_a and κ_L . For more in-depth discussions highlighting the non-Markovianity of such hybrid cavities we refer to Ref. [29] where a full analysis of photonic crystal mirror cavities is provided.

The transmission coefficient $t(\omega) = \langle c_{\text{out}}(\omega) \rangle / \langle b_{\text{in}}(\omega) \rangle$ is easily expressed as $t(\omega) = -\sqrt{2\kappa_R} \langle a(\omega) \rangle / \langle b_{\text{in}}(\omega) \rangle$ in the case of sole driving through the left cavity port and can be analytically derived from Eqs. (96) in the frequency domain

$$t(\omega) = \frac{\sqrt{2\kappa_R}[\epsilon_d(\omega)\mathcal{G}\sqrt{2\gamma_d} - \sqrt{2\kappa_L}]}{\epsilon_a^{-1}(\omega) - \mathcal{G}^2\epsilon_d(\omega)}, \quad (97)$$

where we introduced the susceptibilities $\epsilon_a^{-1}(\omega) = \kappa + i(\omega_a - \omega)$, $\epsilon_d^{-1}(\omega) = \gamma_d + i(\omega_d - \omega)$. This is the main result of the coupled modes theory, which at this point still retains complete generality; in the following we will apply it to the particular scenario of a subwavelength reflective array.

Transfer matrix results - The transfer matrix approach, on the other hand, consists in solving the classical one-dimensional wave propagation in a one-dimensional setup with two mirrors parametrized by the polarizabilities ζ_0 (right mirror) and $\zeta_L(\omega)$ (left, subwavelength array mirror). In linear response theory, one can find the transmission function of the setup for any incoming plane wave at a given frequency ω . We use the parametrization $\zeta_L(\omega) = -ir(\omega)/(1+r(\omega)) = \gamma_d/(\omega - \omega_d)$ for the subwavelength array and choose a fixed $\zeta_0 \gg 1$ (corresponding to a close to unity reflectivity) for the right mirror. The classical transmission coefficient (see Appendix 1) then reads

$$\tilde{t}(\omega) = \frac{1}{(1 - i\zeta_0)[1 - i\zeta_L(\omega)]e^{-i\theta} + \zeta_0\zeta_L(\omega)e^{i\theta}}, \quad (98)$$

where $\theta = \omega\ell/c$. For $\zeta_L(\omega)$ and ζ_0 infinite, the expression above reaches unit absolute value at resonances $\omega_m = m \times \omega_{\text{FSR}}$ for any positive integer m . The resonances are separated by the free spectral range $\omega_{\text{FSR}} = c\pi/\ell$. Let us first fix a given resonance number m such that ω_m lies in the neighborhood of the mirror resonance and see that for finite ζ_0 and assuming $\zeta_L(\omega)$ is flat in frequency and equal to ζ_0 , the transmission can reach unity at a shifted $\omega'_m = \omega_m + \omega_{\text{FSR}}/(\pi\zeta_0)$. The linewidth of such a resonance is then $\kappa_{\text{flat}} = \omega_{\text{FSR}}/(2\pi\zeta_0^2)$. Notice that when the mirrors have unequal reflectivities, the optical resonator has always less than unit transmission. Therefore, for variable susceptibility ζ_L we ask now that a resonance $\bar{\omega}$ should be reached for which $|\zeta_L(\bar{\omega})| = \zeta_0$ such that the transmission is unity. We finally analytically derive (and match to numerical simulations) that this condition gives $\bar{\omega} = \omega_m$ under the condition that $\omega_d = \omega_m + \gamma_d/\zeta_0$. In practice this means that one first fixes γ_d, ζ_0 and the arrays resonance and then adjusts the cavity length to fit such a condition.

For varying γ_d , Fig. 13b shows a scan of the cavity resonance. For $\gamma_d \gg \kappa_{\text{flat}}$, the expected Lorentzian response is obtained (grey, dashed line) while for decreasing γ_d at the level of κ_{flat} , a very narrow (around γ_d/ζ_0) asymmetric Fano profile is obtained. The zero of the hybrid cavity transmission is at ω_d while unity is reached at ω_m .

Notice that the double hybrid cavity has an even narrower linewidth as illustrated in Fig. 13c for the same regimes as provided for Fig. 13b. In addition, the transmission profile is symmetric but has the advantage of presenting two Fano resonances, situated symmetrically with respect to the cavity resonance.

Extraction of parameters - Comparison of the two expressions in Eq. (98) and Eq. (97) can allow for the identification of \mathcal{G} , ω_a and κ_L . First, the zero of the transmission indicates that the numerator of $t(\omega)$ at ω_d is zero, leading immediately to the identification $\mathcal{G} = \sqrt{\kappa_L}\gamma_d$. This indicates a purely dissipative coupling between the surface resonance and the cavity-confined mode, in stark contrast with the situation treated in

Ref. [29] where an additional real photon exchange process occurred between the photonic crystal mirror and the cavity mode. In the next step, asking for unit transmission $|t(\omega)|^2 = 1$, indicates that $\kappa_L = \kappa_R(1 + \zeta_0^2)$ and $\omega_a = \bar{\omega} - \omega_{\text{FSR}}/(2\pi\zeta_0)$.

With the proper definition of the parameters appearing in Eqs. (96), one can proceed in solving various problems involving hybrid cavities with quantum emitter ensembles (eventually in the direction of Fano cavity lasing as in Ref.) or with movable mirrors. In the direction of quantum optomechanics, Ref. [29] has shown that the Fano profile of photonic crystal mirror cavities can be constructively utilized to lead to cooling in the absence of heating. The mechanism is based on sideband resolution by fitting a Stokes, heating sideband inside the Fano resonance. For subwavelength emitter arrays the same can be realized by tailoring the relationship between the cavity length and the array resonance, to move the Fano dip on the opposite side than illustrated in Fig. 13b. In addition, the double sided hybrid cavity is already a natural candidate for sideband resolution as it present symmetrically placed Fano dips.

D. Further remarks

Composite systems made up of flat, standard mirrors and two-dimensional single emitter-thick regular arrays can find a multitude of applications in the direction of quantum technologies. When used in a standard cavity QED scenario, they can act as quick phase switchers with applications in precision spectroscopy of quantum network characterization [18] or in hybrid quantum optomechanical setups with enhanced photon-phonon couplings [81]. In the strong reflectivity limit, subradiant arrays have been interfaced with two-dimensional semiconductor monolayers to show enhanced quantum nonlinear optical properties [20]. The identification of dark collective states between the two mirrors has allowed for the preparation of Bell superpositions states between the two subradiant layers [13], in a double-mirror hybrid setup as discussed above. As such subradiant mirrors are of extremely small mass, their zero point motion is much larger than that of traditional dielectric mirrors used in standard optomechanics: this opens new opportunities for quantum optomechanics at the single photon-phonon level [16, 17].

V. QUANTUM OPTICS WITH MOLECULES

A relatively recent novel direction of research with great promise in the direction of quantum technologies is the engineering of *cavity-dressed materials*. In the field of molecular polaritonics, embedding organic semiconductors in optical cavities allows for the design of

novel materials with enhanced properties such as exciton and charge transport [30–34], superconductive behavior [82, 83] or modified chemical reactivity [37–39, 41, 84] due to light-modified energy potential surfaces. This approach is also extended to study, control and design phase transitions in quantum materials by quantum light [85–89] etc.

Quantum emitters widely utilized in such experiments are of a much more complex nature than the two-level system approximation. We exemplify here how the previously introduced methods (master equation, quantum Langevin equations) and concepts can be extended to additionally include couplings between electronic transitions and vibrations or phonon modes. While this approach is in principle amenable to a wide range of solid-state emitters where phononic couplings play a crucial role, such as quantum dots or vacancy centers in diamond, we focus here on the specific case of molecules. In particular, organic molecules have emerged as tunable and efficient light-matter interfaces due to their relatively large dipole moments, wide range of transition frequencies and narrow linewidths at cryogenic temperatures [90]. As such, single-molecule impurities embedded in solid-state host matrices hold promise as single-photon sources [91–94] or nonlinear optical elements [95]. There also is interest in exploiting the strong inherent coupling between electronic transitions and the molecular vibrational degrees of freedom for the realization of quantum optomechanical effects at the single molecule level [96–98].

In this section, we will mainly follow the approach introduced in Ref. [48] by considering the time evolution of a *polaron* operator (i.e. an “effective”, vibrationally-dressed electronic dipole operator). We proceed with a first-principle derivation of the Holstein Hamiltonian for electron-vibron interactions and derive the standard Franck-Condon physics and absorption/emission properties of molecules. We then illustrate how one can circumvent a major downfall of molecular systems, i.e., they do not have closed transitions, by employing the Purcell effect: a cavity-dressed molecule can then behave as an ideal quantum emitter. Next we analyze molecular dimers as good candidates for the observation and exploration of controllable near-field couplings. Finally we introduce and analyze cooperative processes occurring between near-field coupled disordered molecules leading to what is known as the Förster resonance energy transfer.

A. Holstein Hamiltonian

To include the electron-vibration (*vibronic*) coupling into our formalism, we start with a first-principle derivation for a single electron coupled to a single nuclear coordinate of reduced mass μ . Notice that, for the simplest case of a homonuclear diatomic molecule made of nuclei each with mass m , a single vibrational mode ex-

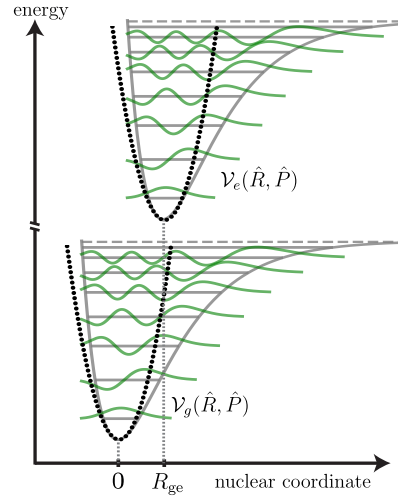


FIG. 14: Displaced oscillator model used to derive the Holstein Hamiltonian. The Morse potential energy landscapes (solid grey) of electronic ground and excited state are approximated as harmonic oscillators (dashed black) and their eigenstates are illustrated in green. The position mismatch between ground and excited state potential energy surfaces R_{ge} gives rise to vibronic coupling.

ists corresponding to relative motion with effective mass $\mu = m/2$; the equilibria coordinates then correspond to the bond length in the ground and excited states. Under the Born-Oppenheimer approximation, the ground and excited state potentials are obtained by solving the Schrödinger equation for each given fixed internuclear distance. We assume that, along the nuclear coordinate, the equilibrium positions for ground (coordinate R_g , state vector $|g\rangle$) and excited (coordinate R_e , state vector $|e\rangle$) electronic orbitals are slightly shifted with respect to each other (as illustrated in Fig. 14). We can then write the total Hamiltonian $\mathcal{H}_{\text{mol}} = \mathcal{H}_{\text{el}} \otimes \mathcal{H}_{\text{vib}}$ as

$$\mathcal{H}_{\text{mol}} = \mathcal{V}_e(\hat{R}, \hat{P}) \otimes \sigma^\dagger \sigma + \mathcal{V}_g(\hat{R}, \hat{P}) \otimes \sigma \sigma^\dagger.$$

where the potential surfaces are described by the quantized position and momentum operator satisfying $[\hat{R}, \hat{P}] = i$. The dynamics takes place now in an infinite-dimensional Hilbert space: in the electronic subspace the algebra is that of a spin 1/2 and is described by projectors $\sigma^\dagger \sigma$ (into the excited state) and $\sigma \sigma^\dagger$ (into the ground state) while in the motional subspace one can for example describe the dynamics in terms of plane waves. However, a great simplification can be obtained by performing a harmonic expansion of the potential surfaces around the minima

$$\mathcal{V}_e(\hat{R}, \hat{P}) = \omega_0 + \frac{\hat{P}^2}{2\mu} + \frac{1}{2}\mu\nu^2 \left(\hat{R} - R_e \right)^2, \quad (99a)$$

$$\mathcal{V}_g(\hat{R}, \hat{P}) = \frac{\hat{P}^2}{2\mu} + \frac{1}{2}\mu\nu^2 \left(\hat{R} - R_g \right)^2. \quad (99b)$$

Finally, we can introduce small oscillations around the equilibria $\hat{Q} = \hat{R} - R_g$ and subsequently $\hat{R} - R_e = \hat{Q} +$

$R_g - R_e =: \hat{Q} - R_{ge}$ leading to

$$\mathcal{H}_{\text{mol}} = \left(\omega_0 + \frac{1}{2} \mu \nu^2 R_{ge}^2 \right) \mathbb{1}_{\text{vib}} \otimes \sigma^\dagger \sigma \quad (100)$$

$$+ \left(\frac{\hat{P}^2}{2\mu} + \frac{1}{2} \mu \nu^2 \hat{Q}^2 \right) \otimes \mathbb{1}_{\text{el}} - \mu \nu^2 R_{ge} \hat{Q} \otimes \sigma^\dagger \sigma. \quad (101)$$

The last term is a renormalization of the bare electronic transition frequency energy which will naturally go away when diagonalizing the Hamiltonian via the polaron transformation resulting in ω_0 as the natural electronic transition frequency. We can now rewrite the momentum and position operators in terms of bosonic operators $\hat{Q} = r_{\text{zpm}}(b^\dagger + b)$, $\hat{P} = ip_{\text{zpm}}(b^\dagger - b)$ by introducing the zero-point motion $r_{\text{zpm}} = 1/\sqrt{2\mu\nu}$ and $p_{\text{zpm}} = \sqrt{\mu\nu}/2$. Reexpressing the terms above via the factor $\sqrt{S} = \mu\nu R_{ge} r_{\text{zpm}}$ (S is the Huang-Rhys factor) yields the Holstein-Hamiltonian [47]

$$\mathcal{H}_{\text{mol}} = (\omega_0 + S\nu) \sigma^\dagger \sigma + \nu b^\dagger b - \sqrt{S}\nu(b^\dagger + b)\sigma^\dagger \sigma, \quad (102)$$

A molecular box illustration is shown in Fig. 15a as a minimal model for a molecule.

One can bring this Hamiltonian into diagonal form via the polaron transformation $U_{\text{pol}}^\dagger = (\mathcal{D}^\dagger)^{\sigma^\dagger \sigma} = |g\rangle\langle g| + \mathcal{D}^\dagger |e\rangle\langle e|$ where the displacement is defined as $\mathcal{D} = \exp(-i\sqrt{2Sp}) = \exp[\sqrt{S}(b^\dagger - b)]$ with the dimensionless momentum quadrature $p = i(b^\dagger - b)/\sqrt{2}$ as generator. The position quadrature is defined analogously as $q = (b^\dagger + b)/\sqrt{2}$. The displacement operator creates a coherent state with amplitude \sqrt{S} when applied to the vibrational ground state $\mathcal{D}|0\rangle_{\text{vib}} = |\sqrt{S}\rangle_{\text{vib}}$. Note that the vibrational creation and annihilation operators transform in the polaron picture as

$$U_{\text{pol}}^\dagger b U_{\text{pol}} = b + \sqrt{S}\sigma^\dagger \sigma, \quad (103a)$$

$$U_{\text{pol}}^\dagger b^\dagger U_{\text{pol}} = b^\dagger + \sqrt{S}\sigma^\dagger \sigma, \quad (103b)$$

and furthermore the following commutation relations are fulfilled $[p, \mathcal{D}^\dagger] = 0$, $[q, \mathcal{D}^\dagger] = -\sqrt{2S}\mathcal{D}^\dagger$. The Hamiltonian in the diagonal basis then becomes $\tilde{\mathcal{H}}_{\text{mol}} = \omega_0 \sigma^\dagger \sigma + \nu b^\dagger b$ and has eigenvectors $\{|g, n\rangle, |e, n\rangle\}$ while the eigenvectors in the original basis can be obtained by an inverse polaron transform and are given by $\{|g, n\rangle, \mathcal{D}|e, n\rangle\}$.

Franck-Condon physics - Let us now ask what is the optical response of the molecule to a weak laser excitation modelled via $\mathcal{H}_\ell = i\eta(\sigma^\dagger e^{-i\omega_\ell t} - \sigma e^{i\omega_\ell t})$. In an interaction picture, reached after performing a transformation of the Hamiltonian with $e^{i\omega_\ell \sigma^\dagger \sigma t}$, one has

$$\tilde{\mathcal{H}} = (\omega_0 - \omega_\ell) \sigma^\dagger \sigma + \nu b^\dagger b + i\eta(\sigma^\dagger \mathcal{D}^\dagger - \sigma \mathcal{D}). \quad (104)$$

Starting with the molecule in the absolute ground state $|g, 0\rangle$, the result of the drive is to excite the electron

to state $|e\rangle$ while exciting motion on the nuclear coordinate to a coherent motional state. One can immediately compute the probability of absorption

$$P_{\text{abs}} = |\langle e, n | \tilde{\mathcal{H}} | g, 0 \rangle|^2 = \langle e, n | \sigma^\dagger \mathcal{D}^\dagger | g, 0 \rangle|^2 = f_S^n, \quad (105)$$

showing a Poissonian distribution $f_S^n = e^{-S} S^n / n!$ of the occupancies of number states $|n\rangle$ with coefficients known as Franck-Condon factors. In particular, the so-called zero-phonon line (transition corresponding to $n = 0$) is reduced by a factor e^{-S} at zero temperature. The Huang-Rhys factor S should be interpreted as the average number of vibrational quanta created upon excitation or deexcitation of the molecule. The probability of the emission process is similarly computed between $|e, 0\rangle$ and final states $|g, n\rangle$ and yields the same Poissonian distribution in n . This is a known result in molecular spectroscopy where the absorption and emission spectra are mirror images of each other. For small $S < 1$ the physics of absorption and emission in a molecule is illustrated in Fig. 15c where the width of the arrows indicate the strength of the optical transitions between eigenstates of the free Hamiltonian (without the Holstein interaction).

The Holstein Hamiltonian in Eq. (102) can be generalized to a more complex molecular box (as illustrated in Fig. 15b) involving n_v independent nuclear coordinates with frequencies ν_k and coupling strengths \sqrt{S}_k . The total Hamiltonian is then expressed as

$$\mathcal{H}_{\text{mol}} = \tilde{\omega}_0 \sigma^\dagger \sigma + \sum_{k=1}^{n_v} \nu_k b_k^\dagger b_k - \sum_{k=1}^{n_v} \sqrt{S}_k \nu_k (b_k^\dagger + b_k) \sigma^\dagger \sigma, \quad (106)$$

where the accumulated frequency shift is $\tilde{\omega}_0 = \omega_0 + \sum_{k=1}^{n_v} S_k \nu_k$. Diagonalization of this Hamiltonian is straightforward as it involves a collective displacement for all nuclear coordinates $U_{\text{pol}}^\dagger = (\prod_k \mathcal{D}_k^\dagger)^{\sigma^\dagger \sigma}$ with $\mathcal{D}_k = \exp(-i\sqrt{2S_k}p_k)$. The expectation value of the displacement operator $\langle \mathcal{D}_k \rangle = \langle \mathcal{D}_k^\dagger \rangle = e^{-S_k \langle p_k^2 \rangle}$ (assuming the vibrational mode to be in a thermal state) can be expressed as $e^{-S_k(\bar{n}_k + 1/2)}$ (expanding the displacement operator and making use of the fact that Gaussian states are characterized by their second-order moments and odd moments are vanishing) where the average thermal occupancy is given by $2\bar{n}_k = \coth(\beta\nu_k/2) - 1$ with $\beta = 1/(k_B T)$.

Branching ratio manipulation - The branching ratio quantifies the rate of emission into the zero-phonon line versus all other lines. For ideal quantum emitters this is automatically unity in the absence of coupling to any other channels of de-excitation. For an isolated molecule this is instead given by $\alpha = \langle \mathcal{D} \rangle^2 = \prod_k \langle \mathcal{D}_k \rangle^2 = e^{-\sum_k S_k}$ (at zero temperature) stemming from loss of excitation into other vibrational levels. Complex molecules have many vibrations: even for small Huang-Rhys factors the sum in the exponential gives a considerable reduction of the oscillator strength of the zero-phonon line. The

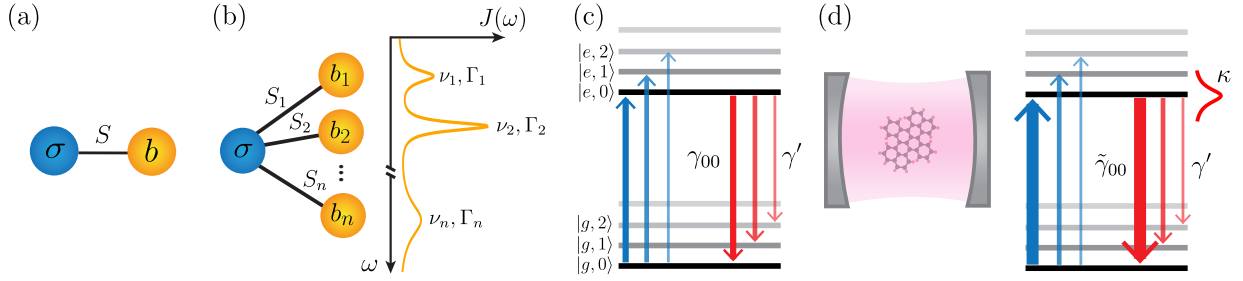


FIG. 15: (a) The dynamics of a molecule with a single nuclear coordinate can be seen as the coupling of an electronic transition operator σ to a single vibrational mode b with a strength given by the Huang-Rhys factor S . (b) For many vibrational modes, a molecule can be constructed by coupling an electronic transition operator σ to n vibrational modes with strengths S_k , frequencies ν_k and linewidths Γ_k described by the (Lorentzian) spectral density function $J(\omega)$. (c) Energy eigenstates of the electron-vibron system denoted by $|g, n\rangle$ and $|e, n\rangle$. The zero phonon line is the $|g, 0\rangle$ to $|e, 0\rangle$ transition. For small $S < 1$ the width of the arrows indicate the strength of the optical transitions. For a molecule with many vibrational levels, spontaneous emission outside the zero phonon line at summed rate γ' can be larger than into it at rate γ_{00} . (d) The enhancement of spontaneous emission via resonant coupling to an optical cavity can lead to a great modification of the strength of the zero phonon line thus turning a molecule into a closed quantum system.

Purcell effect (introduced in Sec. II D), stemming from the resonant interaction of the zero-phonon line transition with a lossy confined optical resonance has been experimentally proven to turn molecular emitters into almost perfect two-level quantum emitters [42]. Assuming that the cavity linewidth is narrow compared to the vibrational frequency $\kappa \ll \nu$ and only couples to the zero-phonon line transition, we can define by $g_{00} = g \langle \mathcal{D} \rangle$ the effective reduced coupling between the cavity and the zero-phonon line with a corresponding cooperativity $\mathcal{C}_{00} = g_{00}^2 / (\kappa \gamma)$. This will lead to an enlarged zero-phonon transition linewidth $\tilde{\gamma}_{00} = \gamma_{00}(1 + \mathcal{C}_{00})$ as illustrated in Fig. 15 while other transitions are unperturbed and sum up to $\gamma' = \gamma - \gamma_{00}$. The cavity-modified branching ratio can then be expressed as

$$\alpha_{\text{cav}} = \frac{\tilde{\gamma}_{00}}{\tilde{\gamma}_{00} + \gamma'} = \frac{(1 + \mathcal{C}_{00})e^{-\sum_k S_k}}{1 + \mathcal{C}_{00}e^{-\sum_k S_k}}, \quad (107)$$

which reproduces the bare molecule result for $\mathcal{C}_{00} = 0$ and goes to unity in the limit that $\mathcal{C}_{00} \rightarrow \infty$. Experimentally, values of \mathcal{C}_{00} close to 100 have been reached [42], showing that almost unity branching ratios can be achieved.

B. Quantum Langevin equations for polarons

We will now proceed by deriving a quantum Langevin equation for a polaron operator $\tilde{\sigma} = \sigma \mathcal{D}^\dagger$ (i.e., a vibrationally dressed electronic dipole operator). This will allow us to include all coherent and incoherent effects at the level of the equations of motion. The collective displacement operator \mathcal{D}^\dagger can refer to a large set of molecular vibrational modes $\mathcal{D}^\dagger = \prod_{k=1}^{n_v} \mathcal{D}_k^\dagger$. The method can also be extended to include coupling to an (eventually infinite) set of phonon modes of the host environment [49, 99]. We will assume a Brownian noise dissipation model (see Appendix 2) for the molecular vibrational modes. Start-

ing with the Holstein Hamiltonian one can derive the following equations of motion for vibrations

$$\dot{q}_k = \nu_k p_k, \quad (108a)$$

$$\dot{p}_k = -2\Gamma_k p_k - \nu_k q_k - \sqrt{2S_k} \nu_k \sigma^\dagger \sigma + \xi_k. \quad (108b)$$

In addition to the environment induced damping at rates $2\Gamma_k$ and associated thermal input noise ξ_k (see Appendix 2 for noise properties), vibrations are driven by their coupling to the electronic degree of freedom. For the electronic transition, the polaron operator can be computed from $\tilde{\sigma} = \dot{\sigma} \mathcal{D}^\dagger + \sigma \mathcal{D}^\dagger$ where the full Langevin equation for σ is derived from the Holstein Hamiltonian and the Lindblad form radiative emission with the transformation indicated by the relation in Eq. (78). We obtain then

$$\begin{aligned} \dot{\tilde{\sigma}} = & -[\gamma - i(\omega_\ell - \omega_0)]\tilde{\sigma} - 2i \sum_k \sqrt{2S_k} \Gamma_k p_k \tilde{\sigma} \quad (109) \\ & + \eta \mathcal{D}^\dagger + \sqrt{2\gamma} \tilde{\sigma}_{\text{in}} + i \sum_k \sqrt{2S_k} \xi_k \tilde{\sigma}. \end{aligned}$$

The equation is derived under the assumption of weak driving $\eta \ll \gamma$ and therefore small occupancy of the electronic excited state $\langle \sigma^\dagger \sigma \rangle \ll 1$ and with special attention devoted to the rules for taking the time derivative of any exponential operator $e^{A(t)}$ with $[\dot{A}(t), A(t)] \neq 0$. Moreover, some of the terms cancel (see Ref. [48] for full details) and an extremely simple equation of motion for the polaron operator is obtained

$$\dot{\tilde{\sigma}} = -[\gamma - i(\omega_\ell - \omega_0)]\tilde{\sigma} + \sqrt{2\gamma} \tilde{\Sigma}_{\text{in}}. \quad (110)$$

Here we have combined the input fields affecting the electronic transition into the expression $\Sigma_{\text{in}} = \eta / \sqrt{2\gamma} + \sigma_{\text{in}}$ and the displaced input field (drive plus noise) is $\tilde{\Sigma}_{\text{in}} = \Sigma_{\text{in}} \mathcal{D}^\dagger$. A solution of the bare electronic dipole operators can be obtained by a formal integration as a sum $\sigma(t) = \sigma_{\text{tr}}(t) + \sigma_{\text{ss}}(t)$ between transient and steady

state solutions

$$\sigma_{\text{tr}}(t) = \sigma(0)\mathcal{D}(t)\mathcal{D}^\dagger(0)e^{-[\gamma-i(\omega_\ell-\omega_0)]t}, \quad (111\text{a})$$

$$\sigma_{\text{ss}}(t) = \sqrt{2\gamma} \int_0^t dt' e^{-[\gamma-i(\omega_\ell-\omega_0)](t-t')} \Sigma_{\text{in}}(t') \mathcal{D}(t)\mathcal{D}^\dagger(t'). \quad (111\text{b})$$

To derive the optical response of the electronic degree of freedom in the presence of its coupling to vibrations one then has to evaluate two-time correlation functions of the displacement operator. This is factorizable as we consider that all vibrational modes are independent from each other, i.e., $\langle \mathcal{D}(t)\mathcal{D}^\dagger(t') \rangle = \prod_k \langle \mathcal{D}_k(t)\mathcal{D}_k^\dagger(t') \rangle$. By expanding the displacement operators and applying the Isserlis' theorem (or Wick's probability theorem for multivariate normal distributions) one obtains

$$\langle \mathcal{D}_k(t)\mathcal{D}_k^\dagger(t') \rangle = e^{-2S_k(\langle p_k^2 \rangle - \langle p_k(t)p_k(t') \rangle)}, \quad (112)$$

where we made use of the fact that the momentum variance is stationary, i.e., $\langle p_k^2 \rangle = \langle p_k(t)^2 \rangle = 1/2 + \bar{n}_k$. This can be easily computed by using the properties for the Brownian noise model listed in the Appendix 2

$$\langle p_k(t)p_k(t') \rangle = \left[\left(\bar{n}_k + \frac{1}{2} \right) \cos(\nu_k \tau) - \frac{i}{2} \sin(\nu_k \tau) \right] e^{-\Gamma_k \tau}, \quad (113)$$

with $\tau = t - t'$. While expressions can be derived for any temperature of the bath, in the following we will, for the sake of simplicity, focus on the zero temperature case for all vibrational modes. This is typically a very good approximation as molecular vibrations typically lie in the range of 1 to 100 THz frequencies and are therefore barely occupied as the condition $\hbar\nu_k \ll k_B T$ is typically fulfilled. The displacement correlation function in this case simplifies to

$$\langle \mathcal{D}_k(t)\mathcal{D}_k^\dagger(t') \rangle = e^{-S_k} e^{S_k \exp[-(\Gamma_k + i\nu_k)\tau]}, \quad (114)$$

which we will make use of in the next subsection to derive analytical expressions for absorption and emission lines and linewidths.

C. Absorption and emission

The absorption and emission spectra of a driven molecule can be readily obtained from Eq. (111). Considering large times $t \gg 1/\gamma$, the first term in Eq. (111) goes towards zero and the average dipole moment can be expressed as (taking the average over both electronic and vibrational degrees of freedom)

$$\langle \sigma(t) \rangle = \eta \int_0^t dt' e^{-(\gamma-i\Delta)(t-t')} \langle \mathcal{D}(t)\mathcal{D}^\dagger(t') \rangle, \quad (115)$$

with the laser detuning $\Delta = \omega_\ell - \omega_0$. The population of the electronic excited state evolves according to $\partial_t \langle \sigma^\dagger \sigma \rangle =$

$-2\gamma \langle \sigma^\dagger \sigma \rangle + 2\eta \Re \langle \sigma(t) \rangle$ meaning that the steady state absorption profile can be directly computed from the expectation value of the coherence $\langle \sigma(t) \rangle$. We define $S_{\text{abs}}(\Delta) = \langle \sigma^\dagger \sigma \rangle$ as the absorption profile for a varying laser frequency with expression

$$S_{\text{abs}}(\Delta_\ell) = 2\eta \int_{-\infty}^t dt' e^{-2\gamma(t-t')} \Re \langle \sigma(t') \rangle. \quad (116)$$

To evaluate this integral, we expand the displacement correlation function from Eq. (114) in a power series

$$\langle \mathcal{D}_k(t)\mathcal{D}_k^\dagger(t') \rangle = e^{-S_k} \sum_{n_k=0}^{\infty} \frac{S_k^{n_k}}{n_k!} e^{-n_k(\Gamma_k + i\nu_k)(t-t')}. \quad (117)$$

The absorption spectrum can then be readily expressed as a sum over all indices $\{n_k\} = n_1, \dots, n_{n_v}$ weighted by the Franck-Condon factors $f_{n_k}^{S_k}$

$$S_{\text{abs}}(\Delta) = \frac{\eta^2}{\gamma} \sum_{\{n_k\}=0}^{\infty} \frac{f_{S_1}^{n_1} \dots f_{S_{n_v}}^{n_{n_v}} [\gamma + \Gamma_{\{n_k\}}]}{[\gamma + \Gamma_{\{n_k\}}]^2 + [\Delta - \nu_{\{n_k\}}]^2}, \quad (118)$$

where the denominator indicates a series of blue-shifted absorption sidebands with increased linewidths $\Gamma_{\{n_k\}} = \sum_{\{n_k\}} n_k \Gamma_k$ at positions $\omega_\ell = \omega + \sum_k \nu_{\{n_k\}}$ with $\nu_{\{n_k\}} = \sum_{\{n_k\}} n_k \nu_k$.

For the definition of the emission spectrum one can consider the transient dynamics of a molecule which is partially excited at time $t = 0$: $\langle \sigma^\dagger \sigma(0) \rangle = p_0$. The emission spectrum is then defined as the Fourier transform $S_{\text{em}}(\omega) = 2\Re \int_0^\infty d\tau \langle \mathcal{T} \{ \sigma^\dagger(\tau) \sigma(0) \} \rangle e^{-i\omega\tau}$ (where \mathcal{T} denotes time ordering) and can be computed as (normalized by p_0)

$$S_{\text{em}}(\omega) = \sum_{\{n_k\}=0}^{\infty} \frac{2f_{S_1}^{n_1} \dots f_{S_{n_v}}^{n_{n_v}} [\gamma + \Gamma_{\{n_k\}}]}{[\gamma + \Gamma_{\{n_k\}}]^2 + [\omega - \omega_0 + \nu_{\{n_k\}}]^2}. \quad (119)$$

The denominator indicates a series of red-shifted Stokes lines at frequencies $\omega = \omega_0 - \nu_{\{n_k\}}$.

D. Near-field effects: vibronic dimer model

Effects showing quantum coherence in electronically excited molecules, carrying the signature of entanglement have been experimentally investigated in a combination of single molecule spectroscopy and quantum chemistry techniques [50]. An ideal candidate for such investigations is the vibronic dimer, well-known model to describe the interplay between electronic and vibrational interactions in molecular aggregates and which has been studied both theoretically [100–102] and experimentally [50, 103]. As opposed to the pure electronic dimer discussed in Sec. II B, this model gives rise to a more complex energy landscape with states possessing both electronic and vibrational

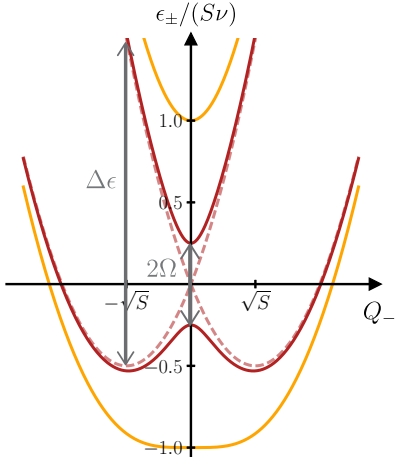


FIG. 16: Potential energy surfaces ϵ_{\pm} of the vibronic dimer model as a function of the (dimensionless) relative motion coordinate Q_- for $\Omega = 0$ (red dashed), $2\Omega = \Delta\epsilon/4$ (red solid) and $2\Omega = \Delta\epsilon$ (orange).

character.

The model consists of two molecules (indexed here by 1 and 2), each with a single electronic ground and excited state and each coupled to a single harmonic nuclear coordinate $q_{1/2}$ with Huang-Rhys factor S . The molecules are coupled to each other electronically (e.g. via dipole-dipole interaction) with strength Ω . Assuming that the excited state energies of the two molecules are identical and using the single excitation manifold with states $|e\rangle_1 \otimes |g\rangle_2$ and $|g\rangle_1 \otimes |e\rangle_2$, the Hamiltonian of the dimer can be represented by

$$\mathcal{H}_{\text{dim}} = \begin{pmatrix} -\sqrt{2S}\nu q_1 & \Omega \\ \Omega & -\sqrt{2S}\nu q_2 \end{pmatrix} + \frac{\nu}{2} \sum_{i=1,2} (p_i^2 + q_i^2) \mathbb{1}, \quad (120)$$

where $\mathbb{1}$ is a 2×2 unity matrix. Introducing symmetrized coordinates $Q_{\pm} = (q_1 \pm q_2)/\sqrt{2}$ and electronic operators $\sigma_{\pm} = (\sigma_1 \pm \sigma_2)/\sqrt{2}$, the Hamiltonian transforms to

$$\tilde{\mathcal{H}}_{\text{dim}} = \begin{pmatrix} \Omega & -\sqrt{S}\nu Q_- \\ -\sqrt{S}\nu Q_- & -\Omega \end{pmatrix} - \sqrt{S}\nu Q_+ \mathbb{1} \quad (121) \\ + \frac{\nu}{2} (P_+^2 + P_-^2 + Q_+^2 + Q_-^2) \mathbb{1},$$

from which one can see that only the coordinate Q_- couples between electronic states in the collective basis. The coordinate Q_+ instead leads to a constant shift and therefore can eventually be eliminated by a proper choice of the origin. The Hamiltonian in Eq. (121) can be easily diagonalized leading to the eigenvalues for the excited state potential energy surfaces

$$\epsilon_{\pm} = \frac{\nu}{2} (Q_+^2 + Q_-^2) - \sqrt{S}\nu Q_+ \pm \sqrt{S\nu^2 Q_-^2 + \Omega^2}. \quad (122)$$

The potential energy surfaces are plotted in Fig. 16 for various coupling strengths Ω . One can see that the coupling lifts the degeneracy of the potential surfaces at

$Q_- = 0$ and leads to a splitting of 2Ω . Depending on Ω , the lower energy surface either has two minima or just a single minimum. An important quantity is the reorganization energy $\Delta\epsilon = 2S\nu$ defined as the vertical energy separation between the potential curves at each minimum for zero coupling $\Omega = 0$ [as illustrated in Fig. 16]. One finds that a double minimum of the lower energy surface located at $Q_{\pm}^{\pm} = \pm\sqrt{S[1 - \Omega^2/(S^2\nu^2)]}$ exists when the level splitting 2Ω is smaller than the reorganization energy $|2\Omega| < \Delta\epsilon$.

E. Förster resonance energy transfer

We now apply the formalism developed in the previous sections to the near-field energy transfer between two molecules, the so-called *Förster resonance energy transfer* (FRET). FRET is the main excitation transfer mechanism in photosynthetic light harvesting complexes, where energy is transferred with high efficiency from a light-harvesting antenna through a network of molecules (chromophores) to a reaction centre [2, 3]. Although a lot of progress has been made in understanding and unravelling the reasons for the high efficiency of the photosynthetic energy transfer occurring in nature over the last years, there is still ongoing debate e.g. about the role of quantum coherence or entanglement in the energy transfer process [104, 105]. In the sense of this tutorial, FRET can be seen as a truly *cooperative* process since it involves a complex interplay between electronic and nuclear degrees of freedom as well as both coherent and incoherent couplings. Generally speaking, the requirement for FRET is a spectral overlap between the emission profile of the donor molecule and the absorption profile of the acceptor, giving rise to a resonant transfer process typically accompanied by quick vibrational relaxation [106].

Here we exemplify the application of the QLEs formalism to derive a perturbative expression for the FRET rate between two near-field coupled molecules D and A with energy mismatch $\Delta = \omega_D - \omega_A$, first by considering a simple configuration where each molecule has a single vibrational mode b_D and b_A (with corresponding vibrational frequencies ν_D and ν_A and Huang-Rhys factors S_D and S_A). We will assume an initially excited donor molecule which can undergo a resonant exchange with the acceptor's excited state vibrational manifold. In a standard scenario, a unidirectional process emerges as the acceptor quickly relaxes to its vibrational ground state $\Gamma_D \gg \Omega$. We start with the equations of motion for the polaron-transformed dipole operators $\tilde{\sigma}_D = \mathcal{D}_D^\dagger \sigma_D$ and $\tilde{\sigma}_A = \mathcal{D}_A^\dagger \sigma_A$ with the displacement operators $\mathcal{D}_D = e^{\sqrt{S_D}(b_D^\dagger - b_D)}$ and $\mathcal{D}_A = e^{\sqrt{S_A}(b_A^\dagger - b_A)}$ which shows coherent coupling induced by the dipole-dipole

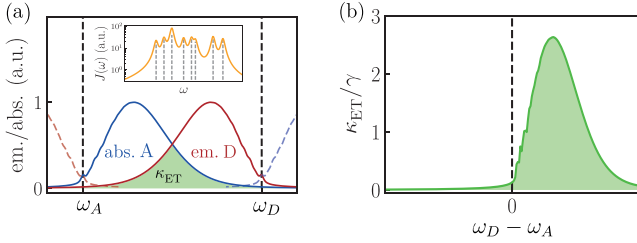


FIG. 17: Energy transfer in donor-acceptor configurations. (a) Overlap between acceptor emission spectrum and donor absorption spectrum leads to the FRET process. The results assume a given vibrational spectral energy $J(\omega)$ (assumed here to be identical for both molecules) shown in the inset, for 8 vibrational modes considered. (b) Numerical analysis of the energy transfer rate shows a unidirectional flow from the higher energy molecule (donor) to the lower energy one (acceptor) optimized around a detuning corresponding to the overlap of the donor electronic state to a high density of vibrational states in the acceptor excited state manifold.

near-field exchange of virtual photons

$$\dot{\sigma}_D = -(\gamma_D + i\omega_D)\tilde{\sigma}_D - i\Omega\tilde{\sigma}_A\mathcal{D}_A\mathcal{D}_D^\dagger + \sqrt{2\gamma}\tilde{\sigma}_D^{\text{in}}, \quad (123\text{a})$$

$$\dot{\sigma}_A = -(\gamma_A + i\omega_A)\tilde{\sigma}_A - i\Omega\tilde{\sigma}_D\mathcal{D}_D\mathcal{D}_A^\dagger + \sqrt{2\gamma}\tilde{\sigma}_A^{\text{in}}. \quad (123\text{b})$$

To derive a perturbative expression for the energy transfer rate, we consider a scenario with an initial full excitation of D and no excitation of A . Then from above one can derive an equation of motion for the acceptor's population

$$\dot{P}_A = -2\gamma_A P_A + 2\Omega\Im\langle\sigma_A^\dagger\sigma_D\rangle + \sqrt{2\gamma_A}\langle\sigma_A^\dagger\sigma_A^{\text{in}} + \sigma_A^{\dagger,\text{in}}\sigma_A\rangle, \quad (124)$$

which shows how the two particle correlations appear as source terms for the acceptor population. The procedure to compute $2\Omega\Im\langle\sigma_A^\dagger\sigma_D\rangle$ involves then formal integration of the equation of motion for the acceptor polaron operator (as detailed in the Appendix 3) under the assumption that $\Gamma_D, \Gamma_A \gg \gamma_D, \gamma_A$. Finally, one arrives at an expression for the energy transfer rate showing proportionality to the donor population $2\Omega\langle\sigma_A^\dagger\sigma_D\rangle = \kappa_{\text{ET}}P_D(t)$

$$\kappa_{\text{ET}} = \sum_{n_D, n_A} \frac{2\Omega^2 f_{SD}^{n_D} f_{SA}^{n_A} (n_D \Gamma_D + n_A \Gamma_A)}{(n_D \Gamma_D + n_A \Gamma_A)^2 + [\Delta - n_D \nu_D - n_A \nu_A]^2}, \quad (125)$$

where, for simplicity, we have set $\gamma_D = \gamma_A$. The denominator of the above expression asks that the resonance is $\omega_D - n_D \nu_D = \omega_A + n_A \nu_A$ is fulfilled, i.e. fluorescence lines of the donor $|e_D, 0\rangle \rightarrow |g_D, n_D\rangle$ have to overlap with absorption lines of the acceptor $|g_A, 0\rangle \rightarrow |e_A, n_A\rangle$, both of which are weighted by the respective Franck-Condon factors.

In the case of many vibrational modes n for donor and acceptor, we can generalize the result by writing general

displacements $\mathcal{D}_A = \prod_{k=1}^{n_v} \mathcal{D}_A^k$ and $\mathcal{D}_D = \prod_{k=1}^{n_v} \mathcal{D}_D^k$ for all vibrational modes. The rate is computed by assuming multiple paths of energy transfer between the two molecules involving all vibrational modes. We assume an initially electronically excited state with no vibrations present $|e_D; 0_1, 0_2 \dots 0_{n_v}\rangle$ of molecule D and ground state without vibrations $|g_A; 0_1, 0_2 \dots 0_{n_v}\rangle$ for molecule A . The emission of molecule D leads it into state $|g_D; m_1, \dots, m_k, \dots, m_{n_v}\rangle$ and resonant interactions can occur with state $|e_A; l_1, \dots, l_k, \dots, l_{n_v}\rangle$ of molecule A . Summing over all these processes leads to an analytical cumbersome expression for κ_{ET} (listed in Appendix 3) seen simply as a generalization of the energy transfer rate from above. Such an analytical result is the discrete version of the well established integral formulation [106] describing the overlap between the emission spectrum of molecule D and absorption spectrum of molecule A as illustrated in Fig. 17a for a donor-acceptor pair with 8 vibrational modes and spectral density $J(\omega) = \sum_k 2S_k \nu_k^2 \Gamma_k / [\Gamma_k^2 + (\omega - \nu_k)^2]$ stemming from the coupling of the molecular vibrations to some external phonon bath allowing for vibrational relaxation at rates Γ_k . The process is unidirectional as shown in Fig. 17b as $\omega_D - \omega_A$ dictates the direction of the energy flow.

F. Further remarks

We have covered here the electron-vibron interaction and described the optical response to a weak classical optical drive. We have however hinted that coupling to confined optical modes can lead to strong modifications on the matter side, such as the described model of a molecule turned into an efficient quantum emitter [42]. Indeed, many experimental and theoretical efforts have been recently targeted into the direction of cavity charge and energy transport enhancement [30–34], Förster resonance energy transfer (FRET) enhancement [35, 36, 107–109], modified chemical reactivity [37–39, 41, 84], polariton dynamics [110, 111], etc. On the theory side a large effort is aimed at translating standard cavity QED concepts (as introduced in Sec. IID) with two-level systems into the realm of molecules. To this end, theoretical efforts consider a generalized light-electronic-vibrations problem modeled as a Holstein-Tavis-Cummings Hamiltonian. Investigations aim at providing an understanding of the vibrationally induced cavity polariton asymmetry [111, 112], vibrationally dressed polaritons [113], dark vibronic polaritons [114, 115], developing a cavity Born-Oppenheimer theory [51, 116] or deriving relevant simplified models for large scale numerics in the mesoscopic limit [117].

We also remark that molecules are natural quantum mechanical platforms interfacing electronic and vibrational degrees of freedom via an interaction that resembles the radiation pressure Hamiltonian (via a boson-spin replacement) utilized in quantum optomechanics; as vibration at

terahertz frequencies are practically in the ground state even at room temperature and the strength of the coherent coupling can be comparable to the vibrational frequency, molecules could be a good platform for studying quantum state transfer between light and motion [98]. Moreover, molecules are good single photon emitters as they are characterized by large emission rates and they allow for highly efficient collection schemes, thus utilizable in applications for photon-photon entanglement generation and optical quantum computing [118].

VI. CONCLUSIONS

Quantum systems, comprised of many particles, inherently coupled via common reservoirs (the electromagnetic vacuum, optical resonators, optical waveguides, etc.) can exhibit *cooperative* behavior with some specific properties scaling more favorably than what would be expected from a collection of uncoupled particles. In order to analytically and numerically understand the cooperativity of light-matter platforms, we have detailed two alternative approaches based on either the time evolution of the density operator (master equation approach) or of system operators (stochastic quantum Langevin equations). Based on this toolbox, this tutorial introduced a set of equations successfully applied to chains, rings and arrays of quantum emitters or ensembles of molecules within the confined mode of optical resonators.

A first set of applications that we have tackled are based on effects stemming from the dipole-dipole interaction occurring in dense quantum emitter ensembles. This interaction allows for the hopping of excitations in one or two-dimensional regular arrays and for the engineering of energy bands with special properties such as bandgaps, Dirac points or Chern numbers. Thus, such systems are ideal platforms for the investigation of topological quantum photonics with built-in nonlinearities. Their subradiant properties allow for applications in quantum metrology, in the design of high-fidelity photon-storage platforms and in the generation of entangled Bell states of two or more quantum emitter arrays (hinting towards quantum networks of spatially distant subwavelength arrays). Their enhanced reflectivity properties render them useful as extremely light mechanical resonators for quantum nano-optomechanical applications or as metasurfaces with enhanced optical nonlinearities at the level of a single photon. Also, subradiant rings illuminated by incoherent light can provide a natural

gain medium via supported waveguide resonances leading to thresholdless nano-lasers.

A second set of applications that we have discussed are based on the enhancement of the photon-emitter coupling in cavity QED. We have analyzed two-dimensional arrays as quick phase switchers or as integrated elements in hybrid cavity devices. The hybrid cavity approach, where flat mirrors are replaced with frequency dependent mirrors (such as subwavelength arrays or photonic crystal mirrors) can lead to narrow linewidths useful for example in resolved sideband optomechanics. We provided an input-output theory, valid outside Markovian regimes with wide applicability. In the same context of cavity QED, we provided a simple theory of superradiant lasers with potential applications in enhancing the stability of atomic clocks.

As molecular systems, quantum dots, vacancy centers in solid state hosts are increasingly important for quantum technology applications, it is crucial to understand and to tailor the electron-vibration interaction. We provided here a first-principle derivation of the Holstein Hamiltonian for electron-vibron interactions in simple molecular systems and extended the QLEs approach to polaron physics. This theory leads to very simple analytical insight in the understanding of molecular spectral lines, their absorption and emission profiles and processes such as FRET migration of energy in donor-acceptor configurations. We also made the analytical connection between the molecular dimer model, widely used in quantum chemistry for studying vibronic quantum coherence and the dipole-dipole interaction Hamiltonian.

Acknowledgments

We acknowledge useful discussion with A. Dantan. We acknowledge financial support from the Max Planck Society and from the German Federal Ministry of Education and Research, co-funded by the European Commission (project RouTe), project number 13N14839 within the research program “Photonik Forschung Deutschland”. This work was funded by the Deutsche Forschungsgemeinschaft (DFG, German Research Foundation) – Project-ID 429529648 – TRR 306 QuCoLiMa (“Quantum Cooperativity of Light and Matter”). M. R. acknowledges financial support from the International Max Planck Research School - Physics of Light (IMPRS-PL).

[1] I. H. Deutsch, “Harnessing the power of the second quantum revolution,” *PRX Quantum* **1**, 020101 (2020).

[2] T. Förster, “Zwischenmolekulare Energiewanderung und Fluoreszenz,” *Ann. Phys.* **437**, 55–75 (1948).

[3] R. E. Blankenship, *Molecular Mechanisms of Photosynthesis*, 2nd Edition (John Wiley & Sons, Inc., Hoboken, NJ, 2014).

[4] J. Perczel, J. Borregaard, D. E. Chang, H. Pichler, S. F. Yelin, P. Zoller, and M. D. Lukin, “Topological quantum optics in two-dimensional atomic arrays,” *Phys. Rev.*

Lett. **119**, 023603 (2017).

[5] R. J. Bettles, J. Minar, C. S. Adams, I. Lesanovsky, and B. Olmos, “Topological properties of a dense atomic lattice gas,” *Phys. Rev. A* **96**, 041603 (2017).

[6] J. Perczel, J. Borregaard, D. E. Chang, S. F. Yelin, and M. D. Lukin, “Topological quantum optics using atomlike emitter arrays coupled to photonic crystals,” *Phys. Rev. Lett.* **124**, 083603 (2020).

[7] G. Facchinetti, S. D. Jenkins, and J. Ruostekoski, “Storing light with subradiant correlations in arrays of atoms,” *Phys. Rev. Lett.* **117**, 243601 (2016).

[8] A. Asenjo-Garcia, M. Moreno-Cardoner, A. Albrecht, H. J. Kimble, and D. E. Chang, “Exponential improvement in photon storage fidelities using subradiance and “selective radiance” in atomic arrays,” *Phys. Rev. X* **7**, 031024 (2017).

[9] D. E. Chang, J. S. Douglas, A. González-Tudela, C.-L. Hung, and H. J. Kimble, “Colloquium: Quantum matter built from nanoscopic lattices of atoms and photons,” *Rev. Mod. Phys.* **90**, 031002 (2018).

[10] L. Ostermann, H. Ritsch, and C. Genes, “Protected state enhanced quantum metrology with interacting two-level ensembles,” *Phys. Rev. Lett.* **111**, 123601 (2013).

[11] M. T. Manzoni, M. Moreno-Cardoner, A. Asenjo-Garcia, J. V. Porto, A. V. Gorshkov, and D. E. Chang, “Optimization of photon storage fidelity in ordered atomic arrays,” *New Journal of Physics* **20**, 083048 (2018).

[12] A. W. Glaetzle, K. Ender, D. S. Wild, S. Choi, H. Pichler, M. D. Lukin, and P. Zoller, “Quantum spin lenses in atomic arrays,” *Phys. Rev. X* **7**, 031049 (2017).

[13] P.-O. Guimond, A. Grankin, D. V. Vasilyev, B. Vermersch, and P. Zoller, “Subradiant Bell states in distant atomic arrays,” *Phys. Rev. Lett.* **122**, 093601 (2019).

[14] Y.-X. Zhang and K. Mølmer, “Subradiant emission from regular atomic arrays: Universal scaling of decay rates from the generalized Bloch theorem,” *Phys. Rev. Lett.* **125**, 253601 (2020).

[15] J. Rui, D. Wei, A. Rubio-Abadal, S. Hollerith, J. Zeiher, D. M. Stamper-Kurn, C. Gross, and I. Bloch, “A subradiant optical mirror formed by a single structured atomic layer,” *Nature* **583**, 369–374 (2020).

[16] E. Shahmoon, M. D. Lukin, and S. F. Yelin, “Chapter one - collective motion of an atom array under laser illumination,” (Academic Press, 2019) pp. 1–38.

[17] E. Shahmoon, M. D. Lukin, and S. F. Yelin, “Quantum optomechanics of a two-dimensional atomic array,” *Phys. Rev. A* **101**, 063833 (2020).

[18] D. Plankensteiner, C. Sommer, H. Ritsch, and C. Genes, “Cavity antiresonance spectroscopy of dipole coupled subradiant arrays,” *Phys. Rev. Lett.* **119**, 093601 (2017).

[19] D. Plankensteiner, C. Sommer, M. Reitz, H. Ritsch, and C. Genes, “Enhanced collective Purcell effect of coupled quantum emitter systems,” *Phys. Rev. A* **99**, 043843 (2019).

[20] D. S. Wild, E. Shahmoon, S. F. Yelin, and M. D. Lukin, “Quantum nonlinear optics in atomically thin materials,” *Phys. Rev. Lett.* **121**, 123606 (2018).

[21] S. Haroche and D. Kleppner, “Cavity Quantum Electrodynamics,” *Phys. Today* **42**, 24–30 (1989).

[22] P. Berman, *Cavity Quantum Electrodynamics*, Advances in atomic, molecular, and optical physics (Academic Press, 1994).

[23] H. Walther, B. T. Varcoe, B. Englert, and T. Becker, “Cavity Quantum Electrodynamics,” *Rep. Prog. Phys.* **69**, 1325 (2006).

[24] S. Haroche and J.-M. Raimond, *Exploring the Quantum: Atoms, Cavities, and Photons* (Oxford University Press, 2013).

[25] R. H. Dicke, “Coherence in spontaneous radiation processes,” *Phys. Rev.* **93**, 99–110 (1954).

[26] M. Gross and S. Haroche, “Superradiance: An essay on the theory of collective spontaneous emission,” *Physics Reports* **93**, 301 – 396 (1982).

[27] J. Bohnet, Z. Chen, J. Weiner, D. Meiser, M. Holland, and J. K. Thompson, “A steady-state superradiant laser with less than one intracavity photon,” *Nature* **484**, 78 (2012).

[28] M. A. Norcia, M. N. Winchester, J. R. K. Cline, and J. K. Thompson, “Superradiance on the millihertz linewidth strontium clock transition,” *Science Advances* **2** (2016).

[29] O. Cernotik, A. Dantan, and C. Genes, “Cavity quantum electrodynamics with frequency-dependent reflectors,” *Phys. Rev. Lett.* **122**, 243601 (2019).

[30] E. Orgiu, J. George, J. Hutchinson, E. Devaux, J. F. Dayen, B. Doudin, F. F. Stellacci, C. Genet, J. Schachenmayer, C. Genes, G. Pupillo, P. Samori, and T. W. Ebbesen, “Conductivity in organic semiconductors hybridized with the vacuum field,” *Nat. Mater.* **14**, 1123 – 1129 (2015).

[31] J. Schachenmayer, C. Genes, E. Tignone, and G. Pupillo, “Cavity-enhanced transport of excitons,” *Phys. Rev. Lett.* **114**, 196403 (2015).

[32] J. Feist and F. J. Garcia-Vidal, “Extraordinary exciton conductance induced by strong coupling,” *Phys. Rev. Lett.* **114**, 196402 (2015).

[33] D. Hagenmüller, J. Schachenmayer, S. Schütz, C. Genes, and G. Pupillo, “Cavity-enhanced transport of charge,” *Phys. Rev. Lett.* **119**, 223601 (2017).

[34] D. Hagenmüller, S. Schütz, J. Schachenmayer, C. Genes, and G. Pupillo, “Cavity-assisted mesoscopic transport of fermions: Coherent and dissipative dynamics,” *Phys. Rev. B* **97**, 205303 (2018).

[35] X. Zhong, T. Chervy, S. Wang, J. George, A. Thomas, J. Hutchinson, E. Devaux, C. Genet, and T. W. Ebbesen, “Non-radiative energy transfer mediated by hybrid light-matter states,” *Angew. Chem.* **55**, 6202 (2016).

[36] X. Zhong, T. Chervy, L. Zhang, A. Thomas, J. George, C. Genet, J. Hutchinson, and T. W. Ebbesen, “Energy transfer between spatially separated entangled molecules,” *Angew. Chem.* **56**, 9034 (2017).

[37] J. A. Hutchinson, T. Schwartz, C. Genet, E. Devaux, and T. W. Ebbesen, “Modifying chemical landscapes by coupling to vacuum fields,” *Angew. Chem. Int. Ed.* **51**, 1592–1596 (2012).

[38] J. Galego, F. Garcia-Vidal, and J. Feist, “Suppressing photochemical reactions with quantized light fields,” *Nat. Commun.* **7**, 13841 (2017).

[39] F. Herrera and F. C. Spano, “Cavity-controlled chemistry in molecular ensembles,” *Phys. Rev. Lett.* **116**, 238301 (2016).

[40] J. Galego, F. J. Garcia-Vidal, and J. Feist, “Many-molecule reaction triggered by a single photon in polaritonic chemistry,” *Phys. Rev. Lett.* **119**, 136001 (2017).

[41] L. A. Martinez-Martinez, R. F. Ribeiro, J. Campos-González-Angulo, and J. Yuen-Zhou, “Can ultrastrong coupling change ground-state chemical reactions?” *ACS Photonics* **5**, 167–176 (2018).

[42] D. Wang, H. Kelkar, D. Martin-Cano, D. Rattenbacher,

A. Shkarin, T. Utikal, S. Götzinger, and V. Sandoghdar, “Turning a molecule into a coherent two-level quantum system,” *Nature Physics* (2019).

[43] R. Loudon, *The Quantum Theory of Light*, Oxford (Clarendon Press, 1973).

[44] M. Scully and M. Zubairy, *Quantum Optics* (Cambridge University Press, 1997).

[45] C. Gardiner and P. Zoller, *Quantum noise: a handbook of Markovian and non-Markovian quantum stochastic methods with applications to quantum optics*, Vol. 56 (Springer Science & Business Media, 2004).

[46] D. Walls and G. Milburn, *Quantum Optics*, Springer Study Edition (Springer Berlin Heidelberg, 2012).

[47] T. Holstein, “Studies of polaron motion: Part I. The molecular-crystal model,” *Annals of Physics* **8**, 325 – 342 (1959).

[48] M. Reitz, C. Sommer, and C. Genes, “Langevin approach to quantum optics with molecules,” *Phys. Rev. Lett.* **122**, 203602 (2019).

[49] M. Reitz, C. Sommer, B. Gurlek, V. Sandoghdar, D. Martin-Cano, and C. Genes, “Molecule-photon interactions in phononic environments,” *Phys. Rev. Research* **2**, 033270 (2020).

[50] F. P. Diehl, C. Roos, A. Duymaz, B. Lunkenheimer, A. Köhn, and T. Basche, “Emergence of coherence through variation of intermolecular distances in a series of molecular dimers,” *J. Phys. Chem. Lett.* **5**, 262 (2014).

[51] J. Flick, M. Ruggenthaler, H. Appel, and A. Rubio, “Atoms and molecules in cavities, from weak to strong coupling in quantum-electrodynamics (QED) chemistry,” *114*, 3026–3034 (2017).

[52] D. Plankensteiner, L. Ostermann, H. Ritsch, and C. Genes, “Selective protected state preparation of coupled dissipative quantum emitters,” *Sci. Rep.* **5**, 16231 (2015).

[53] M. Hebenstreit, B. Kraus, L. Ostermann, and H. Ritsch, “Subradiance via entanglement in atoms with several independent decay channels,” *Phys. Rev. Lett.* **118**, 143602 (2017).

[54] M. B. Plenio, “Logarithmic negativity: a full entanglement monotone that is not convex,” *Phys. Rev. Lett.* **95**, 090503 (2005).

[55] J. G. Bohnet, Z. Chen, J. M. Weiner, K. C. Cox, and J. K. Thompson, “Linear-response theory for superradiant lasers,” *Phys. Rev. A* **89**, 013806 (2014).

[56] C. Sommer, M. Reitz, F. Mineo, and C. Genes, “Molecular polaritonics in dense mesoscopic disordered ensembles,” (2020), [arXiv:2010.07155 \[quant-ph\]](https://arxiv.org/abs/2010.07155).

[57] R. Alaei, B. Gurlek, M. Albooyeh, D. Martín-Cano, and V. Sandoghdar, “Quantum metamaterials with magnetic response at optical frequencies,” *Phys. Rev. Lett.* **125**, 063601 (2020).

[58] K. E. Ballantine and J. Ruostekoski, “Optical magnetism and Huygens’ surfaces in arrays of atoms induced by cooperative responses,” *Phys. Rev. Lett.* **125**, 143604 (2020).

[59] R. Bekenstein, I. Pikovski, H. Pichler, E. Shahmoon, S. F. Yelin, and M. D. Lukin, “Quantum metasurfaces with atom arrays,” *Nature Physics* **16**, 676–681 (2020).

[60] A. Grankin, P. O. Guimond, D. V. Vasilyev, B. Vermeresch, and P. Zoller, “Free-space photonic quantum link and chiral quantum optics,” *Phys. Rev. A* **98**, 043825 (2018).

[61] R. J. Bettles, S. A. Gardiner, and C. S. Adams, “Enhanced optical cross section via collective coupling of atomic dipoles in a 2D array,” *Phys. Rev. Lett.* **116**, 103602 (2016).

[62] E. Shahmoon, D. S. Wild, M. D. Lukin, and S. F. Yelin, “Cooperative resonances in light scattering from two-dimensional atomic arrays,” *Phys. Rev. Lett.* **118**, 113601 (2017).

[63] R. J. Bettles, M. D. Lee, S. A. Gardiner, and J. Ruostekoski, “Quantum and nonlinear effects in light transmitted through planar atomic arrays,” *Communications Physics* **3**, 141 (2020).

[64] L. Ostermann, D. Plankensteiner, H. Ritsch, and C. Genes, “Protected subspace Ramsey spectroscopy,” *Phys. Rev. A* **90**, 053823 (2014).

[65] R. Holzinger, D. Plankensteiner, L. Ostermann, and H. Ritsch, “Nanoscale coherent light source,” *Phys. Rev. Lett.* **124**, 253603 (2020).

[66] W. P. Su, J. R. Schrieffer, and A. J. Heeger, “Solitons in polyacetylene,” *Phys. Rev. Lett.* **42**, 1698–1701 (1979).

[67] J. K. Asbóth, L. Oroszlány, and A. Pályi, *A Short Course on Topological Insulators* (Springer, New York, 2016).

[68] N. Ramsey, *Molecular beams* (Oxford University Press, New York, 1990).

[69] M. Moreno-Cardoner, D. Plankensteiner, L. Ostermann, D. E. Chang, and H. Ritsch, “Subradiance-enhanced excitation transfer between dipole-coupled nanorings of quantum emitters,” *Phys. Rev. A* **100**, 023806 (2019).

[70] J. A. Needham, I. Lesanovsky, and B. Olmos, “Subradiance-protected excitation transport,” *New Journal of Physics* **21**, 073061 (2019).

[71] K. E. Ballantine and J. Ruostekoski, “Subradiance-protected excitation spreading in the generation of collimated photon emission from an atomic array,” *Phys. Rev. Research* **2**, 023086 (2020).

[72] A. E. Miroshnichenko, S. Flach, and Y. S. Kivshar, “Fano resonances in nanoscale structures,” *Rev. Mod. Phys.* **82**, 2257–2298 (2010).

[73] C. J. Chang-Hasnain and W. Yang, “High-contrast gratings for integrated optoelectronics,” *Adv. Opt. Photon.* **4**, 379–440 (2012).

[74] W. Zhou, D. Zhao, Y.-C. Shuai, H. Yang, S. Chuwongin, A. Chadha, J.-H. Seo, K. X. Wang, V. Liu, Z. Ma, and S. Fan, “Progress in 2D photonic crystal Fano resonance photonics,” *Progress in Quantum Electronics* **38**, 1–74 (2014).

[75] M. F. Limonov, M. V. Rybin, A. N. Poddubny, and Y. S. Kivshar, “Fano resonances in photonics,” *Nature Photonics* **11**, 543–554 (2017).

[76] S. Zeytinoğlu, C. Roth, S. Huber, and A. Imamoglu, “Atomically thin semiconductors as nonlinear mirrors,” *Physical Review A* **96**, 031801 (2017).

[77] P. Back, S. Zeytinoğlu, A. Ijaz, M. Kroner, and A. Imamoglu, “Realization of an electrically tunable narrow-bandwidth atomically thin mirror using monolayer MoSe₂,” *Phys. Rev. Lett.* **120**, 037401 (2018).

[78] G. Scuri, Y. Zhou, A. A. High, D. S. Wild, C. Shu, K. De Greve, L. A. Jauregui, T. Taniguchi, K. Watanabe, P. Kim, M. D. Lukin, and H. Park, “Large excitonic reflectivity of monolayer MoSe₂ encapsulated in hexagonal boron nitride,” *Phys. Rev. Lett.* **120**, 037402 (2018).

[79] K. Jacobs, *Stochastic Processes for Physicists: Understanding Noisy Systems* (Cambridge University Press, New York, 2010).

[80] C. Genes, D. Vitali, P. Tombesi, S. Gigan, and M. Aspelmeyer, “Ground-state cooling of a micromechanical oscillator: Comparing cold damping and cavity-assisted cooling schemes,” *Physical Review A* **77**, 033804 (2008).

[81] A. Dantan, B. Nair, G. Pupillo, and C. Genes, “Hybrid cavity mechanics with doped systems,” *Phys. Rev. A* **90**, 033820 (2014).

[82] M. A. Sentef, M. Ruggenthaler, and A. Rubio, “Cavity quantum-electrodynamical polaritonically enhanced electron-phonon coupling and its influence on superconductivity,” *Sci. Adv.* **4**, 6969–6969 (2018).

[83] A. Thomas, E. Devaux, K. Nagarajan, T. Chervy, M. Seidel, D. Hagenmüller, S. Schütz, J. Schachenmayer, C. Genet, G. Pupillo, and T. W. Ebbesen, “Exploring superconductivity under strong coupling with the vacuum electromagnetic field,” [arXiv:1911.01459](https://arxiv.org/abs/1911.01459) (2019).

[84] T. Kampschulte and J. H. Denschlag, “Cavity-controlled formation of ultracold molecules,” *New Journal of Physics* **20**, 123015 (2018).

[85] M. Kiffner, J. R. Coulthard, F. Schlawin, A. Ardavan, and D. Jaksch, “Manipulating quantum materials with quantum light,” *Phys. Rev. B* **99**, 085116 (2019).

[86] X. Wang, E. Ronca, and M. A. Sentef, “Cavity quantum electrodynamic Chern insulator: Towards light-induced quantized anomalous Hall effect in graphene,” *Phys. Rev. B* **99**, 235156 (2019).

[87] J. Rohn, M. Hörmann, C. Genes, and K. P. Schmidt, “Ising model in a light-induced quantized transverse field,” *Phys. Rev. Research* **2**, 023131 (2020).

[88] M. A. Sentef, J. Li, F. Künzel, and M. Eckstein, “Quantum to classical crossover of Floquet engineering in correlated quantum systems,” *Phys. Rev. Research* **2**, 033033 (2020).

[89] Y. Ashida, A. Imamoğlu, J. Faist, D. Jaksch, A. Cavalleri, and E. Demler, “Quantum electrodynamic control of matter: Cavity-enhanced ferroelectric phase transition,” *Phys. Rev. X* **10**, 041027 (2020).

[90] C. Toninelli, I. Gerhardt, A. S. Clark, A. Reserbat-Plantey, S. Götzinger, Z. Ristanović, M. Colautti, P. Lombardi, K. D. Major, I. Deperasińska, W. H. Pernice, F. H. L. Koppens, B. Kozankiewicz, A. Gourdon, V. Sandoghdar, and M. Orrit, “Single organic molecules for photonic quantum technologies,” *Nature Materials* (2021).

[91] T. Basché, W. E. Moerner, M. Orrit, and H. Talon, “Photon antibunching in the fluorescence of a single dye molecule trapped in a solid,” *Phys. Rev. Lett.* **69**, 1516–1519 (1992).

[92] F. De Martini, G. Di Giuseppe, and M. Marrocco, “Single-mode generation of quantum photon states by excited single molecules in a microcavity trap,” *Phys. Rev. Lett.* **76**, 900–903 (1996).

[93] B. Lounis and W. E. Moerner, “Single photons on demand from a single molecule at room temperature,” *Nature* **407**, 491–493 (2000).

[94] S. Pazzagli, P. Lombardi, D. Martella, M. Colautti, B. Tiribilli, F. S. Cataliotti, and C. Toninelli, “Self-assembled nanocrystals of polycyclic aromatic hydrocarbons show photostable single-photon emission,” *ACS Nano* **12**, 4295–4303 (2018).

[95] A. Maser, B. Gmeiner, T. Utikal, S. Götzinger, and V. Sandoghdar, “Few-photon coherent nonlinear optics with a single molecule,” *Nature Photonics* **10**, 450–453 (2016).

[96] P. Roelli, C. Galland, N. Piro, and T. J. Kippenberg, “Molecular cavity optomechanics as a theory of plasmon-enhanced Raman scattering,” *Nat. Nanotechnol.* **11**, 164–169 (2016).

[97] T. Neuman, R. Esteban, G. Giedke, M. K. Schmidt, and J. Aizpurua, “Quantum description of surface-enhanced resonant Raman scattering within a hybrid-optomechanical model,” *Phys. Rev. A* **100**, 043422 (2019).

[98] F. Benz, M. K. Schmidt, A. Dreismann, R. Chikkaraddy, Y. Zhang, A. Demetriadou, C. Carnegie, H. Ohadi, B. de Nijs, R. Esteban, J. Aizpurua, and J. J. Baumberg, “Single-molecule optomechanics in ‘picocavities’,” *Science* **354**, 726–729 (2016).

[99] C. Clear, R. C. Schofield, K. D. Major, J. Iles-Smith, A. S. Clark, and D. P. S. McCutcheon, “Phonon-induced optical dephasing in single organic molecules,” *Phys. Rev. Lett.* **124**, 153602 (2020).

[100] A. Witkowski and W. Moffitt, “Electronic spectra of dimers: Derivation of the fundamental vibronic equation,” *J. Chem. Phys.* **33**, 872–875 (1960).

[101] M. J. Riley and E. R. Krausz, “The symmetric dimer: Effects of second-order vibronic coupling,” *Chemical Physics* **148**, 229–240 (1990).

[102] A. Eisfeld, L. Braun, W. T. Strunz, J. S. Briggs, J. Beck, and V. Engel, “Vibronic energies and spectra of molecular dimers,” *J. Chem. Phys.* **122**, 134103 (2005).

[103] M. Lippitz, C. G. Hübner, T. Christ, H. Eichner, P. Bordat, A. Herrmann, K. Müllen, and T. Basché, “Coherent electronic coupling versus localization in individual molecular dimers,” *Phys. Rev. Lett.* **92**, 103001 (2004).

[104] G. S. Engel, T. R. Calhoun, E. L. Read, T.-K. Ahn, T. Mančal, Y.-C. Cheng, R. E. Blankenship, and G. R. Fleming, “Evidence for wavelike energy transfer through quantum coherence in photosynthetic systems,” *Nature* **446**, 782–786 (2007).

[105] A. Streltsov, G. Adesso, and M. B. Plenio, “Colloquium: Quantum coherence as a resource,” *Rev. Mod. Phys.* **89**, 041003 (2017).

[106] V. May and O. Kühn, *Charge and energy transfer dynamics in molecular systems* (Wiley-VCH Verlag GmbH, New York, 2011).

[107] F. J. Garcia-Vidal and J. Feist, “Long-distance operator for energy transfer,” *Science* **357**, 1357 (2017).

[108] M. Du, L. A. Martínez-Martínez, R. F. Ribeiro, Z. Hu, V. M. Menon, and J. Yuen-Zhou, “Theory for polariton-assisted remote energy transfer,” *Chem. Sci.* **9**, 6659–6669 (2018).

[109] M. Reitz, F. Mineo, and C. Genes, “Energy transfer and correlations in cavity-embedded donor-acceptor configurations,” *Scientific Reports* **8**, 9050 (2018).

[110] T. Schwartz, J. A. Hutchinson, J. Léonard, C. Genet, S. Haacke, and T. W. Ebbesen, “Polariton dynamics under strong Light–Molecule coupling,” *ChemPhysChem* **14**, 125–131.

[111] A. Canaguier-Durand, C. Genet, A. Lambrecht, T. W. Ebbesen, and S. Reynaud, “Non-markovian polariton dynamics in organic strong coupling,” *The European Physical Journal D* **69**, 24 (2015).

[112] T. Neuman and J. Aizpurua, “Origin of the asymmetric light emission from molecular exciton polaritons,” *Optica* **5**, 1247–1255 (2018).

[113] M. A. Zeb, P. G. Kirton, and J. Keeling, “Exact states and spectra of vibrationally dressed polaritons,” *ACS*

Photonics **5**, 249–257 (2018).

[114] F. Herrera and F. C. Spano, “Dark vibronic polaritons and the spectroscopy of organic microcavities,” *Phys. Rev. Lett.* **118**, 223601 (2017).

[115] F. Herrera and F. C. Spano, “Theory of nanoscale organic cavities: The essential role of vibration-photon dressed states,” *ACS Photonics* **5**, 65–79 (2018).

[116] J. Flick, H. Appel, M. Ruggenthaler, and A. Rubio, “Cavity Born–Oppenheimer approximation for correlated electron–nuclear-photon systems,” *Journal of Chemical Theory and Computation* **13**, 1616–1625 (2017).

[117] J. del Pino, F. A. Y. N. Schröder, A. W. Chin, J. Feist, and F. J. Garcia-Vidal, “Tensor network simulation of non-Markovian dynamics in organic polaritons,” *Phys. Rev. Lett.* **121**, 227401 (2018).

[118] R. Lettow, Y. L. A. Rezus, A. Renn, G. Zumofen, E. Ikonen, S. Götzinger, and V. Sandoghdar, “Quantum interference of tunably indistinguishable photons from remote organic molecules,” *Phys. Rev. Lett.* **104**, 123605 (2010).

[119] U. Weiss, *Quantum Dissipative Systems*, Series in modern condensed matter physics (World Scientific, 1999).

Appendix

1. One dimensional transfer matrix theory

For an arbitrary scatterer (mirror, atom, etc.) at a fixed position, we assume the modes on the left as Ae^{-ikx} (left propagating) and Be^{ikx} (right propagating) and on the right as Ce^{-ikx} (left propagating) and De^{ikx} (right propagating), as illustrated in Fig. 18. We assume the scatterer to have a complex reflectivity r and transmittivity t . The two are connected as $t = 1 + r$ and in the absence of absorption one has $|t|^2 + |r|^2 = 1$. The outgoing fields can be related to the incoming fields as

$$A = rB + tC, \quad (1a)$$

$$D = tB + rC. \quad (1b)$$

Note that in the case where one has no incoming wave from the right ($C = 0$), this simply gives $D = tB$ and $A = rB$. The fields on the left can be connected to the fields on the right via

$$\begin{pmatrix} A \\ B \end{pmatrix} = \frac{1}{t} \begin{pmatrix} t^2 - r^2 & r \\ -r & 1 \end{pmatrix} \begin{pmatrix} C \\ D \end{pmatrix}. \quad (2)$$

For the two-mirror arrangement considered in Sec. IV C, each mirror can be characterized by its polarizability ζ_j , $j = R, L$, where the polarizability generally depends on frequency $\zeta_j = \zeta_j(\omega)$. The transmission and reflection coefficients for each mirror are given by $t_j = 1/(1 - i\zeta_j)$ and $r_j = i\zeta_j/(1 - i\zeta_j)$, respectively and the transfer matrix of each mirror reads

$$\mathbf{T}_j = \begin{pmatrix} 1 + i\zeta_j & i\zeta_j \\ -i\zeta_j & 1 - i\zeta_j \end{pmatrix}, \quad (3)$$

while the matrix for free space propagation is given by $\mathbf{T}_f = \text{diag}(e^{i\theta}, e^{-i\theta})$ where $\theta = \omega\ell/c$. The transfer matrix of the whole system is then obtained by multiplying the three individual matrices

$$\begin{aligned} \mathbf{T} &= \mathbf{T}_R \mathbf{T}_f \mathbf{T}_L & (4) \\ &= \begin{pmatrix} (1 + i\zeta_R)(1 + i\zeta_L)e^{i\theta} + \zeta_R \zeta_L e^{-i\theta} & i(1 - i\zeta_L)\zeta_R e^{-i\theta} + i\zeta_L(1 + i\zeta_R)e^{i\theta} \\ -i(1 + i\zeta_L)\zeta_R e^{i\theta} - i\zeta_L(1 - i\zeta_R)e^{-i\theta} & (1 - i\zeta_R)(1 - i\zeta_L)e^{-i\theta} + \zeta_R \zeta_L e^{i\theta} \end{pmatrix}, \end{aligned}$$

from which the cavity transmission coefficient can be obtained as $t = 1/T_{22}$.

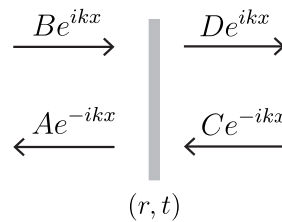


FIG. 18: In- and outgoing waves for an arbitrary scatterer with reflectivity and transmission coefficients (r, t) .

2. Brownian noise model for vibrational relaxation

A particular case of dissipation arises in the case of a quantum harmonic oscillator with free energy $\mathcal{H} = \nu(p^2 + q^2)/2$ interacting with a heat bath of (mutually independent) harmonic oscillators. In the Brownian motion model

$$\dot{q} = \nu p, \quad (5a)$$

$$\dot{p} = -2\Gamma p - \nu q + \xi, \quad (5b)$$

the decay 2Γ stems from the correlations of the stochasting input noise ξ which is only affecting the momentum quadrature. This model is a consequence of displacement-displacement interactions between the oscillator and an infinite surrounding bath $\mathcal{H}_{\text{int}} = -q \sum_k \alpha_k Q_k$ with coupling coefficients α_k [119]. The correlations of the input noise ξ at a given bath temperature in the time domain read [80]

$$\langle \xi(t)\xi(t') \rangle = \int_{-\infty}^{\infty} \frac{d\omega}{2\pi} e^{-i\omega(t-t')} S_{\text{th}}(\omega). \quad (6)$$

where we defined the thermal noise spectrum $S_{\text{th}}(\omega)$

$$S_{\text{th}}(\omega) = \frac{2\Gamma\omega}{\nu} \left[\coth \frac{\hbar\omega}{2k_B T} + 1 \right]. \quad (7)$$

While generally, the noise is not delta-correlated, one can approximate Eq. (6) in the limit of large temperatures as (using that in this limit $\bar{n} + 1/2 \approx k_B T/(\hbar\nu)$ with the average thermal occupancy $\bar{n} = [\exp(\hbar\nu/k_B T) - 1]^{-1}$ and $\coth(x) \approx 1/x$ for $x \ll 1$)

$$\langle \xi(t)\xi(t') \rangle \approx 2\Gamma(2\bar{n} + 1)\delta(t - t') + i\frac{2\Gamma}{\nu}\delta'(t - t'), \quad (8)$$

where $\delta'(t - t')$ is the time derivative of the delta function. From the spectrum evaluated at $\pm\nu$ one can obtain the cooling and heating contributions: $S_{\text{th}}(\nu) = 4\Gamma(\bar{n} + 1)$ and $S_{\text{th}}(-\nu) = 4\Gamma\bar{n}$. Generally, from these properties one can always estimate the damping rate as $2\Gamma = (S_{\text{th}}(\nu) - S_{\text{th}}(-\nu))/2$ and the equilibrium thermal occupancy as $\bar{n} = S_{\text{th}}(-\nu)/[S_{\text{th}}(\nu) + S_{\text{th}}(-\nu)]$. In the case of small temperatures $k_B T/(\hbar\nu) \ll 1$, the thermal spectrum becomes very asymmetric $S_{\text{th}}(\omega) = [4\omega\Gamma/\nu]\theta(\omega)$ as it vanishes for negative frequencies (we introduced the Heaviside function $\theta(\omega)$). Generally, one can proceed with a Fourier domain analysis of the steady state of the equations above which leads to $p(\omega) = \epsilon(\omega)\xi(\omega)$ and $q(\omega) = i\nu p(\omega)/\omega$ with the mechanical susceptibility describing the response of the phonon bath

$$\epsilon(\omega) = \frac{i\omega}{\omega^2 - \nu^2 + 2i\Gamma\omega}. \quad (9)$$

One can also make use of the fact that the noise is always delta-correlated in Fourier domain $\langle \xi(\omega)\xi(\omega') \rangle = S_{\text{th}}(\omega)\delta(\omega + \omega')$. One can then proceed by computing the time-domain correlations (using that $\epsilon(-\omega) = \epsilon^*(\omega)$)

$$\langle p(t)p(t') \rangle = \frac{1}{2\pi} \int_{-\infty}^{\infty} d\omega e^{-i\omega(t-t')} |\epsilon(\omega)|^2 S_{\text{th}}(\omega), \quad (10a)$$

$$\langle q(t)q(t') \rangle = \frac{1}{2\pi} \int_{-\infty}^{\infty} d\omega e^{-i\omega(t-t')} \frac{\nu}{\omega} |\epsilon(\omega)|^2 S_{\text{th}}(\omega). \quad (10b)$$

Generally, these expressions can be solved by a contour integral in the complex plane. We note that the integral of the momentum correlation function diverges and generally requires the introduction of a cutoff frequency $\Lambda > \nu$ to keep it finite. However, for $\Gamma \ll \nu$, the expression for $|\epsilon(\omega)|^2 S_{\text{th}}(\omega)$ is sharply peaked around $\pm\nu$. In this case, one can expand around the poles $\omega = \nu + \delta$ and $\omega = \nu - \delta$ with $|\delta| \ll |\nu|$ and only keep leading order terms in δ . The integrals in Eq. (10) can then be approximated as the Fourier transforms of Lorentzian lineshapes which is much easier to solve and results in (for $t > t'$)

$$\langle p(t)p(t') \rangle = \left[\left(\bar{n} + \frac{1}{2} \right) \cos(\nu\tau) - \frac{i}{2} \sin(\nu\tau) \right] e^{-\Gamma|\tau|}, \quad (11)$$

with $\tau = t - t'$.

3. Derivation of the FRET rate

Let us evaluate the term $2\Omega\Im\langle\sigma_A^\dagger\sigma_D\rangle$ which is the one that give rise to energy transfer between the two molecules. Formal integration of the equation of motion for the acceptor gives

$$\sigma_A^\dagger(t) = \sigma_A(0)e^{-(\gamma_A-i\omega_A)t}\mathcal{D}_A(0)\mathcal{D}_A^\dagger(t) + \int_0^t dt' e^{-(\gamma_A-i\omega_A)(t-t')}\left[i\Omega\sigma_D^\dagger(t') + \sqrt{2\gamma}\sigma_A^{\dagger,\text{in}}(t')\right]\mathcal{D}_A(t')\mathcal{D}_A^\dagger(t). \quad (12)$$

Due to the quick vibrational relaxation, we can make a great simplification by neglecting the backaction of the acceptor's dipole moment onto the donor and assume free evolution for the donor

$$\dot{\tilde{\sigma}}_D \approx -(\gamma_D + i\omega_D)\tilde{\sigma}_D + \sqrt{2\gamma}\tilde{\sigma}_D^{\text{in}}. \quad (13)$$

Integrating this, one can calculate the term $2\Omega\Im\langle\sigma_A^\dagger\sigma_D\rangle$ which requires the correlation function (assuming $t \geq t' \geq 0$ and $t \gg 1/\Gamma_D$)

$$\langle\mathcal{D}_D(0)\mathcal{D}_D^\dagger(t')\mathcal{D}_D(t)\mathcal{D}_D^\dagger(0)\rangle = e^{-S_D}e^{S_D e^{-(\Gamma_D-i\nu_D)(t-t')}}e^{-S_D e^{-(\Gamma_D+i\nu_D)t'}}e^{S_D e^{-(\Gamma_D-i\nu_D)t'}}, \quad (14)$$

where the four-operator correlation function can be reduced to a two-operator correlation function by commuting $\mathcal{D}_D^\dagger(0)$ with $\mathcal{D}_D(t)$ and $\mathcal{D}_D^\dagger(t')$ and using that $\mathcal{D}_D(0)\mathcal{D}_D^\dagger(0) = \mathbb{1}$. Under the assumption of $\Gamma_D, \Gamma_A \gg \gamma_D, \gamma_A$, one can finally arrive at an expression for the energy transfer rate showing proportionality to the donor population $2\Omega\langle\sigma_A^\dagger\sigma_D\rangle = \kappa_{\text{ET}}P_D(t)$ (assuming $\gamma_D = \gamma_A$):

$$\kappa_{\text{ET}} = \sum_{n_D, n_A} \frac{2\Omega^2 f_{S_D}^{n_D} f_{S_A}^{n_A} (n_D \Gamma_D + n_A \Gamma_A)}{(n_D \Gamma_D + n_A \Gamma_A)^2 + [\Delta - n_D \nu_D - n_A \nu_A]^2}. \quad (15)$$

The denominator of the above expression asks that the resonance is $\omega_D - n_D \nu_D = \omega_A + n_A \nu_A$ is fulfilled, i.e. fluorescence lines of the donor $|e_D, 0\rangle \rightarrow |g_D, n_D\rangle$ have to overlap with absorption lines of the acceptor $|g_A, 0\rangle \rightarrow |e_A, n_A\rangle$, both of which are weighted by the respective Franck-Condon factors. In the case of many vibrational modes n for donor and acceptor, we can generalize the result by writing general displacements $\mathcal{D}_A = \prod_{k=1}^n \mathcal{D}_A^k$ and $\mathcal{D}_D = \prod_{k=1}^n \mathcal{D}_D^k$ for all vibrational modes. The equations of motion can then be expressed in the same form as in Eqs. (123)

$$\dot{\tilde{\sigma}}_D = -(\gamma + i\omega_D)\tilde{\sigma}_D - i\Omega\tilde{\sigma}_A\mathcal{D}_A\mathcal{D}_D^\dagger + \sqrt{2\gamma}\tilde{\sigma}_D^{\text{in}}, \quad (16a)$$

$$\dot{\tilde{\sigma}}_A = -(\gamma + i\omega_A)\tilde{\sigma}_A - i\Omega\tilde{\sigma}_D\mathcal{D}_D\mathcal{D}_A^\dagger + \sqrt{2\gamma}\tilde{\sigma}_A^{\text{in}}, \quad (16b)$$

except that now the displacement is produced by all modes. We assume that the two molecules have the same vibrational properties $\langle\mathcal{D}_A^k(t')\mathcal{D}_A^{k,\dagger}(t)\rangle = \langle\mathcal{D}_D^k(t')\mathcal{D}_D^{k,\dagger}(t)\rangle$. This leads to a generalized energy transfer rate

$$\kappa_{\text{ET}} = \sum_{\{m_k=0\}}^{\infty} \sum_{\{l_k=0\}}^{\infty} 2 \prod_{k=1}^n e^{-2S_k} \frac{S_k^{(m_k+l_k)}}{m_k!l_k!} \frac{\sum_{k=1}^n (m_k + l_k) \Gamma_k \Omega^2}{[\sum_{k=1}^n (m_k + l_k) \Gamma_k]^2 + [\omega_D - \omega_A - \sum_{k=1}^n (m_k + l_k) \nu_k]^2}. \quad (17)$$

Here the sums go over all indices $\{m_k\} = m_1, \dots, m_n$ and $\{l_k\} = l_1, \dots, l_n$ referring to the possible occupancies of all n vibrational modes of the two involved molecules.